

© 2007

Rambod Hadidi

ALL RIGHTS RESERVED

**GENERIC PROBABILISTIC INVERSION TECHNIQUE FOR
GEOTECHNICAL AND TRANSPORTATION ENGINEERING APPLICATIONS**

by

RAMBOD HADIDI

A Dissertation submitted to the
Graduate School-New Brunswick
Rutgers, The State University of New Jersey
in partial fulfillment of the requirements

for the degree of

Doctor of Philosophy

Graduate Program in Civil and Environmental Engineering

written under the direction of

Dr. Nenad Gucunski

and approved by

New Brunswick, New Jersey

May, 2007

ABSTRACT OF THE DISSERTATION

GENERIC PROBABILISTIC INVERSION TECHNIQUE FOR GEOTECHNICAL AND TRANSPORTATION ENGINEERING APPLICATIONS

BY RAMBOD HADIDI

Dissertation Director:

Dr. Nenad Gucunski

A wide range of important problems in civil engineering can be classified as inverse problems. In such problems, the observational data related to the performance of a system is known, and the characteristics of the system or the input are sought. There are two general approaches to the solution of inverse problems: deterministic and probabilistic. Traditionally, inverse problems in civil engineering have been solved using a deterministic approach. In this approach, the objective is to find a model of the system that its theoretical response best fits the observed data. In deterministic approach to the solution of inverse problems, it is implicitly assumed that the uncertainties in data and theoretical models are negligible. However, this assumption is not valid in many applications, and therefore, effects of data and modeling uncertainties on the obtained

solution should be evaluated. In this dissertation, a general probabilistic approach to the solution of the inverse problems is introduced, which offers the framework required to obtain uncertainty measures for the solution. Techniques for direct analytical evaluation and numerical approximation of the probabilistic solution using Monte Carlo Markov Chains (MCMC), with and without Neighborhood Algorithm (NA) approximation, are introduced and explained. The application of the presented concepts and techniques are then illustrated for three important classes of inverse problems in geotechnical and transportation engineering as application examples. These applications are: Falling Weight Deflectometer (FWD) backcalculation, model calibration based on geotechnical instrument measurements, and seismic waveform inversion for shallow subsurface characterization. For each application, the probabilistic formulation is presented; the solution is obtained; and the advantages of the probabilistic approach are illustrated and discussed.

Dedication

To my parents,
For all their unconditional love and support

Acknowledgement

This dissertation is the result of many years of work and study. During these years, I have been guided, accompanied, and supported by many people. These few lines are my opportunity to acknowledge their contributions.

First, I would like to express my sincere gratitude to Dr. Nenad Gucunski, my advisor, for his guidance and support. I thank him as well for providing me an opportunity to grow as a student and an engineer in the unique research environment he creates. I would also like to thank Dr. Ali Maher, whose steadfast support was greatly needed and deeply appreciated.

There are no words to express my gratitude to my parents. Although they have been living thousands of miles away, that has not stopped the wealth of love, support, and advice they have given me. They will always have a special place in my heart.

The writing of a dissertation may seem as a lonely and isolating experience, yet it is obviously not possible without the support of numerous people. Thus, my gratitude goes to many people who directly or indirectly helped me in this journey. Among them are faculty and staff at department of civil and environmental engineering of Rutgers University and my colleagues at Paulus, Sokolowski, and Sartor, LLC.

Support and encouragement from my friends have been essential in completion of this work. Particularly, I'd like to thank Azam and Bahman Kalantari for their kindness, encouragement, and support. Finally, my thanks go to Parisa Shokouhi as well for the happy moments we shared at Rutgers.

Rambod Hadidi, January, 2007

Table of Contents

ABSTRACT OF THE DISSERTATION.....	ii
Dedication	iv
Acknowledgement.....	v
Table of Contents	vi
List of Tables	x
List of Illustrations.....	xi
1 Introduction.....	1
Statement of the Problem	1
Objectives	2
Organization	3
References	5
2 Uncertainties in Measurements	6
Introduction	6
Measurement Specification	7
Evaluation and Expression of Uncertainties in Measurement.....	8
<i>Evaluation of Uncertainty</i>	9
<i>Standard Uncertainty</i>	10
<i>Combined Standard Uncertainty</i>	11
<i>Expanded Uncertainty</i>	11
<i>Uncertainty Interval</i>	12
Generalized Measurement	12
Summary.....	14
References	14
3 Probabilistic Approach to Inverse Problems	15
Introduction	15
Elements of Probability Theory.....	16
<i>Kolmogorov's Concept of Probability</i>	16
<i>Probability Density</i>	17
<i>Homogeneous Probability Density</i>	18
<i>Conjunction of Probabilities</i>	18
<i>Marginal Probability</i>	20
<i>Independent Probabilities</i>	20
Probabilistic Formulation of Inverse Problems	20
<i>Model Space and Data Space</i>	21
<i>State of Information</i>	21
<i>A Priori Information</i>	22
<i>Forward Model</i>	24
<i>General Probabilistic Solution of the Inverse Problem</i>	25
<i>Probabilistic Solution in the Case of Data and Forward Model with Gaussian</i> <i>Uncertainties</i>	26
Appraisal of the Probabilistic Solution.....	28
<i>Central Estimators and Estimators of Dispersion</i>	28
<i>One and Two Dimensional Marginal Probability Densities</i>	29
Summary.....	29

References	30
4 Monte Carlo Evaluation of the Probabilistic Solution	31
Introduction	31
Illustrative Example.....	32
Deterministic Solution.....	33
Analytical Evaluation of the Probabilistic Solution	34
Direct Sampling Evaluation of the Probabilistic Solution.....	36
<i>Monte Carlo Sampling of Probability Distributions.....</i>	<i>37</i>
<i>Markov Chains</i>	<i>39</i>
<i>Metropolis Sampler.....</i>	<i>40</i>
<i>Cascade Metropolis Sampler</i>	<i>41</i>
<i>Monte Carlo Markov Chain (MCMC) Sampling of the Solution of Inverse Problems</i>	<i>42</i>
<i>Appraisal of Results</i>	<i>44</i>
<i>Convergence.....</i>	<i>48</i>
<i>Computational Limitations.....</i>	<i>50</i>
Direct Sampling Solution Using Approximation of the Likelihood Function	51
<i>Neighborhood Algorithm (NA).....</i>	<i>52</i>
<i>Implementation of NA.....</i>	<i>54</i>
<i>Voronoi Diagram</i>	<i>55</i>
<i>Stop Criteria.....</i>	<i>56</i>
<i>Monte Carlo Solution Using Neighborhood Approximation</i>	<i>57</i>
Matlab® Application Program	60
Summary.....	61
References	63
5 Application One: Falling Weight Deflectometer Backcalculation	65
Introduction	65
Background.....	66
<i>Review of FWD Test Procedure</i>	<i>66</i>
<i>Review of Current FWD Backcalculation Procedures</i>	<i>69</i>
Probabilistic Formulation of FWD Backcalculation	74
<i>Model a Priori Information.....</i>	<i>75</i>
<i>Data a Priori Information.....</i>	<i>76</i>
<i>Forward Model</i>	<i>79</i>
<i>Probabilistic Solution.....</i>	<i>85</i>
<i>Computational Time.....</i>	<i>85</i>
Backcalculation of Synthetic Test Data.....	86
<i>Synthetic FWD Test Data.....</i>	<i>86</i>
<i>Backcalculation of Layer Modulus based on Deflection Bowl Using Linear Static</i> <i>Forward Model</i>	<i>88</i>
<i>Backcalculation of Layer Moduli Based on Deflection Bowl Using Linear Dynamic</i> <i>Forward Model</i>	<i>94</i>
<i>Backcalculation of Layer Moduli Based on Deflection Time History Using Linear</i> <i>Dynamic Time Domain Forward Model.....</i>	<i>98</i>
<i>Backcalculation of Layer Moduli and Depth to Bedrock Based on Deflection Time</i> <i>History Using Linear Dynamic Forward Model.....</i>	<i>101</i>

<i>Backcalculation of Layer Moduli and Thickness Based on Deflection Time History Using Linear Dynamic Forward Model</i>	103
<i>Backcalculation Based on Velocity Time History</i>	103
Backcalculation of FWD Test Data.....	106
<i>FWD Test Results</i>	106
<i>Backcalculation Results</i>	107
<i>A Discussion on Data and Modeling Uncertainties</i>	108
Effect of Considering Dynamic Material Properties of Pavement Layers on Backcalculation Results.....	111
<i>Dynamic Moduli and Damping of Pavement Layers</i>	111
<i>Numerical Modeling of Dynamic Moduli and Damping</i>	115
<i>Backcalculation of Layer Moduli Based on Deflection Time History Using Linear Dynamic Frequency Domain Forward Model</i>	118
<i>Pavement Response with Dynamic Moduli</i>	121
Summary.....	124
References.....	125
6 Application Two: Model Calibration Based On Geotechnical Instrument Measurements	128
Introduction.....	128
Background.....	130
<i>Project Overview</i>	130
<i>Site Conditions</i>	132
<i>Ground Improvement Program</i>	133
Development of Predictive Model and Calibration Measurements.....	134
<i>Development of Predictive Model</i>	134
<i>Measurement Results</i>	138
<i>Initial Model Predictions</i>	140
<i>Model Parameters</i>	140
Probabilistic Formulation.....	142
<i>Model a Priori Information</i>	143
<i>Data a Priori Information</i>	143
<i>Forward Model</i>	144
<i>Probabilistic Formulation and Solution</i>	144
Calibration Results.....	145
Summary.....	149
References.....	149
7 Application Three: Seismic Waveform Inversion	150
Introduction.....	150
Probabilistic Formulation of Waveform Inversion Problem.....	151
<i>Model a Priori Information</i>	152
<i>Data a Priori Information</i>	152
<i>Forward Model</i>	153
<i>Probabilistic Formulation and Solution</i>	154
Synthetic Seismic Experiment.....	154
<i>Test Setup</i>	154
<i>Synthetic Waveforms and Forward Model</i>	156

<i>Results of Inversion of Synthetic Seismic Test</i>	158
Inversion of Seismic Pavement Analyzer Data	159
<i>Test Setup</i>	159
<i>Experimental Waveforms</i>	163
<i>Forward Model</i>	167
<i>Results of Inversion of SPA Data</i>	167
Summary	171
References	171
8 Closure	173
Summary and Conclusions	173
<i>FWD Backcalculation</i>	174
<i>Model calibration</i>	175
<i>Seismic Inversion</i>	175
Recommendations for Future Research	176
Appendix A: Spectral Element Method for Analysis of Wave Propagation in Layered Media	178
Introduction	178
Spectral Wave Analysis	181
Spectral Element Formulation	183
<i>Two-Node Layer Element</i>	183
<i>One-Node Half Space Element</i>	186
<i>Assemblage</i>	187
<i>Boundary Conditions and Solution of the System For an Impact Load</i>	187
Numerical Implementation	190
Illustrative Example	191
Summary	192
References	193
Curriculum Vitae	194

List of Tables

Table 5-1 - Geometrical and material properties used for defenition of finite element model.....	83
Table 5-2 – Range of layer moduli values used for evaluation of modeling uncertainties using deflection bowls from static analysis.	89
Table 5-3 - Geometrical and material properties used for development of spectral element results.	116
Table 5-4 – Modulus and damping values used for numerical evaluation of spectral element analysis.	121
Table 6-1 – Initial material properties used for development of predictive model.	139
Table 6-2 – Numerical values of the best fit model obtained from calibration analysis.	145
Table 7-1- Subsurface profile parameters in the generation of synthetic waveform inversion example.	158
Figure 7-3 – Synthetic waveforms used in the inversion.....	158
Table A- 1 – Geometrical and material properties used in the numerical evaluation and verification of the spectral element method [<i>Alkhoury, 2001</i>].	191

List of Illustrations

Figure 3-1 - Illustration of the concept of conjunction of probabilities P and Q , $P \wedge Q$ [Tarantola 2005].	19
Figure 3-2 - Illustration of the probability densities $\rho_M(m)$, $\rho_D(d)$, and $\rho(m,d)$ representing a priori information on model, data, and joint model and data spaces respectively [Tarantola 2005].	23
Figure 3-3 - (left) Forward model with negligible modelization uncertainties (right) and forward model with modeling uncertainties [Tarantola 2005].	25
Figure 3-4 - Representation of the general probabilistic solution of inverse problem as the conjunction of the a priori information, $\rho(m,d)$ and information obtained from forward model $\theta(m,d)$. [Tarantola 2005].	26
Figure 4-1 - Deflection based modulus determination experiment.	33
Figure 4-2 - Graphical representation of the probability densities $\rho(E,\Delta)$, $\theta(E,\Delta)$, and $\sigma(E,\Delta)$ for the modulus determination experiment. It is assumed that $\Sigma_p = 1 \text{ Pa}$ and $\Sigma_\Delta = 0.001 \text{ m}$.	35
Figure 4-3 - Graphical representation of the probability density $\sigma_E(E)$ for the modulus determination experiment. It is assumed that $\Sigma_p = 1 \text{ Pa}$ and $\Sigma_\Delta = 0.001 \text{ m}$.	36
Figure 4-4 - The collection randomly generated samples (right) of a probability distribution (left) allow inference of characteristics of underlying probability distribution [Tarantola 2005].	38
Figure 4-5 - MCMC solution of the deflection based modulus determination experiment. Histogram (top) and kernel density estimate (bottom) of the a posteriori probability density obtained from analysis of 40000 sampled models.	48
Figure 4-6 - Typical Voronoi Diagram in two dimensions.	55
Figure 4-7 - Exact plot (top) and neighborhood approximation (bottom) of the likelihood function with 1000 models. Sampled models, as well as corresponding Voronoi diagram are also shown ($\Sigma_\Delta = 0.001 \text{ m}$).	59
Figure 4-8 - Exact plot of $\sigma(E,P)$ (top) and MCMC solution using neighborhood approximation (bottom) of the modulus determination experiment.	60
Figure 4-9 Histogram of 10000 samples of the one dimensional marginal a posteriori probabilities of (a) modulus and (b) load, and their corresponding kernel density estimates (c and d).	61
Figure 4-10 Snapshot of the input window of ProbInvert, the developed probabilistic inversion application.	62
Figure 5-1 - Schematics of FWD test setup (top) and Dynatest® model 8000 FWD trailer (bottom).	68

Figure 5-2 - Typical measured loading history (top) and pavement response during FWD test at different offsets (bottom).....	69
Figure 5-3 - Coefficient of variation of deflection from short term repeatability experiments [<i>Benson, Nazarian and Harrison, 1994</i>]. D1 thru D6 indicates different deflection sensors.....	78
Figure 5-4 – Axisymmetric ABAQUS® Finite Element mesh with absorbing boundary elements for theoretical modeling of FWD test.....	79
Figure 5-5 - Time history (top) and frequency spectrum (bottom) of idealized time history wavelet.....	81
Figure 5-6 - Predicted pavement surface deflection time histories from ABAQUS® finite element model.....	84
Figure 5-7 - Response of pavement surface deflection time histories [<i>Alkhoury, 2001</i>].	84
Figure 5-8 - Synthetic FWD data for no bedrock (top) and shallow bedrock at 2 m below the surface (bottom).....	87
Figure 5-9 - Deflection bowls for synthetic FWD data.....	87
Figure 5-10 - (a, b and c) Kernel density estimates of marginal a posteriori probabilities for the layer moduli obtained from the probabilistic backcalculation of the deflection bowl with the static forward model without considering modeling uncertainties and (d) comparison of the backcalculated deflection bowls for the pavement section with the most probable layer moduli and the observed data.....	90
Figure 5-11 – Histograms and kernel density estimate of the absolute difference between the calculated maximum deflections from dynamic and static analyses at each receiver location and . The area under each density estimate is equal to one unit. The histograms are scaled to fit in the same figure.....	92
Figure 5-12 - (a, b and c) Kernel density estimates of marginal a posteriori probabilities for the layer moduli obtained from the probabilistic backcalculation of the deflection bowl with the static forward model, which includes the modeling uncertainties, and (d) comparison of the backcalculated deflection bowls for the pavement section with the most probable layer moduli and the observed data.....	93
Figure 5-13 - (a, b and c) Kernel density estimates of marginal a posteriori probabilities for the layer moduli obtained from the probabilistic backcalculation of the deflection bowl with the dynamic forward model and (d) comparison of the backcalculated deflection bowls for the pavement section with the most probable layer moduli and the observed data.....	95
Figure 5-14 -(a, b and c) Kernel density estimates of marginal a posteriori probabilities for the layer moduli obtained from the probabilistic backcalculation of the deflection bowl with the dynamic forward model with high model and data uncertainty and (d) comparison of the backcalculated deflection bowls for the pavement section with the most probable layer moduli and the observed data.....	97
Figure 5-15 - (a, b and c) Kernel density estimates of marginal a posteriori probabilities for the layer moduli obtained from the probabilistic backcalculation of the deflection time	

history with the dynamic forward model and (d) comparison of the backcalculated deflection time histories for the pavement section with the most probable layer moduli and the observed data. The two time histories are overlapping.	100
Figure 5-16 - (a, b, c and d) Kernel density estimates of marginal a posteriori probabilities for the layer moduli and depth to bedrock obtained from the probabilistic backcalculation of the deflection time histories with the dynamic forward model and (e) comparison of the backcalculated deflection time histories for the pavement section with the most probable layer moduli and the observed data.	102
Figure 5-17 - (a, b, and c) Kernel density estimates of marginal a posteriori probabilities for the layer moduli obtained from the probabilistic backcalculation of the velocity time histories with the dynamic forward model and (d) comparison of the backcalculated velocity time histories for the pavement section with the most probable layer moduli and the observed data.	105
Figure 5-18 - Measured loading history (top) and pavement response for FWD test. ...	107
Figure 5-19 -(a, b, and c) Kernel density estimates of marginal a posteriori probabilities for the layer moduli obtained from the probabilistic backcalculation of the experimental deflection time histories with the dynamic forward model and (d) comparison of the backcalculated deflection time histories for the pavement section with the most probable layer moduli and the observed data.	109
Figure 5-20 - Measured velocity time history record at receiver at zero offset.	110
Figure 5-21 - Variation of modulus (top) and damping (bottom) with shear strain for sands [Seed et. al. 1986]. <i>Error! Objects cannot be created from editing field codes.</i> indicates the ratio of the modulus at each frequency to the static modulus.	112
Figure 5-22 - Typical modulus master curves for different asphalt mixtures [Clyne et. al. 2003].	114
Figure 5-23 - Predicted pavement surface deflection time histories from linear spectral element analysis.	117
Figure 5-24 - Comparison of predicted surface defections at different receiver location from time domain and frequency domain models.	118
Figure 5-25 - (a, b and c) Kernel density estimates of marginal a posteriori probabilities for the layer moduli obtained from the probabilistic backcalculation of the deflection time history with the spectral element forward model and (d) comparison of the backcalculated deflection time histories for the pavement section with the most probable layer moduli and the observed data.	120
Figure 5-26 – Sample modulus curve and constant modulus line used for numerical evaluation of the pavement response with spectral element approach. The curve parameters are $\alpha = 2.8$, $\beta = -0.44$, $\delta = -1.48$, $\gamma = -0.56$ and $S_T = 0$ (See equation 5-4).	122
Figure 5-27 - Predicted pavement surface deflection time histories from spectral element analysis with dynamic asphalt layer modulus.	122

Figure 5-28 - Predicted pavement surface deflection time histories from nonlinear spectral element analysis.....	123
Figure 6-1 – Sketch of the generalized subsurface profile	133
Figure 6-2 – Total layer settlement for waste, organic silt/peat and clay strata. E1-7 and E1-2 are the installed extensometers along the modeled cross section.	135
Figure 6-3 – Geometry of developed finite element predictive.....	136
Figure 6-4 – Fill placement timeline at two points along the cross section and idealized fill placement timeline and stages used for model development.	137
Figure 6-5 – Close up view of idealized loading stages.	137
Figure 6-6 – Total layer settlement for waste, organic silt/peat and clay strata from extensometer measurements along the modeled cross section (Extensometer E1-2 and E1-7).	138
Figure 6-7 – Comparison of observed vs. calculated total layer settlement based on initial layer properties for waste, organic silt/peat and clay strata.	141
Figure 6-8 - Comparison of observed vs. calculated total layer settlement based on calibrated layer properties for waste (top), organic silt/peat (middle) and clay (bottom) strata.....	147
Figure 6-9 - One-dimensional kernel density estimates of marginal probability densities of model parameters for permeability of waste (a), organic silt/peat (b), and clay (c) layer. Similar information is also presented for the compression index of waste (d), organic silt/peat (e), and clay (f) layer.	148
Figure 7-1 - Schematics of the synthetic seismic waveform inversion test setup	155
Figure 7-2 - Finite element model with the test setup superimposed on the mesh	157
Figure 7-3 – Synthetic waveforms used in the inversion.....	158
Figure 7-4 - (a, b, c, d and e) Kernel density estimates of marginal a posteriori probabilities for the layer compressional wave velocities.	161
Figure 7-5 - (a, b, c, and d) Two dimensional kernel density estimates of marginal a posteriori probabilities for the layer compressional wave velocities.....	162
Figure 7-6 – Schematics of SPA.....	160
Figure 7-7 –A/D counts from accelerometers A1, A2, A3, and the high frequency hammer from a test on a flexible section.	165
Figure 7-8 – Hamming window function and A/D counts from accelerometers A1, A2, A3 after the windowing operation.	166
Figure 7-9 – - Kernel density estimates of marginal a posteriori probabilities for the layer thickness (a and b) and layer moduli (c, d, and e) obtained from the probabilistic inversion of the acceleration time histories.	169
Figure 7-10 – Comparison of the acceleration time histories for the pavement section with the most probable layer moduli and the observed data.....	170

Figure A-1 - Two-node axi-symmetrical layer element [Alkhoury, 2001].....	184
Figure A-2 - One-node axi-symmetrical half space element. [Alkhoury, 2001].	187
Figure A-3 – Spatial distribution of the load [Alkhoury, 2001].	188
Figure A-4 - Time history of the idealized time wavelet.....	188
Figure A-5 - Frequency spectrum of the idealized wavelet.....	189
Figure A-6 – Coefficients of Fourier-Bessel series for a circular load of a radius $a = 0.15m$	190
Figure A-7 - Predicted pavement surface deflection time histories from the spectral element analysis.	192
Figure A-8 - Predicted pavement surface deflection time histories from the spectral element analysis [Alkhoury et al.,2001].	192

1 Introduction

Statement of the Problem

A wide range of tasks in civil engineering includes solution of inverse problems. In such problems, the observational data regarding the performance of a system is known and the information about the system is sought. Examples of inverse problems in civil engineering are interpretation of geophysical and nondestructive test data, determination of material constitutive parameters from laboratory or field data, earthquake location estimation, and interpretation of geotechnical instrumentation readings.

There are two general approaches to the solution of inverse problems: deterministic and probabilistic approaches. In deterministic approach to inverse problems, which has been historically used for applications in civil engineering [Santamarina, Fratta, 1998], the objective is to find the model of a system that its theoretical response best fits the observed data. The obtained best fit model is then generally chosen to represent the inverse problem solution. This approach provides a single model as the solution of the problem, meaning that no uncertainty in the observed data or in the theoretically calculated model predictions is considered. However, data and

modeling uncertainties are always present, and their effect on the obtained results should be evaluated. Additionally, there are many situations, where there is information about the expected results prior to the solution of the inverse problem. For example, this information can be in the form of the limits of expected values or general trend of the results. Such information is important and should be included in the solution of the inverse problem.

The probabilistic approach to the solution inverse problems, which is a new approach in civil engineering, provides the framework required for obtaining the solution of the inverse problem and offers mathematical techniques to include prior information about the solution and to evaluate uncertainty measures [Tarantola, 2005]. The introduction and application of the probabilistic approach to problems in civil engineering is the main focus of this research.

Objectives

The objectives of this research are:

- introduction of the probabilistic approach to the solution of inverse,
- presentation of the required mathematical background,
- development of computational tools required for the implementation of the approach, and
- illustration of its application and advantages for the solution of inverse problems in geotechnical and transportation engineering.

Three inverse problems in geotechnical and transportation engineering were selected as application examples. These problems are:

- Falling Weight Deflectometer (FWD) backcalculation,
- Model calibration based on geotechnical instrument measurements, and
- Seismic waveform inversion.

Organization

Following the introduction, the concept of uncertainty in the solution of inverse problems is formally introduced in chapter two, and its importance is highlighted.

In chapter three, the probabilistic solution of inverse problems is introduced as the main tool in evaluation of uncertainties in the solution of inverse problems. An overview of the major concepts used in probabilistic approach is then provided and the mathematical formulation for the probabilistic solution is presented in general terms using the introduced concepts.

Chapter four presents several techniques for numerical evaluation of the probabilistic solution. In this chapter, direct application of the developed formulation for simple problems is discussed. For complex problems that direct application of the developed formulation is not feasible, a numerical technique for the solution of the problem using Monte Carlo Markov Chains (MCMC) is introduced and explained. To further reduce computational time of obtaining a solution for complex problems, the introduced MCMC technique is integrated with the recently developed Neighborhood

Algorithm (NA) to obtain an approximation to the probabilistic solution. Details of integration of NA with MCMC are presented, discussed, and explained in this chapter.

Chapters five through seven provide the application examples. In chapter five, FWD backcalculation problem is considered. The probabilistic formulation of this problem is introduced and the results of probabilistic backcalculation of synthetic and experimental data are presented. Using the synthetic test data, different approaches to backcalculation, such as backcalculation using deflection bowl or time history records, are studied and compared. The results of these comparisons are also presented in this chapter.

In chapter six, a brownfield redevelopment project is used as an example to demonstrate how the probabilistic approach to the solution of inverse problems can be used to calibrate a predictive model and complement the application of the observational method in geotechnical engineering. In this chapter, an overview of the mentioned brownfield redevelopment project is provided and the results of the calibration of a settlement prediction model using the probabilistic approach are presented and discussed.

Chapter seven presents the probabilistic approach to inversion of the seismic waveforms for evaluation of soil and pavement layer moduli and thicknesses. The probabilistic formulation of this problem is introduced and the results of probabilistic backcalculation of synthetic and experimental data are presented.

Finally, chapter eight provides the summary of the research and offers recommendations for future research.

References

- Santamarina, J. C. and Fratta D. (1998), “Introduction to Discrete Signals and Inverse Problems in Civil Engineering”, ASCE Press, Reston, VA.
- Tarantola, A. (2005), “Inverse Problem Theory”, SIAM, Philadelphia, PA.

2 Uncertainties in Measurements

“To measure is to know.”

Lord Kelvin (1824-1907)

Introduction

In comparison to the traditional deterministic approach, the main advantage of the probabilistic approach to the solution of inverse problems is its ability to quantify the uncertainties of the obtained results. Evaluation of these uncertainties requires a probabilistic representation of uncertainties of the input parameters of an inverse problem. Therefore, to provide the required background, the concept of uncertainty is formally introduced in this chapter.

The concept of uncertainty, as it relates to direct physical measurements, is a very familiar and accepted concept in engineering. In simple terms, it is a representation of the likely values of the measurement results. The concept of uncertainty is sometimes confused with the concept of error. Error refers to the difference between the true value of the quantity subject to measurement, called *measurand*, and the measurement result. A measurement can unknowingly be very close to the unknown value of the measurand, thus having a negligible error; however, it may have a large uncertainty. Since the exact value of a measurand can never be evaluated, error is an abstract concept, which can

never be quantified. However, uncertainty is a measure that can be and should be quantified for every measurement.

The probabilistic presentation of uncertainties in direct measurements is formalized by International Organization for Standardization (ISO) and United States National Institute of Standards and Technology (NIST) [*ISO, 1993, Taylor and Kuyatt, 1994*]. According to the recommendations of ISO and NIST, measurement uncertainties should be expressed explicitly using probabilistic concepts. This presentation is the first step towards the implementation of the probabilistic approach to the solution of inverse problems, where the direct physical measurements are one of the inputs to the problem.

In this chapter, important ISO and NIST concepts and guidelines for presentation of uncertainties in direct measurements are reviewed. Following this review, the notion of measurement is generalized to include indirect measurement of physical quantities in inverse problems. It is shown that using this generalized notion, any inverse problem can be viewed as a measurement, which its uncertainties should be evaluated. Such evaluation can be accomplished using a probabilistic approach to the solution of inverse problems. Therefore, the probabilistic approach can be considered as an extension of NIST and ISO guidelines to include generalized measurements.

Measurement Specification

The first step in making a measurement is to specify the measurand. The specification of a measurand, which specifies how the measurement should be carried out, is directly related to the required accuracy of the measurement. For example, if the length of a bar is to be determined with micrometer accuracy, its specification should

include the temperature and pressure at which the measurement is supposed to be carried out. The uncertainty of the length measurement, if temperature and pressure are not specified, is so high that micrometer accuracy can not be achieved, even if the accuracy of the measurement instrument is adequate. Theoretically, it is possible to find the minimum level of uncertainty attainable for any given measurement specification. However, in most practical applications, the minimum level is not usually achieved. The measurement specification and the associated minimum level of uncertainty attainable should be always considered in interpretation of measurement results, even when no uncertainty measure is provided.

Evaluation and Expression of Uncertainties in Measurement

Once a measurement is carried out according to a given specification, the associated measurement uncertainties arising from different source of uncertainty should be evaluated, combined, and expressed with the measurement results. Sole presentation of the measurement value without any uncertainty measure does not provide the complete picture and might be misleading. ISO and NIST [ISO, 1993, Taylor and Kuyatt, 1994] provide general recommendation for expressing uncertainties in direct physical measurements. These recommendations form a basis for probabilistic expression of measurement uncertainties, which can be directly used in the probabilistic approach to the solution of inverse problems. This section presents the major concepts and recommendation of NIST, which for the most part are adopted from ISO.

Evaluation of Uncertainty

In the NIST approach, any source of uncertainty in the measurement is categorized in two classes based on the method used for its evaluation:

- *Type A Uncertainties*: Uncertainties that are evaluated by statistical methods
- *Type B Uncertainties*: Uncertainties that are evaluated by other means

Evaluation of “Type A” uncertainties is based on any valid statistical method, such as evaluation of the mean and standard deviation of a series of measurements or by performing analysis of variances (ANOVA). For example, uncertainties of measurement instruments provided by manufacturer’s specifications or calibration reports are generally evaluated as “Type A” uncertainties.

A “Type B” evaluation is based on non statistical evaluation, such as subjective evaluation based on scientific or engineering judgment, previous measurement data, experience with or general knowledge of the behavior of the instrument and measurand, and information published in reference books and handbooks.

Most sources of uncertainty can be evaluated either as a Type A or a Type B uncertainty. For example, the uncertainty in a measurement due to a change of the observers can be evaluated statistically with analysis of a series of observations from a group of independent observers, or it can be simply evaluated as a Type B using the previous experience and judgment for that type of measurement.

It should be mentioned that NIST’s classification of uncertainties is different than the traditional classification that divides uncertainties into “random” and “systematic”.

There is not always a simple one to one correspondence between these two classifications. Depending on how the measured quantity is used in mathematical equations, a random uncertainty arising from a random effect may become systematic and vice versa. For example, the uncertainty in a correction value applied to a measurement result to compensate for a systematic effect can produce a random or systematic uncertainty.

In routine engineering applications, direct statistical evaluation of the measurement uncertainties from all sources of uncertainty is not generally feasible and some of the measurement uncertainties should be evaluated as a Type B uncertainty. For example, in the measurement of settlement, in addition to uncertainty of measurement instrument, uncertainties in the measurement process due to other factors, such as uncertainty in positioning of instruments, or uncertainties due to change of the observer should also be evaluated and included in the uncertainty measure.

Standard Uncertainty

In NIST approach, the basic quantity representing uncertainty (Type A or B) from a single source is the standard uncertainty, denoted by symbol s , which is the standard deviation of the measurement when only one source of uncertainty is considered. In this representation, a Gaussian distribution for the source of uncertainty is implicitly considered and it is quantified by the value of the standard deviation.

Combined Standard Uncertainty

A measurement is usually subject to uncertainties from different sources. Ideally, the standard uncertainty should be evaluated for each source of uncertainty in the measurement as a Type A or a Type B uncertainty and then combined together to provide a single uncertainty measure. In other words, if all the uncertainties in the measurement process are characterized by standard uncertainties s_i , these individual uncertainties should be combined to represent *combined standard uncertainty*, s_c , of the measurement. Such combination can be obtained by calculating the square root of the sum of the squares of individual standard uncertainties s_i . This method, which is based on the probability theory, is sometimes referred to as *law of propagation of uncertainty*. The combined standard uncertainty is the quantity reported as the uncertainty in measurements.

Expanded Uncertainty

The combined standard uncertainty is the main quantity used in presentation of the measurement results. However, NIST also recognizes the presentation of uncertainty as *expanded uncertainty* in the form of $d_{obs} \pm S$, where d_{obs} is the measured value and S is half of the uncertainty interval. The relationship between expanded and standard uncertainty is presented by $S = ks_c$, where s_c is the combined standard uncertainty and k is called the *coverage factor*. Typically k is between 2 and 3. Assuming a Gaussian distribution, $k = 2$ defines an interval with a confidence level of 95 percent, whereas $k = 3$ defines an interval with a confidence level of 99 percent.

Uncertainty Interval

Uncertainties of measurements are also sometimes specified in the form of uncertainty interval, where for a given measurement, the upper and lower limits of the measurement value are identified. In such cases, given the upper and lower limits of the measurement result, denoted by d_{upper} and d_{lower} , the uncertainty can be calculated by assuming the best estimated value as $(d_{upper} + d_{lower})/2$ and calculating a corresponding combined standard uncertainty for the measurement, s_c . The combined standard uncertainty is then calculated such that there is a certain probability that the measurement result is between d_{upper} and d_{lower} . For example, for a 50 percent probability choose $s_c = (d_{upper} - d_{lower})/2$, for a 67 percent probability select $s_c = (d_{upper} - d_{lower})/2$, and for a 99 percent probability use $s_c = (d_{upper} - d_{lower})/\sqrt{3}$.

NIST also presents guidelines to convert uncertainties stated in other forms to combined standard uncertainty. A detailed account of these guidelines is provided in the cited references [Taylor and Kuyatt, 1994].

Generalized Measurement

In general, a measurement is considered to be a direct evaluation of a quantity subject to measurement. An inverse problem on the other hand is an indirect evaluation of the parameters of interest in the problem through measurement of another set of parameters and using the theoretical relationships between these two sets of parameters. Since the ultimate objective of an inverse problem is also measurement of the parameters

of interest in the problem, an inverse problem can also be considered a complex and indirect measurement using physical theories [Tarantola, 2005]. Such a measurement is referred to here as a *generalized measurement*. In principle, there is no difference between a direct measurement and a generalized measurement. In fact, the measurements that are considered direct measurements are simple forms of inverse problems. For example, measurement of the weight by a spring scale is a simple direct measurement, which can be considered a simple inverse problem. In this problem the parameter of interest is the weight of an object, which is evaluated indirectly by measurement of the deflection of a spring. In this example, the physical theory linking the observed parameter (deflection) to the parameter of interest (weight) is a very simple linear relationship. The solution of the problem is trivial, which is often solved using a calibrated gauge.

Similar to direct measurements, there are uncertainties associated with any generalized measurement. These uncertainties are basically due to uncertainties in physical measurements and uncertainties inherent in physical theories that are used in generalized measurements. These uncertainties should be evaluated and presented with the results of generalized measurements. However, evaluation of these uncertainties can not be performed using the NIST guidelines. Since the NIST approach deals with direct measurements only, there is a great emphasis on the use of Gaussian probabilities for expression of uncertainties. Although use of Gaussian probabilities is very appropriate for representing uncertainties in direct measurements, they can not in general represent uncertainties in generalized measurements, where the uncertainty may follow other distributions. The probabilistic approach to the solution of inverse problems provides the required tools to evaluate uncertainties in generalized measurements. In this sense, the

probabilistic approach to solution of inverse problems can be considered as an extension of NIST and ISO guidelines to include generalized measurements.

Summary

Basic and established guidelines in the presentation of uncertainties in direct measurements were introduced and reviewed in this chapter. These guidelines are the first step towards the probabilistic solution of the inverse problems, where the simple physical measurements are one of the inputs to the problem. The notion of inverse problem as a generalized measurement was also introduced in this chapter. It has been stated that using this generalized notion, any inverse problem can be viewed as a measurement, which its uncertainties should be evaluated and presented with the measurement result. In this sense, the probabilistic approach to solution of inverse problems can be considered as an extension of NIST and ISO guidelines to include generalized measurements.

References

- International Organization for Standardization (1993), “Guide to the Expression of Uncertainty in Measurement”, International Organization for Standardization, Geneva, Switzerland.
- Tarantola, A. (2005), “Inverse Problem Theory”, SIAM, Philadelphia, PA.
- Taylor B. N. and Kuyatt C. E. (1994), “Guidelines for Evaluation and Expressing Uncertainty of NIST Measurement Results”, Technical Note 1297, United States National Institute of Standards and Technology (NIST), United States Department of Commerce, Washington, DC.

3 Probabilistic Approach to Inverse Problems

“Far better an approximate answer to the right question, which is often vague, than the exact answer to the wrong question, which can always be made precise.”

John Tukey, Statistician (1915-2000)

Introduction

Inverse problem is a mathematical problem where the objective is to obtain information about a parameterized system (i.e. model) from observational data, theoretical relationships between system parameters and data, and any available a priori information. The most general form of the inverse problem theory is obtained using a probabilistic point of view, where the a priori information on the problem parameters and theoretical relationships is represented by probability distributions. In this approach, the solution of the inverse problem is itself a probability distribution representing the combined information about model parameters and theoretical relationships. The inverse problem solution with probabilistic approach in simple cases will reduce to the same solution obtained from the traditional deterministic approach. However, with this approach, more information about the solution is obtained and more complex inverse problems can be solved.

This chapter provides an introduction to the mathematical theory of inverse problems from a probabilistic point of view. This introduction is mainly based on the formulation of the theory presented by Tarantola [Tarantola 2005, Mosegaard and Tarantola 2002, Tarantola 2004, Tarantola and Valette 1982]. Following this

introduction, elements of probability theory required in formulating the probabilistic solution are initially introduced. General probabilistic approach to inverse problems is then formulated, solution of the problem is defined, and common techniques for appraisal of the solution are introduced. Due to introductory nature of the chapter, there has been a conscious effort to present the main ideas and important results with less emphasis on mathematical derivations and proofs. Interested readers can find a detailed mathematical treatment of the subject in the cited references.

Elements of Probability Theory

Probability theory is essential to the probabilistic formulation of inverse problems presented here. Therefore, this section contains a review of the elements of probability theory which are important for the analysis of inverse problems.

Kolmogorov's Concept of Probability

The Kolmogorov's [1933] definition of probability, clarifies the underlying mathematical structure of probability and allows a formal presentation of the concepts based on which the probabilistic solution of inverse problems are based.

Consider a point x that can be materialized anywhere inside a space of points denoted as χ . The point x may for example be realized in the domain A of χ ($A \subset \chi$). The probability of realization of a point can be completely described, if to every domain A of χ a positive number $P(A)$ can be assigned having three properties:

- For any domain A of χ , $P(A) > 0$.

- If A_i and A_j are two disjoint domains of χ , then

$$P(A_i \cup A_j) = P(A_i) + P(A_j).$$

- If $A \rightarrow \text{Empty domain}$, then $P(A) > 0$.

The $P(A)$, which satisfies the above criteria, is called the *probability* of A and defines a probability distribution over χ . It should be mentioned that in this definition, it is not assumed that the probability is necessarily normalized to unity (i.e. $P(\chi) = 1$). If the probability is not normalized, it is sometimes referred to as a *measure*. Some probabilities are not normalizable (i.e. $P(\chi) = \infty$). In such cases, only *relative probabilities* can be computed.

Generally, any type of coordinate system can be selected to represent points in space χ ; however, for most applications, including for the applications considered in this work, the Cartesian coordinate system is the most convenient system. The formulation of probabilistic approach presented here assumes that the Cartesian coordinates are the coordinates used to define the problem. In special cases where the coordinates are not Cartesian, the presented formulation should be slightly modified [Tarantola 2005].

Probability Density

A probability distribution, $P(A)$, can also be represented by its *probability density function*, $p(x)$, which is defined as:

$$P(A) = \int_A p(x) \delta x \quad (3-1)$$

where $\delta x = \delta x_1 \delta x_2 \dots, \delta x_n$ is a volume element.

Homogeneous Probability Density

The *homogeneous probability distribution* is a probability distribution that assigns to each domain of the space a probability proportional to its volume or:

$$M(A) = kV(A) \quad (3-2)$$

where $M(A)$ represents the homogenous probability distribution, k is a proportionality constant, and $V(A)$ is the volume of A of χ , which is defined as:

$$V(A) = \int_A \delta x \quad (3-3)$$

Combining equations (3-1), (3-2) and (3-3), it is easy to show that density function of homogenous probability density denoted by $\mu(x)$ is:

$$\mu(x) = k \quad (3-4)$$

where k is a constant. It should be remembered that in coordinate systems other than Cartesian coordinate system, the homogeneous probability density may not be constant.

Conjunction of Probabilities

Consider two probability distributions P and Q . The conjunction of these probabilities is a probability distribution denoted by $P \wedge Q$ which has the following properties:

- $P \wedge Q = Q \wedge P$;
- For any subset A , $(P \wedge Q)(A) = 0$; if and only if $P(A) = 0$ and $Q(A) = 0$;

- If M denotes the homogenous probability distribution $P \wedge M = P$

It is easy to show that if P and Q are represented by density functions $p(x)$ and $q(x)$, the simplest way to define $(p \wedge q)(x)$, the probability density of $P \wedge Q$, is given by:

$$(p \wedge q)(x) = kp(x)q(x) \quad (3-5)$$

where k is a constant. A graphical representation of conjunction of probabilities is depicted in Figure 3-1.

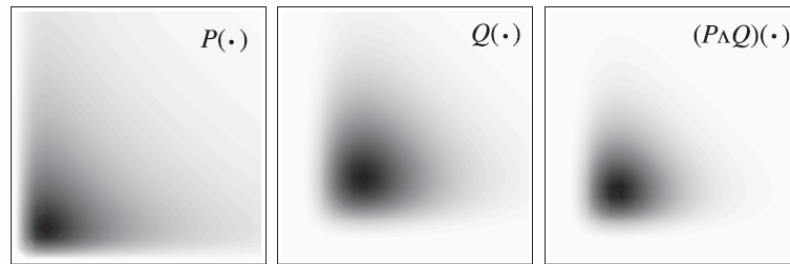


Figure 3-1 - Illustration of the concept of conjunction of probabilities P and Q , $P \wedge Q$ [Tarantola 2005].

The concept of conjunction of probabilities is somewhat analogous to the concept of intersection in set theory. The intersection of two sets is a set which its members are shared by both sets. Similarly, conjunction of two probability distributions is a probability distribution which assigns probabilities to every domain equivalent to multiplication of the probabilities assigned to that domain by individual probabilities. In other words, the domains with high probability will also have high probability under conjunction of probabilities. However, the domains that have low probabilities under either of distributions will have low probability under the conjunction of probabilities as well.

Marginal Probability

If the space is divided into two subspaces according to $\chi = U \times V$, given the joint probability density $p(u, v)$, it is possible to derive marginal probability densities as:

$$p_u(u) = \int_V p(u, v) \delta v \quad \text{and} \quad p_v(v) = \int_U p(u, v) \delta u \quad (3-6)$$

where u and v are points in subspace U and V respectively.

Independent Probabilities

If the u and v are independent parameters, their joint probability can be expressed as:

$$p(u, v) = p_u(u) p_v(v) \quad (3-7)$$

Probabilistic Formulation of Inverse Problems

Inverse problem is a mathematical problem where the objective is to obtain information about a parameterized system (i.e. model) from observational data, theoretical relationship between system parameters and data, and any available a priori information. [Tarantola 2005, Parker, 1994, Menke 1984]. There are three major components to any inverse problem:

- Parameterization of the physical system in terms of a set of model parameters that from a given point of view completely describes the system.
- A set of physical laws called forward model that for a given set of model parameters, makes prediction about the results of measurements.
- Use of the measurements of observable parameters to infer or invert the actual values of the model parameters.

To be able to mathematically formulate the probabilistic solution of an inverse problem, there are a few concepts that should be introduced.

Model Space and Data Space

For any given inverse problem, it is possible to select a set of model parameters that will adequately describe the model (i.e. parameterization). The choice of these parameters is not unique. However, once a particular parameterization of the system is chosen, it is possible to introduce a space of values that describe possible values of model parameters. This abstract space is termed the *model space*, and is denoted by M , which represents all the conceivable models. Individual models, $m = \{m_1, m_2, \dots\}$ are basically points in the model space.

In an inverse problem, the values of parameters m are the main interest; however, they are not directly measurable. The goal of inverse problem is to obtain information on the values of m by making direct observation on another set of parameters denoted as d_{obs} . Similar to the concept of model space, it is possible to introduce an abstract idea of *data space* D , which is the space of all conceivable observed responses. The actual observed response is in fact a point in this space represented by $d_{obs} = \{d_{obs1}, d_{obs2}, \dots\}$.

State of Information

In the probabilistic approach, any information about the problem, including the solution of the problem, is expressed by probability distributions that are interpreted

using the concept of the state of information. The state of information is an intuitive concept associated with the concept of probability. In addition to the statistical interpretation of probability, a probability distribution can be also interpreted as a subjective degree of knowledge of the true value of a given parameter. The subjective interpretation of the probability theory is usually named Bayesian, in honor of British mathematician Thomas Bayes (1763). The Bayesian interpretation of probability is a very common concept in everyday life, which is used in many situations, such as in weather forecast reports. For example, the forecast predicting a certain probability for having precipitation presents the subjective knowledge of the meteorologist based on all the available information. In civil engineering problems, the subjective knowledge about any parameter prior to any measurement may also be represented by a probability distribution. If there is no a priori information on the value of the parameter, this lack of information can also be represented by a homogeneous probability distribution, where all the possible models have the same probability. The other extreme situation is that when the exact value of the parameter is known from a direct measurement. This precise information can be also represented by a Dirac delta probability distribution. In general, the spread of the probability distribution is an indication of how precise the knowledge about the underlying parameter is; the narrower the spread of the distribution, the more precise the prior information.

A Priori Information

In the probabilistic approach presented, the probability distribution representing the state of information on the model parameters prior to the solution is denoted by

$\rho_M(m)$, and is termed the *model a priori probability* density function. Similarly, the a priori information on the observed data prior to the solution can be expressed as *data a priori probability* density function, which is denoted by $\rho_D(d)$. The a priori information on model parameters (represented by $\rho_M(m)$) is independent of a priori information on the data (represented by $\rho_D(d)$). This notion of independence can be used to define a joint probability over the joint model and data space, $\chi = (M, D)$, as a product of the two marginal probability densities. This probability is denoted by:

$$\rho(m, d) = \rho_M(m) \rho_D(d) \quad (3-8)$$

where $\rho(m, d)$ is referred to as *joint a priori probability* density function and k is a normalization constant. This probability can be graphically depicted as a “cloud of probability” centered on the observed data and a priori model, as shown in Figure 3-2.

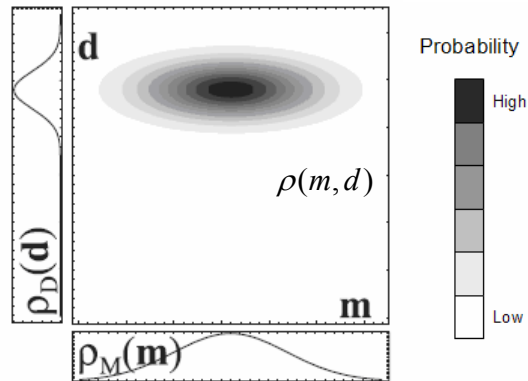


Figure 3-2 - Illustration of the probability densities $\rho_M(m)$, $\rho_D(d)$, and $\rho(m, d)$ representing a priori information on model, data, and joint model and data spaces respectively [Tarantola 2005].

Forward Model

The forward model is a set of physical laws that for a given set of model parameters, $m \in M$, predicts the value of observable parameters, $d \in D$. The forward model can be expressed as:

$$d = g(m) \quad (3-9)$$

where $g(m)$ is the forward model operator. If the model predictions are exact and without any uncertainty, a single response is predicted for a given model. However, the forward model predictions are rarely exact and there are modeling approximations involved. In the probabilistic approach, the effect of this approximation can be represented by a probability density function, $\theta(m, d)$. In this representation, for a given model parameter, instead of a single value of d , a probability in the data space is predicted representing the modeling uncertainties. This concept, as well as the probability $\theta(m, d)$, referred to as *forward model probability density function*, is conceptually depicted in Figure 2-3. It should be pointed out that evaluation of modeling uncertainties is a complex task, and in many cases, there is only limited published research available. For the applications presented in the chapters that follow, modeling uncertainties have been assigned based on experience or limited analysis. Further research is required to evaluate the modeling uncertainties for each application.

It is worthy to mention that for the formulation presented here, the forward model is considered to be a general model and no simplifying assumptions, such as the linearity assumption, are made. For example, if the forward model operator, $g(\cdot)$, is a linear operator (i.e. $d = Gm$, where G is a matrix), significant simplification of the inverse problem theory can be obtained [Menke 1984]. However, to present a uniform approach

to both linear and non-linear inverse problems, for the treatment presented here a general nonlinear operator is considered.

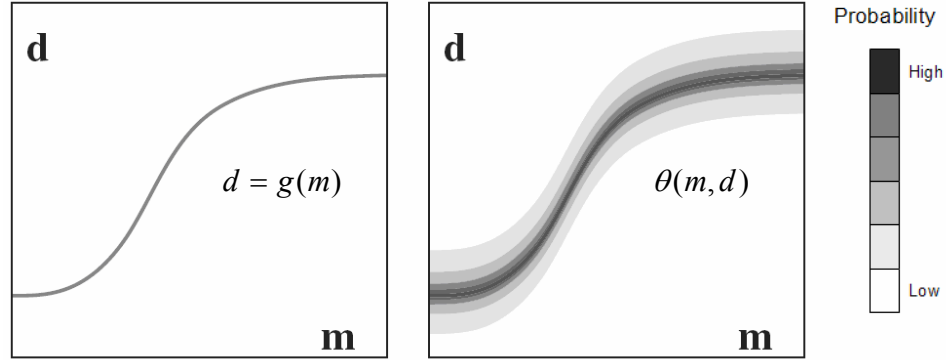


Figure 3-3 - (left) Forward model with negligible modelization uncertainties (right) and forward model with modeling uncertainties [Tarantola 2005].

General Probabilistic Solution of the Inverse Problem

In the probabilistic framework, the solution of an inverse problem is a probability distribution combining the a priori information, $\rho(m, d)$ (i.e. *experimental information*), with information obtained from the forward model, $\theta(m, d)$ (i.e. *theoretical information*). Since the predictions of the forward model are assumed to be independent of a priori information, the combination can be accomplished by conjunction operation [Tarantola, 2005], which can be visualized as the multiplication of two probabilities. The resulting probability, denoted by $\sigma(m, d)$, is basically the solution of the problem, and it is termed a posteriori probability, where its density function is represented by [Tarantola, 2005]:

$$\sigma(m, d) = k\theta(m, d)\rho(m, d) \quad (3-10)$$

where k is a normalization constant. The conjunction operation and the obtained probability are depicted in Figure 3-4.

Having defined the a posteriori probability, marginal probability densities on model and data spaces are defined respectively as:

$$\sigma_M(m) = \int_D \sigma(m, d) \delta d \quad \text{and} \quad \sigma_D(d) = \int_M \sigma(m, d) \delta m \quad (3-11)$$

where $\sigma_M(m)$ is model a posteriori probability density function, and $\sigma_D(d)$ is the data a posteriori probability density function. The model a posteriori probability, as defined above, is often the prime quantity of interest in the solution of an inverse problem.

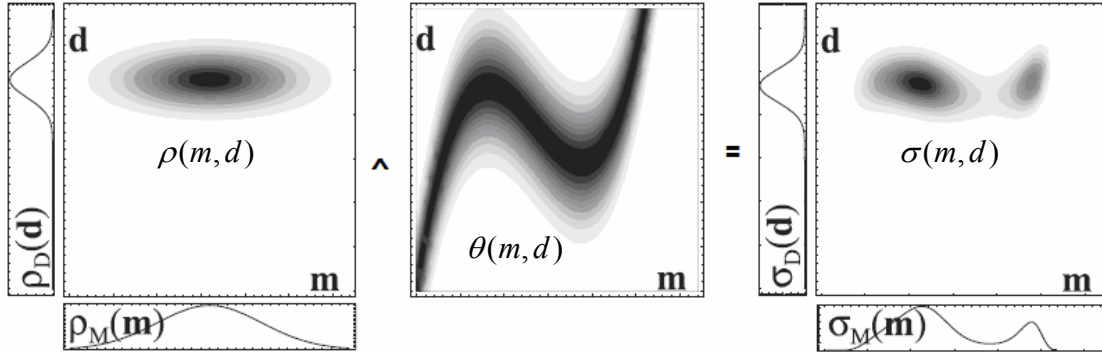


Figure 3-4 - Representation of the general probabilistic solution of inverse problem as the conjunction of the a priori information, $\rho(m, d)$ and information obtained from forward model $\theta(m, d)$. [Tarantola 2005].

Probabilistic Solution in the Case of Data and Forward Model with Gaussian Uncertainties

Substituting Equation (3-10) into Equation (3-11), and using Equation (3-8), the model a posteriori probability distribution (i.e. the problem solution in the model space) can be evaluated as:

$$\sigma_M(m) = k \rho_M(m) \int_D \rho_D(d) \theta(m, d) \delta d \quad (3-12)$$

or

$$\sigma_M(m) = k\rho_M(m)\lambda(m) \quad (3-13)$$

where $\lambda(m)$ is the likelihood function:

$$\lambda(m) = \int_D \rho_D(d)\theta(m,d)\delta d \quad (3-14)$$

If it is assumed that the data uncertainties are represented by a Gaussian probability, such as:

$$\rho_D(d) = k \exp\left(-\frac{1}{2}(d - d_{obs})^T C_d^{-1}(d - d_{obs})\right) \quad (3-15)$$

where C_d is the covariance matrix representing observational uncertainties, and that the forward model uncertainties can be presented by:

$$\theta(m,d) = k \exp\left(-\frac{1}{2}(d - g(m))^T C_T^{-1}(d - (g(m)))\right) \quad (3-16)$$

where C_T is the covariance matrix representing forward model uncertainties. It can be shown that the likelihood function can be represented by [Tarantola 2005]:

$$\lambda(m) = k \exp\left(-\frac{1}{2}(d_{obs} - g(m))^T (C_T^{-1} + C_d^{-1})(d_{obs} - (g(m)))\right) \quad (3-17)$$

This result is important because it shows that, by the Gaussian assumption, observational and modeling uncertainties simply combine by addition of their respective covariances. It is worthy to mention that, by inspection of Equations (3-13) and (3-17), it can be observed that, if there is no a priori information (i.e. $\rho_M(m) = \mu(m)$), the maximum of the a posteriori probability occurs at the maximum of the likelihood function. Additionally, the maximum of the likelihood function occurs when the observed data fits best the model predictions in a weighted least square sense. If the covariance matrices are multiplications of the identity matrix, it can also be shown that the maximum of the likelihood function is the L_2 norm best fit model to the observed data. This is the

same solution obtained in the deterministic approach. Therefore, it can be concluded that the deterministic solution is a very special case of the probabilistic solution.

Appraisal of the Probabilistic Solution

It has been stated and illustrated that the solution of the inverse problem, the a posteriori probability distribution, is the conjunction of two probability distributions representing experimental and theoretical information about the problem. Although the a posteriori probability distribution contains all the information regarding the problem solution, it is generally desirable to quantify this information. In other words, it is desirable to appraise the obtained solution. Two important classes of quantities are generally presented as quantifying measures of the a posteriori probability distribution: (1) central estimators and estimators of dispersion, and (2) one and two dimensional marginal probability densities.

Central Estimators and Estimators of Dispersion

The a posteriori mean model (or the expected value) is a central estimator, which represents the most probable solution. It is calculated using following integral:

$$\langle m \rangle = \int_M m \sigma_M(m) \delta m \quad (3-18)$$

where $\langle . \rangle$ indicates the mean or expected value. It should be mentioned that depending on the shape of probability distribution, the mean value may or may not coincide with the maximum of probability density. The dispersion estimator associated with the mean is the covariance matrix and is given by:

$$C_M = \int_M (m - \langle m \rangle)(m - \langle m \rangle)^T \sigma_M(m) \delta m \quad (3-19)$$

Since the concept of mean and covariance is derived for unimodal probability densities, for complex problems, where the posteriori probability density is complex and may have several modes, one should be careful in interpretation of the mean and covariance.

One and Two Dimensional Marginal Probability Densities

Another quantity of interest in presentation of probabilistic solution is the one dimensional marginal probability density of variable m_i :

$$\Gamma(m_i) = \int \dots \int \sigma_M(m) \prod_{\substack{k=1 \\ k \neq i}} \delta m_k \quad (3-20)$$

where Γ indicates the marginal probability density. Joint marginal probability density of two parameters can be defined in a similar manner:

$$\Gamma(m_i, m_j) = \int \dots \int \sigma_M(m) \prod_{\substack{k=1 \\ k \neq i \\ k \neq j}} \delta m_k \quad (3-21)$$

Evaluation of the integrals presented in equations (3-18) thru (3-21) generally has to be performed numerically. However, when the a priori and forward model probability distributions are simple, it is possible to obtain closed form formulas that can be directly used in evolution of estimator quantities and marginal probabilities [Menke 1984].

Summary

The mathematical theory of inverse problems from a probabilistic view was introduced in this chapter. The basic concepts and elements of the theory were presented and the general solution of the inverse problem was defined as the a posteriori

probability, which combines the a priori information about the problem with the information obtained by measuring some observable parameters (data) and theoretical information gained from a forward model. The obtained general solution was then formulated for the case where the data a priori and forward model probabilities are Gaussian. Two important classes of quantities that are used for appraisal of the results, namely, (1) central estimators and estimators of dispersion, and (2) one and two dimensional marginal probability densities, were also introduced and defined.

References

- Kokmogorov, A.N., (1933), “Grundbegriffe der Wahrscheinlichkeitsrechnung “, Springer, Berlin, Germany
- Menke, W. (1984), “Geophysical Data Analysis: Discrete Inverse Theory”, Academic Press Inc. Orlando, FL.
- Mosegaard K. and Tarantola, A. (2002), “International Handbook of Earthquake and Engineering Seismology – Chapter 16: Probabilistic Approach to Inverse Problems”, Academic Press, San Diego, CA.
- Parker, R. L., (1994), “Geophysical Inverse Theory”, Princeton University Press, Princeton, NJ.
- Tarantola, A. (2005), “Inverse Problem Theory”, SIAM, Philadelphia, PA.
- Tarantola , A, (2004), “Probability and Measurements”, Submitted to Cambridge University Press for publication.
- Tarantola, A. and Valette, B. (1982), “Inverse Problem=Quest for Information”, Journal of Geophysics, 50, p. 159-170.

4 Monte Carlo Evaluation of the Probabilistic Solution

Chance, too, which seems to rush along with slack reins, is bridled and governed by law.”

Boethius, Roman Philosopher, c.a. 480-525

Introduction

Probabilistic formulation of inverse problems leads to the definition of the solution as a probability distribution in the model space [Tarantola 2005]. This probability distribution combines a priori information on the model parameters with new information obtained by measuring some observable parameters (data) and theoretical information gained from a forward model. For simple problems, it is possible to use the derived mathematical equations directly and obtain an analytical solution of the inverse problem. However, in general, due to the large number of the model parameters or the complexity of the theory linking the data and the model parameters, it may not be possible to describe the solution analytically. In such cases, one technique to evaluate the solution is to randomly generate a large collection of models according to the a posteriori probability distribution and analyze and display the models in such a way that information about the underlying probability is conveyed. This approach can be accomplished using a class of computational techniques referred to as Monte Carlo methods.

This chapter introduces Monte Carlo techniques for evaluation of the probabilistic inverse problem solution. To provide a context for practical applications and illustrate the presented concepts and techniques, a simple inverse problem example, along with its deterministic solution and analytical probabilistic solution, is initially introduced and is used throughout the chapter. For complex problems where obtaining an analytical solution is not feasible, a numerical technique using Monte Carlo Markov Chains (MCMC) is introduced and its application is illustrated. To further reduce the computational time in the solution of the complex problems, the MCMC technique is integrated with the recently developed Neighborhood Algorithm (NA). NA and its integration with MCMC are described, and its application is illustrated using the previously introduced example. It should be mentioned that there are other techniques available for the evaluation of the probabilistic solution of inverse problems; however, a thorough discussion of these techniques are beyond the scope of this research.

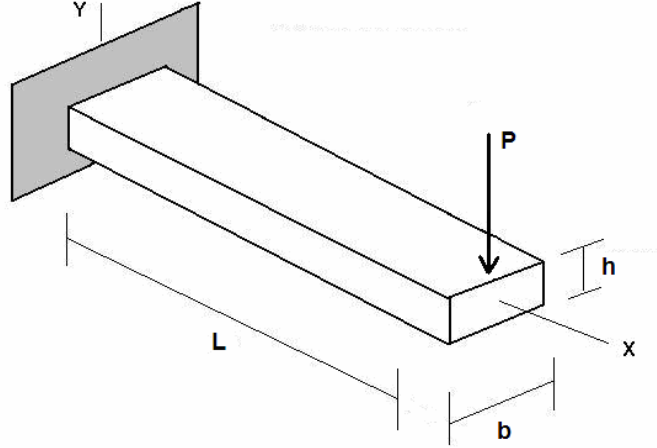
Illustrative Example

A simple deflection based modulus determination experiment is presented below, and it is used as the illustrative example throughout this chapter.

Deflection Based Modulus Determination Experiment: *The objective of the experiment is to determine the elastic modulus of a cantilever beam from the measurement of the deflection of the beam. As depicted in Figure 4-1, the experiment is conducted by placing a known load P at a measured length L from the fixed end of the beam and measuring the deflection Δ . In this inverse problem, modulus is the model parameter of interest and deflection is the observed data. The forward model predicting the deflection for any given modulus is simply obtained using mechanics of materials principles as:*

$$\Delta = \frac{PL^3}{EI} \quad (4-1)$$

where E is the modulus and I is the moment of inertia of the beam.



$$L = 0.5 \text{ m}, b = 0.05 \text{ m}, h = 0.01 \text{ m}, P = 100 \text{ N}, \Delta_{obs} = 0.043 \text{ m}$$

Figure 4-1 - Deflection based modulus determination experiment.

Deterministic Solution

In the deterministic approach, the objective is to find a set of model parameters which minimizes the difference between the model prediction and the observed data (i.e.

$$|g(m) - d_{obs}|).$$

Deterministic Solution of the Modulus Determination Experiment: Based on the traditional deterministic solution, the modulus of the beam can be evaluated by:

$$\min \left| \frac{PL^3}{EI} - \Delta_{obs} \right| \rightarrow E = \frac{PL^3}{I\Delta_{obs}} \quad (4-2)$$

Using the numerical values provided in Figure 4-1, $E = 69.8 \text{ GPa}$, which suggests that the material is probably an aluminum alloy. It should be mentioned that in the deterministic approach, no estimate of uncertainty is obtained.

Analytical Evaluation of the Probabilistic Solution

If the a priori and forward model probability distributions are simple, it might be possible to obtain a closed form analytical solution of the problem by direct application of the presented relationships. This technique is illustrated below; however, in practice, analytical solution can rarely be obtained, and only a numerical estimate of the solution can be calculated.

Analytical Evaluation of the Probabilistic Solution of the Modulus Determination Experiment: To obtain a probabilistic solution, the a priori and forward model probability densities should be defined. Let's assume a Gaussian a priori probability for observed data with the standard deviation Σ_{Δ} ,

$$\rho_{\Delta}(\Delta) = \frac{1}{\sqrt{2\pi}} \cdot \frac{1}{\Sigma_{\Delta}} \exp\left(-\frac{1}{2} \frac{(\Delta - \Delta_{obs})^2}{\Sigma_{\Delta}^2}\right), \text{ and an independent homogeneous a priori}$$

probability density for modulus, E (representing no specific a priori information on the model parameter), $\rho_E(E) = k$, where k is a constant.

As presented, in probabilistic approach, the uncertainties in forward model can also be incorporated in the solution. For many reasons, such as inherent simplifying assumptions in the derivation of the equation, uncertainties in evaluation of the model coefficients, etc, the given forward model, $\Delta = PL^3 / IE$, can never be exact. Let's assume that the leading cause of uncertainty in the forward model in this experiment is the uncertainty in the magnitude of the applied load. The forward model probability density can then be represented by the following probability density function:

$$\theta(E, \Delta) = \frac{1}{\sqrt{2\pi}} \cdot \frac{1}{\Sigma_p L^3 / IE} \exp\left(-\frac{1}{2} \frac{(\Delta - PL^3 / IE)^2}{(\Sigma_p L^3 / IE)^2}\right) \quad (4-3)$$

where Σ_p is the standard deviation representing uncertainty in load P . This equation simply means that for a given modulus, E , rather than predicting a single deflection value, a Gaussian probability in the data space is predicted by the forward model, which incorporates the modeling uncertainties.

The solution of the inverse problem, the conjunction of probability densities, is then given by:

$$\sigma(E, \Delta) = \rho(E, \Delta)\theta(E, \Delta) = \rho_E(E)\rho_{\Delta}(\Delta)\theta(E, \Delta) \quad (4-4)$$

or

$$\sigma(E, \Delta) = k \exp \left(-\frac{1}{2} \frac{(E - PL^3 / I\Delta)^2}{(\Sigma_p L^3 / I\Delta)^2} - \frac{1}{2} \frac{(\Delta - \Delta_{obs})^2}{\Sigma_\Delta^2} \right) \quad (4-5)$$

where k is a constant. Probabilities $\rho(E, \Delta) = \rho_E(E)\rho_\Delta(\Delta)$, $\theta(E, \Delta)$, and $\sigma(E, \Delta)$ are depicted in Figure 2-7.

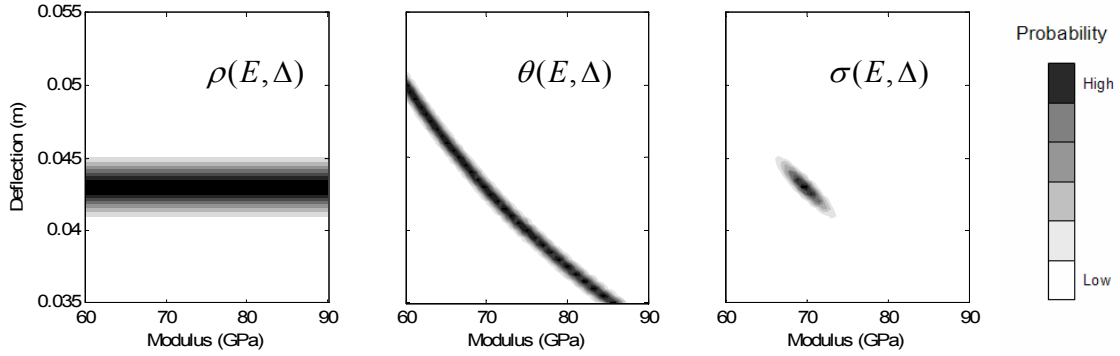


Figure 4-2 - Graphical representation of the probability densities $\rho(E, \Delta)$, $\theta(E, \Delta)$, and $\sigma(E, \Delta)$ for the modulus determination experiment. It is assumed that $\Sigma_p = 1 \text{ Pa}$ and $\Sigma_\Delta = 0.001 \text{ m}$.

The maximum of the probability density $\sigma(E, \Delta)$, is located at $E = 69.8 \text{ GPa}$, which is the solution identified in deterministic approach. However, it can be observed that in addition to the reported value of the modulus, the solution depicted in Figure 4-2 conveys information about the uncertainties of the obtained results.

Appraisal of the Probabilistic Solution of the Modulus Evaluation Experiment:

The information contained in the solution probability density function can be quantified in terms of central and dispersion estimators, such as mean and variance. Often times, for complex problems, these quantities are the only results that are reported.

For this example, the a posteriori probability density on model space is simply:

$$\sigma_E(E) = \int_{\Delta} k \exp \left(-\frac{1}{2} \frac{(E - PL^3 / I\Delta)^2}{(\Sigma_p L^3 / I\Delta)^2} - \frac{1}{2} \frac{(\Delta - \Delta_{obs})^2}{\Sigma_\Delta^2} \right) \delta\Delta \quad (4-6)$$

This integral is numerically evaluated and the results are depicted in Figure 4-3.

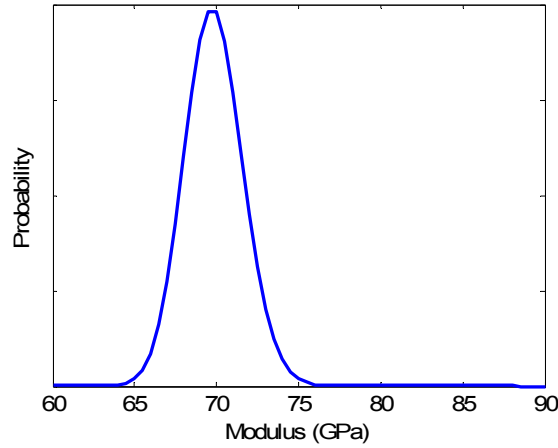


Figure 4-3 - Graphical representation of the probability density $\sigma_E(E)$ for the modulus determination experiment. It is assumed that $\Sigma_p = 1 \text{ Pa}$ and $\Sigma_\Delta = 0.001 \text{ m}$.

Using the numerically evaluated probability density, $\sigma_E(E)$, mean and variance quantities can be evaluated as: $\langle \sigma_E(E) \rangle = 69.8 \text{ GPa}$ and $\sqrt{C_E} = 1.8 \text{ GPa}$, where $\sqrt{C_E}$ is the variance of $\sigma_E(E)$.

Direct Sampling Evaluation of the Probabilistic Solution

The ultimate objective of the direct sampling solution technique presented here is to randomly generate a large representative collection of models according to the model a posteriori probability distribution, $\sigma_M(m)$, and analyze and display the sampled models to derive information about the underlying a posteriori probability distribution. In addition to the basic question of how to generate such samples, there are several other issues, such as stability, convergence, and error estimates of the direct sampling approach that need to be discussed and addressed. These issues are discussed and addressed in this section.

Monte Carlo Sampling of Probability Distributions

It is only when the problem is very simple; the analytical techniques can be used to characterize the solution. For more complex problems, one needs to perform an extensive numerical exploration of the model space and characterize the probabilities for each point in the model space. Except for the problems with a very small number of dimensions, this exploration cannot be systematic. In such cases, well-designed random (or pseudorandom) explorations can be used to solve the problem. These random methods are generally referred to as Monte Carlo methods.

The term “Monte Carlo”, as it refers to computation calculations, was apparently first used by the Enrico Fermi, Stanislaw Marcin Ulam, and John von Neumann as a code name at Los Alamos laboratories for stochastic simulations in development of the atomic bomb. The name Monte Carlo, an illusion to the famous casino in Monaco, refers to the fact that these techniques use the law of random numbers in a similar way that is used in casinos. Today, the Monte Carlo methods refer to any simulation that involves the use of random numbers. Despite the wide spread use of these methods and numerous descriptions of them in articles and books, it is not possible to find a complete and comprehensive definition of Monte Carlo Methods. This is in part due to intuitive nature of these techniques, which are used in a wide range of areas including physics, biology, chemistry, and financial markets. In general, Monte Carlo methods provide approximate solutions to a variety of mathematical problems by performing statistical random sampling experiments. The methods apply to problems with no probabilistic nature as well as to those with inherent probabilistic structure. While most applications of Monte Carlo methods are performed on computers today, there are many applications using

coin-flipping, card-drawing, or needle-tossing experiments. However, advent of the computers and their ever increasing computational capabilities, made it possible to successfully apply Monte Carlo methods to more complex problems, including complex inverse problems. A good review of historical development of Monte Carlo methods in the context of inverse problems is given by Sambridge and Mosegaard [2002].

The fundamental idea behind Monte Carlo methods is that inference regarding the characteristic of the parameters of interest can be gained by repeatedly drawing random samples from the population of interest and observing the behavior of the parameters over the samples. Such an approach is graphically illustrated in Figure 4-4 for a two dimensional probability distribution.

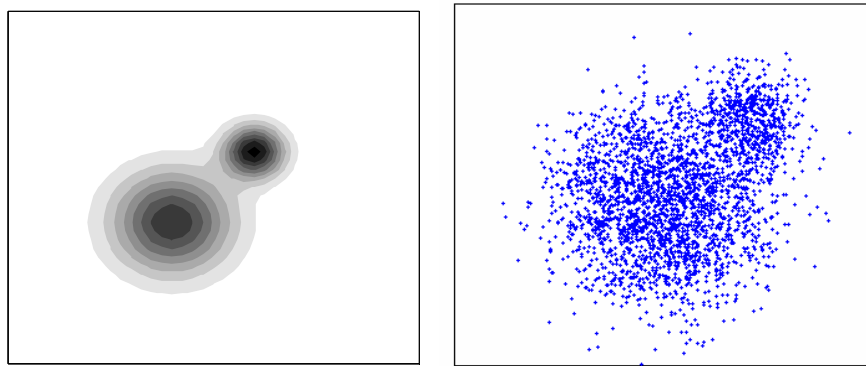


Figure 4-4 - The collection randomly generated samples (right) of a probability distribution (left) allow inference of characteristics of underlying probability distribution [Tarantola 2005].

The fundamental question here is that given a probability distribution, defined analytically or numerically, how random samples according to a desired probability distribution can be generated? Markov chains provide the mathematical tools required for generation of such samples.

Markov Chains

A *Markov chain*, named after the Russian mathematician Andrey Markov (1856-1922), is a sequence of random numbers such that the next value or *state* of the sequence depends only on the previous stage [Bhat and Miller, 2002]. This dependency is mathematically described by *transition kernel*, $\psi(x_{n+1}|x_n)$, which is the probability distribution representing conditional probability of transition to x_{n+1} from x_n . Thus a sequence of random numbers x_1, x_2, \dots, x_n can be generated such that next state x_{n+1} is distributed according to the transition kernel $\psi(x_{n+1}|x_n)$. A realization of the sequence is called a Markov chain. It is assumed here that transitional kernel does not change as the sequence progresses, making the chain *homogenous in time*. It can be shown that given certain conditions [Tierney, 1994] the chain will forget its starting state and the distribution of the random numbers will converge to a *stationary or target distribution*, denoted as Ψ . In other words, as the sequence grows larger, the sample points x_n will become dependent samples of stationary distribution Ψ . The central question here is that given $\Psi(x)$ as the desired stationary probability, how $\psi(x)$ should be constructed so that Markov chain converges to $\Psi(x)$. Metropolis sampler [Metropolis et al 1953] is one technique for generating desired Markov chains with a given target distribution.

Metropolis Sampler

Metropolis sampler [Metropolis et al 1953] is a special case of Metropolis-Hasting sampler [Hasting 1970]. The sampler is a set of rules that generates a Markov chain with a given desired target probability, $\Psi(x)$. To define the rules, consider a Markov chain with a given state x_n . To move to the next state, the Metropolis sampler obtains a random *candidate state*, y (generated randomly most often from a uniform distribution). If the value of $\Psi(y) > \Psi(x_n)$ the candidate point is accepted and $x_{n+1} = y$. If $\Psi(y) < \Psi(x_n)$, the candidate point is only accepted with a probability of $\Psi(y)/\Psi(x_n)$. Otherwise, the candidate point is rejected and $x_{n+1} = x_n$. It can be shown that the Markov chain generated in this manner will converge to $\Psi(x)$. The Metropolis sampler can be represented by the following generalized algorithm:

- Initialize the chain to x_1
- At n th state, randomly generate a candidate point y (usually derived from a uniform distribution).
- If $\Psi(y) > \Psi(x_n)$ accept the candidate and set $x_{n+1} = y$;
- if $\Psi(y) < \Psi(x_n)$ decide randomly to accept the transition with a probability of $\Psi(y)/\Psi(x_n)$, if the candidate is accepted set $x_{n+1} = y$; otherwise set $x_{n+1} = x_n$
- Set $n = n + 1$ and repeat steps 2 through 5

The above rules are also referred to as the *Metropolis acceptances rule*.

Cascade Metropolis Sampler

The Markov chain in metropolis sampler only applies the Metropolis acceptance rule once with $\Psi(x)$ target probability. Assume that the sampler is modified such that the acceptance rule is applied in cascade each time with different target probabilities, $\Psi(x), \Psi'(x), \Psi''(x), \dots \Psi^n(x)$. It can be shown that the stationary probability of the chain is simply obtained as multiplication of probabilities or $\Psi(x) \times \Psi'(x) \times \Psi''(x) \times \dots \times \Psi^n(x)$.

The cascade application of Metropolis acceptance rule at each state x_n can be implemented by application of the following set of rules to generate the next state of the chain:

- At n th state, randomly generate a candidate point y (usually derived from a uniform distribution)
- If $\Psi(y) > \Psi(x_n)$ then go to next step; if $\Psi(y) < \Psi(x_n)$ decide randomly to go to next step with a probability of $\Psi(y)/\Psi(x_n)$; If move to next step is rejected then set $x_{n+1} = x_n$, $n = n + 1$ and go to step 1.
- If $\Psi'(y) > \Psi'(x_n)$ then go to next step; if $\Psi'(y) < \Psi'(x_n)$ decide randomly to go to next step with a probability of $\Psi'(y)/\Psi'(x_n)$; If move to next step is rejected then set $x_{n+1} = x_n$, $n = n + 1$ and go to step 1.
-
-

-
- If $\Psi^n(y) > \Psi^n(x_n)$ then accept the candidate and set $x_{n+1} = y$; if $\Psi^n(y) < \Psi^n(x_n)$ decide randomly to accept the transition (i.e. $x_{n+1} = y$) with a probability of $\Psi^n(y)/\Psi^n(x_n)$; If the candidate is rejected then set $x_{n+1} = x_n$, $n = n + 1$ and go to step 1.

Monte Carlo Markov Chain (MCMC) Sampling of the Solution of Inverse Problems

As presented in the previous chapter, the probabilistic solution of the inverse problem is the a posteriori probability, which can be presented as:

$$\sigma_M(m) = \rho_M(m)L(m) \quad (4-7)$$

where $\sigma_M(m)$ is the a posteriori probability density on the model space, $\rho_M(m)$ is the a priori probability density and $\lambda(m)$ is the likelihood function. For the applications considered in this research, it has been assumed that data and forward model uncertainties are Gaussian. It has been shown in previous chapter that for Gaussian data and forward model uncertainties, $\lambda(m)$ can be represented by:

$$\lambda(m) = k \exp\left(-\frac{1}{2}(d - g(m))^T (C_T^{-1} + C_d^{-1})(d - (g(m)))\right) \quad (4-8)$$

where C_T is the covariance matrix representing forward model uncertainties and C_d is the covariance matrix representing observational uncertainties. Equation 4-7 and 4-8 form the basis for the development of Monte Carlo sampling algorithm for the solution of inverse problems.

The goal of the sampling algorithm is to sample the model space at a rate proportional to model a posteriori probability ($\sigma_M(m)$). To achieve this goal, using Metropolis acceptance rule, the algorithm first generates samples of model space according to the model a priori probability $\rho_M(m)$, then these samples are accepted or rejected using cascade implementation of Metropolis acceptance rule based on their fit to observed data defined by likelihood function $\lambda(m)$. In other words the sampling algorithm is a cascade implementation of metropolis algorithm with probabilities $\rho_M(m)$ and $\lambda(m)$. This means that models that are consistent with a priori information as well as observations are sampled most often whereas models that are incompatible with either a priori information or observational data are sampled rarely. The algorithm described above can be written as:

- Initialize the chain to model m_1
- At n th state, randomly generate a candidate model y (usually derived from a uniform distribution).
- If $\rho_M(y) > \rho_M(m_n)$ then go to next step; if $\rho_M(y) < \rho_M(m_n)$ decide randomly to go to next step with a probability of $\rho_M(y) / \rho_M(m_n)$; If move to next step is rejected then set $m_{n+1} = m_n$, $n = n + 1$ and go to step 2.
- If $\lambda(y) > \lambda(m_n)$ then accept the candidate and set $x_{n+1} = y$; if $\lambda(y) < \lambda(m_n)$ decide randomly to go to accept the transition (i.e. $m_{n+1} = y$) with a probability of $\lambda(y) / \lambda(m_n)$; If the candidate is rejected then set $m_{n+1} = m_n$, $n = n + 1$ and go to step 2.

The output of the algorithm consists of a collection of models that their statistical properties are asymptotically proportional to a posteriori probability distribution in the model space. More comprehensive description of this algorithm can be found in other references [Mosengaard and Tarantola 1995].

Appraisal of Results

Central and Dispersion Estimators

Central and dispersion estimators for appraisal of inverse problem solution were introduced in the previous chapter as integrals in the model space. In MCMC approach, these integrals should be evaluated numerically. Since in MCMC applications the integrand of these integrals is not explicitly defined and is only sampled at certain random points, these evaluations are generally obtained using Monte Carlo integration techniques over the model space. A brief description of Monte Carlo integration techniques is presented below. Detail mathematical treatment of this subject can be found in other references [Hammersley and Handscomb 1964].

Numerical Monte Carlo integration can be simply viewed as evaluation of expected value of a function $f(x)$, denoted by $E[f(x)]$ where x is a random variable distributed according to $p(x)$.

$$E[f(x)] = \int f(x)p(x)\delta x \quad (4-9)$$

In general, x is considered to be in multidimensional space and $f(x)$ and $p(x)$ are functions of x . If a sequence of random variables x_i , distributed according to $p(x)$ can be generated, the integral in Equation (4-9) can be evaluated by:

$$E[f(x)] \approx \frac{1}{N} \sum_{i=1}^N f(x_i) = \bar{f} \quad (4-10)$$

where $\bar{}$ sign indicates the average value and N is the number of random variables used to evaluate the integral. This is simply evaluation of the expected value of $f(x)$. The law of large numbers ensures that the Monte Carlo estimate converges to the true value of the integral:

$$E[f(x)] = \lim_{N \rightarrow \infty} \frac{1}{N} \sum_{i=1}^N f(x_i) \quad (4-11)$$

The uncertainty in Monte Carlo integration is basically the standard deviation of the estimate of $E[f(x)]$, which can be estimated by:

$$\varepsilon = \frac{1}{\sqrt{N}} \sqrt{\overline{f^2} - \bar{f}^2} \quad (4-12)$$

where $\overline{f^2} = \frac{1}{N} \sum_{i=1}^N f^2(x_i)$. It is notable that the error of Monte Carlo integration is independent of dimension of the space and is simply dependent on the number of random variables. This property of Monte Carlo integration makes it more efficient than traditional quadrature techniques for evaluation of integrals in high dimensional spaces (5 or higher). This property is especially appealing for evaluation of integrals in inverse problems, which often should be evaluated over a high dimensional space. Using this technique, the integrals for estimation of central and dispersion estimators can be evaluated as simple sums over sampled models.

Marginal Probability Densities

Evaluation of marginal probabilities is often carried out by constructing the histogram or density estimates of the collected samples in MCMC. A histogram is the simplest non-parametric density estimator and the one that is most frequently encountered. To construct a histogram, the interval covered by the samples is divided into equal sub-intervals, known as “bins”. Every time a sample value falls into a particular bin, then a block of height one and width equal to the bin width is placed on top of histogram at that particular bin. Once this operation is repeated for all the samples, the obtained graph is called the histogram of the collected samples and is an estimate of the underlying probability density. The major shortcoming of histogram is that it does not provide a smooth evaluation of the probability density.

Histogram is a special form of general probability density estimators. In constructing the histogram, once a sample falls in a bin, a unit box function centered at the midpoint of the bin is added to the histogram. This is known as box kernel density estimate. If instead of a box function, a smooth function is used, the final density estimate would be smooth. In this research, a Gaussian density estimate with an optimal bandwidth is used as the kernel density estimator function. The discussion of the details of implementation of this technique and selection of an optimal bandwidth are beyond the interest of this text and are presented in other references [*Bowman and Azzalini, 1997*]. In this text only results of the probability estimates are presented.

To illustrate the ideas and methods presented, the example of deflection based modulus evaluation experiment is considered again.

MCMC Evaluation of the Probabilistic Solution of the Modulus Determination

Experiment: As presented previously, assuming a Gaussian distribution for modeling uncertainties, the forward model probability density for this example can be represented by:

$$\theta(E, \Delta) = \frac{1}{\sqrt{2\pi}} \cdot \frac{1}{\Sigma_p L^3 / IE} \exp\left(-\frac{1}{2} \frac{(\Delta - PL^3 / IE)^2}{(\Sigma_p L^3 / IE)^2}\right) \quad (4-13)$$

Furthermore, similar to the previous example, let's assume a Gaussian a priori probability for observed data with the standard deviation of Σ_Δ , which is represented by $\rho_\Delta(\Delta) = \frac{1}{\sqrt{2\pi}} \cdot \frac{1}{\Sigma_\Delta} \exp\left(-\frac{1}{2} \frac{(\Delta - \Delta_{obs})^2}{\Sigma_\Delta^2}\right)$. Finally, let's consider a homogeneous a priori probability density for model parameter, represented by $\rho_E(E) = k$, which represents no specific a priori information on the model parameter, where k is a constant.

It has been shown in previous chapter that if data and forward model uncertainties are Gaussian, the likelihood function follows a Gaussian distribution, which its covariance is the sum of the covariances of the forward model and data a priori. Using this result, the likelihood function can be represented by:

$$\lambda(E) = k \exp\left(-\frac{1}{2} \frac{(\Delta_{obs} - \frac{PL^3}{EI})^2}{\Sigma_\Delta^2 + (\Sigma_p L^3 / EI)^2}\right) \quad (4-14)$$

Using the numerical values provided previously, the MCMC solution of the problem can be obtained using the described direct sampling method. The histogram of 40000 sampled models and the corresponding probability density estimate are shown in Figure 4-5. The probability density estimate is obtained using a Gaussian kernel density estimate. Based on the results presented in Figure 4-5, it can be observed that the estimates of the a posteriori probability are very close to the one obtained by analytical techniques.

Appraisal of MCMC Solution of the Modulus Determination Experiment Using

Monte Carlo Integration: As presented in previous chapter, the mean and variance of the evaluated solution can be calculated by:

$$\langle E \rangle = \int_E E \sigma_E(E) dE \quad C_E = \int_E dE (E - \langle E \rangle)(E - \langle E \rangle)^T \sigma_E(E) \quad (4-15)$$

Using Monte Carlo integration, these integrals can be evaluated as simple sums over sampled a posteriori models:

$$\langle E \rangle = \frac{1}{N} \sum_{i=1}^N E_i \quad C_E = \frac{1}{N} \sum_{i=1}^N (E_i - \langle E \rangle)^2 \quad (4-16)$$

Using the numerically evaluated probability density, $\sigma_E(E)$, mean and variance quantities can be evaluated as: $\langle \sigma_E(E) \rangle = 69.9 \text{ GPa}$ $\sqrt{C_E} = 1.8 \text{ GPa}$.

Convergence

One important issue in application of MCMC is to decide when to stop the chain and evaluate the underlying probability based on the collected samples. This issue has been explored both theoretically and empirically in literature. In fact, an active and important subfield of MCMC research is focused on the investigation and development of techniques to determine if a chain with finite number of samples have converged to underlying probability distribution and can be used as a reliable basis for estimation of the properties of the target distribution.

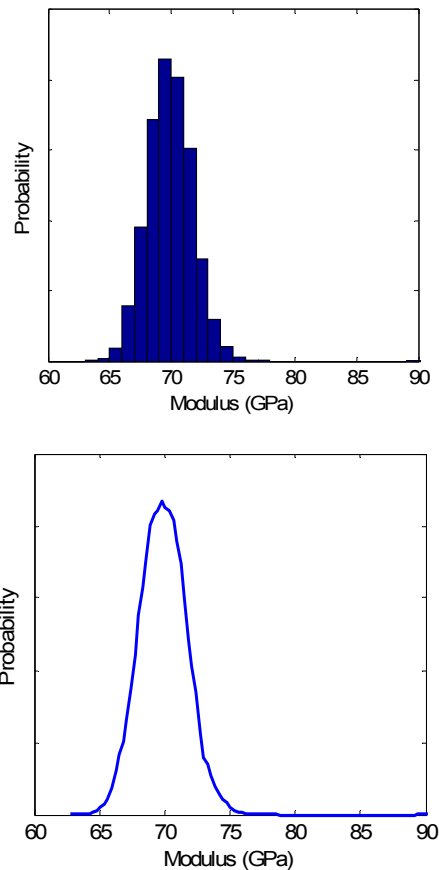


Figure 4-5 - MCMC solution of the deflection based modulus determination experiment. Histogram (top) and kernel density estimate (bottom) of the a posteriori probability density obtained from analysis of 40000 sampled models.

Theoretically, it has been shown [Tierney, 1994] that if a chain has three conditions of irreducibility, aperiodicity, and invariance, then in limit, as the number of the samples increases, the chain will converge to the target probability distribution. For a Markov chain, irreducibility implies that it is possible to visit any state to from any other given state in a finite number of steps. Aperiodicity means that the Markov chain does not circle around in the states with a finite period and a finally, invariance refers to the property of the chain that it will always converge to a unique distribution. It can be shown that [Robert and Casella, 1999] the Markov chain generated by Metropolis algorithm satisfies these conditions and therefore in the limit, as the number of samples approaches to infinity, the chain will converge to underlying probability distribution.

Although this result proves the ultimate convergence of the chain, the primary concern in implementation of MCMC methods is to decide if the chain has reasonably converged in a finite number of steps. There has been very limited success in developing theoretical techniques for determination of the convergence of a chain. In general, there is no golden rule to determine the convergence. Available techniques aim at determination of the convergence through empirical diagnostic methods [e.g. Gelman and Rubin, 1992, Raftery and Lewis, 1992, Geweke, 1992, Roberts, 1992, Ritter and Tanner 1992, Zellner and Min 1995]. Cowles and Carlin [1996] give a comprehensive review of the available convergence diagnostics techniques. However, none of these techniques is general and it is possible to find examples where each method fails. These techniques can be divided into two general categories, techniques that rely on a single long chain to achieve

convergence and techniques that are based on comparison of several chains that are generated simultaneously.

In the implementation used in this research, the convergence is assessed by diagnostic technique proposed by Gelman and Rubin [1992]. In this technique, several chains using the same probability are generated and compared. The lack of convergence of chains is determined from comparison of the mean of each chain to other means and to the mean obtained from mixing all chains together. If the calculated mean for each chain is close to the mean from other chains and to the mean obtained from mixing all the chains together, it can be assumed that chains have converged to the underlying probability. This comparison is carried out by calculating a scale reduction factor, \hat{R} , as follows:

$$\sqrt{\hat{R}} = \sqrt{\left(\frac{n-1}{n} + \frac{m+1}{mn} \frac{B}{W}\right)} \quad (4-17)$$

where B is the variance between the means from m chains each with n numbers and W is the average of the m within chain-chain variances. For slowly mixing chains, the value of scale reduction factor, \hat{R} , is greater than one and approaches to one as chains converge. Gelman and Rubin suggest running chains until the scale reduction factor is close to one and preferably below 1.2. Further details about this diagnostic technique and other available techniques can be found in cited references.

Computational Limitations

As illustrated, MCMC technique is a general technique for solution of the inverse problems and estimation of the a posteriori probabilities. However, to obtain the solution,

a large number of models should be sampled and the likelihood function for each of them should be evaluated, which in turn requires the solution of the forward model. The number of required samples is a function of the dimension of the model space and the required precision in determination of the model parameters. However, as a general rule, as the number of the model parameters or required precision increases, the required number of samples increases as well. With the speed of modern computers, this might not be a problem for inverse problems that have forward models with a short computational time. However, for inverse problems where the computational time of the forward model is substantial, the time required for generation and evaluation of a large number of samples is prohibitive. In such cases, more sophisticated approaches should be used. The approach presented in the next section is one of the possible approaches.

Direct Sampling Solution Using Approximation of the Likelihood Function

As illustrated, MCMC heavily relies on running the forward model and evaluating the likelihood function. Consequently, it becomes inefficient once the required computational time of forward model increases. One approach for the solution of the inverse problems with computationally time consuming forward models (say more than few seconds) is to construct an approximation of the likelihood function over the model space with limited and targeted evaluations of forward model and use this approximation for evaluation of MCMC solution of the inverse problems. Using this approach, the number of forward model evolutions will be limited, which in turn reduces the required solution time. In this approach, the solution of the inverse problem will be carried out in two steps:

- *Approximation stage*: generation of approximate likelihood function and,
- *MCMC stage*: evolution of MCMC solution of the problem using generated approximation.

The approximation stage is implemented here using the recently developed Neighborhood Algorithm (NA) as the search and approximation tool [Sambridge, 1999]. A brief description of neighborhood algorithm is presented below. The MCMC has been described in previous section.

Neighborhood Algorithm (NA)

Neighborhood algorithm is a recently developed search and approximation algorithm. The objective of the algorithm is to find the optimum of an objective function by preferentially sampling the good regions of the space, which have higher values of function. This algorithm falls in the same class of global optimization methods such as simulated annealing and genetic algorithm and can be directly applied for optimization problems. However, rather than seeking a single optimal point, NA provides an approximation of the objective function, which is preferentially sampled more at the good regions of the space. The approximation constructed by NA (i.e. Neighborhood approximation) is used here to approximate the likelihood function for the solution of inverse problems using MCMC.

NA approximation of likelihood function has several important features that are essential for obtaining MCMC solution of the inverse problem. The neighborhood

approximation is a global approximation to likelihood function through out the model space. Additionally, neighborhood approximation is preferentially sampled more at the regions of the model space with high value of the likelihood function resulting in a better approximation in important regions of the model space. Given the right control parameters, NA can locate the global optimum of the likelihood function and it will not get trapped in a local optimum. This feature of the algorithm makes it especially useful in the solution of highly nonlinear inverse problems, where the likelihood function might have several peaks. Finally, the value of likelihood function using neighborhood approximation can be efficiently calculated for every point in the model space.

NA is a global optimization algorithm. Consequently, an additional result of the approximation stage is the identification of the maximum of the likelihood function (i.e. maximum likelihood point). As shown in previous section, in certain situations, the maximum of the likelihood function is the deterministic solution of the inverse problem. So, in these situations, the probabilistic approach presented here also identifies the deterministic solution as an intermediate step. In other words, for these problems, the search stage can be thought of as deterministic solution of the problem and MCMC stage as uncertainty evaluation stage.

Finally, it should be mentioned that the accuracy of the obtained MCMC solution is directly related to the goodness of the approximation used for likelihood function, which is a function of the degree to which important regions of the model space are sampled. There is no general technique for evaluation of goodness of an approximation, intuitively, the more exploration in model space, the better the approximation.

Implementation of NA

The basic premise of NA algorithm is to use previously evaluated samples to construct an approximation to the objective function through out the model space and use this approximation to guide generation of new models for which the forward model has to be evaluated. In general, the objective function can be any function, however, for the inverse problem solution presented here, the objective function is the likelihood function. The generalized algorithm can be presented as follows:

- Construct the approximate likelihood function surface from the previous n_p models for which the function value has been calculated (i.e. forward model has been solves);
- Use this approximation to generate the next n_s samples in the prospective regions of the space and find the function value for them;
- Add n_s to n_p and repeat all the steps again.

The two important missing detail of the above algorithm is how to construct the approximate likelihood function surface and how to generate new samples. NA algorithm uses a mathematical construct knows as Voronoi diagram [*Voronoi, 1908*] to construct the approximate surface and generate new samples.

Voronoi Diagram

Voronoi diagram is a unique way of dividing the n -dimensional space into n regions called cells. Each cell is simply the nearest neighborhood region about one of the previous samples as measured by a particular distance measure (most often L_2 norm). A set of two-dimensional Voronoi cells about 30 random samples is presented in Figure 4-6.

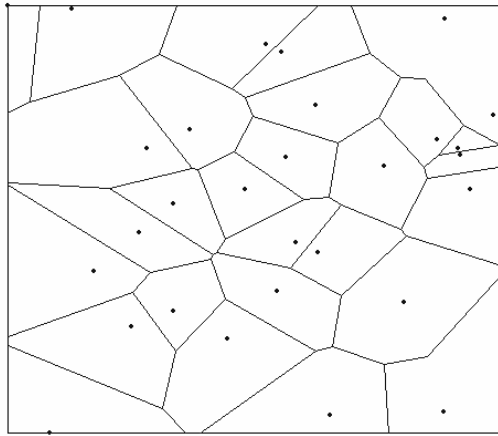


Figure 4-6 - Typical Voronoi Diagram in two dimensions.

Voronoi diagram provides a basis for construction of an approximation to objective function. In NA, the approximate value of the likelihood function within each Voronoi cell is assumed to be constant and equal to the value of the likelihood function evaluated for the point inside the cell. Once this approximation (i.e. neighborhood approximation) is constructed, NA uses this surface to guide the selection of the new samples. Using the concept of Voronoi cells, NA algorithm can be re-written as follows:

- Generate initial n_s samples in model space;

- Solve the forward model for the most recent samples and choose n_r models with highest objective function values,
- Generate n_s new models by drawing random samples in the Voronoi cells of each n_r models (i.e. n_s/n_r samples in each cell).
- Go to step 2.

This algorithm preferentially draws samples in the regions of the model space with high function value. The algorithm has only two control parameter n_s and n_r which can be reduced to only one by setting $n_s = n_r$. At each step during the progress of algorithm, the maximum of the function can be easily identified among the set of sampled points and the approximate function can be created using neighborhood approximation.

Stop Criteria

An important issue in implementation of NA is to determine when to stop the algorithm. Since the objective of the algorithm is to optimize the objective function by preferentially sampling the good regions of the space, the stop criteria should be directly related to how precise the optimum point is located. Consider the following two stop criteria, which both should be satisfied to stop the algorithm:

- The cell corresponding to the identified optimum has not changed for last n_s sampled points

- The distance (in L_2 sense) between identified optimum and last n_s sampled points is less than ε , the required precision.

These two criteria ensure that the region containing the optimum point is sampled adequately and additional sampling is not likely to change the location and precision of the identified optimum. These criteria were used as the stop criteria for the algorithm.

Monte Carlo Solution Using Neighborhood Approximation

Once the approximation to likelihood function is constructed, it can be used to obtain MCMC solution of inverse problem. If this approximation is denoted as $\lambda^{NA}(m)$, the solution can be represented as:

$$\sigma_M^{NA}(m) = \rho_M(m) \lambda^{NA}(m) \quad (4-18)$$

where $\sigma_M^{NA}(m)$ is the a posteriori probability density obtained by using neighborhood approximation, and $\rho_M(m)$ is the model a priori probability density. MCMC techniques as described above can be directly applied to obtain the solution $\sigma_M^{NA}(m)$ and determine estimator quantities and marginal probabilities.

To illustrate the application of the direct sampling using NA approximation of the likelihood function, the modulus determination experiment is considered again. However, to further demonstrate the advantage of the probabilistic approach in comparison to the deterministic approach, the experiment design is slightly modified.

Deflection Based Modulus and Load Determination Experiment: In previous examples, the beam modulus was the only model parameter that had to be determined

from the solution of the inverse problem. For this example, it is assumed that in addition to the modulus, the exact magnitude of the load is also unknown and only an approximate magnitude is known. Therefore, in this example, there are two model parameters load, P , and modulus, E , which should be determined using one measured data value. It should be mentioned that in this case there is an infinite number of deterministic solutions. However, there is always a unique probabilistic solution to the problem. In reality, the a priori information on the model parameters, such as judgment on the type of material or simply an estimate of the load, might be enough to limit the solution to a set of probable solutions. However, there is no structured procedure in the deterministic approach to include such information in the solution process. However, they can be easily included in the probabilistic approach.

Assume that there is no specific a priori information on modulus, i.e. it is represented by a homogenous a priori probability. However, based on the available information, a Gaussian a priori probability for load, P , can be formed, which conveys the expected value of the load. These probabilities are represented by:

$$\rho_{P_{pri}}(P) = \frac{1}{\sqrt{2\pi}} \cdot \frac{1}{\Sigma_{P_{pri}}} \exp\left(-\frac{1}{2} \frac{(P - P_{pri})^2}{\Sigma_{P_{pri}}^2}\right) \quad (4-19)$$

$$\rho_E(E) = \mu(E) = k$$

where P_{pri} and $\Sigma_{P_{pri}}$ are the mean and variance of the a priori distribution. For this example, since the uncertainty of the load is considered as an a priori information, the likelihood function can be simplified as:

$$\lambda(E, P) = k \exp\left(-\frac{1}{2} \frac{(\Delta_{obs} - \frac{PL^3}{EI})^2}{\Sigma_{\Delta}^2}\right) \quad (4-20)$$

Having defined the elements of the problem, the MCMC solution of the problem using NA is presented below. The solution consists of two stages, approximation stage and MCMC stage.

Approximation Stage: The neighborhood approximation of the likelihood function, obtained using neighborhood algorithm, is presented in Figure 4-7. Since the likelihood function in this example is simple, for comparison purposes, exact plot of the function is also presented. It should be remembered that this exact plot is generally not available. By inspection of this figure, it can be observed that the neighborhood approximation is relatively coarse where the value of the function is low and it becomes dense near the regions of the function with high values. It should be also noted that the likelihood function in this case is a function which has infinite number of maximum points. This type of behavior is not easy to approximate. However, it can be observed that the neighborhood approximation has reasonably captured the behavior of the function.

MCMC Stage: The two dimensional a posteriori histograms of 10000 sampled models obtained using the neighborhood approximation of the likelihood function are presented in Figure 4-8. For comparison purposes, the analytical solution is also presented in this figure. Histogram and kernel density estimates of one dimensional posteriori marginal probabilities for each parameter are also presented in Figure 4-9.

Using the numerically evaluated probability density, mean and variance quantities for the modulus and load are presented below:

$$\begin{aligned} \langle \sigma_E(E) \rangle &= 72.6 \text{ GPa}, & \sqrt{C_E} &= 10.66 \text{ GPa} \\ \langle \sigma_p(p) \rangle &= 100.4 \text{ GPa}, & \sqrt{C_p} &= 10.18 \text{ GPa} \end{aligned}$$

It can be observed that the approximate solution has captured the essential features of the exact analytical solution.

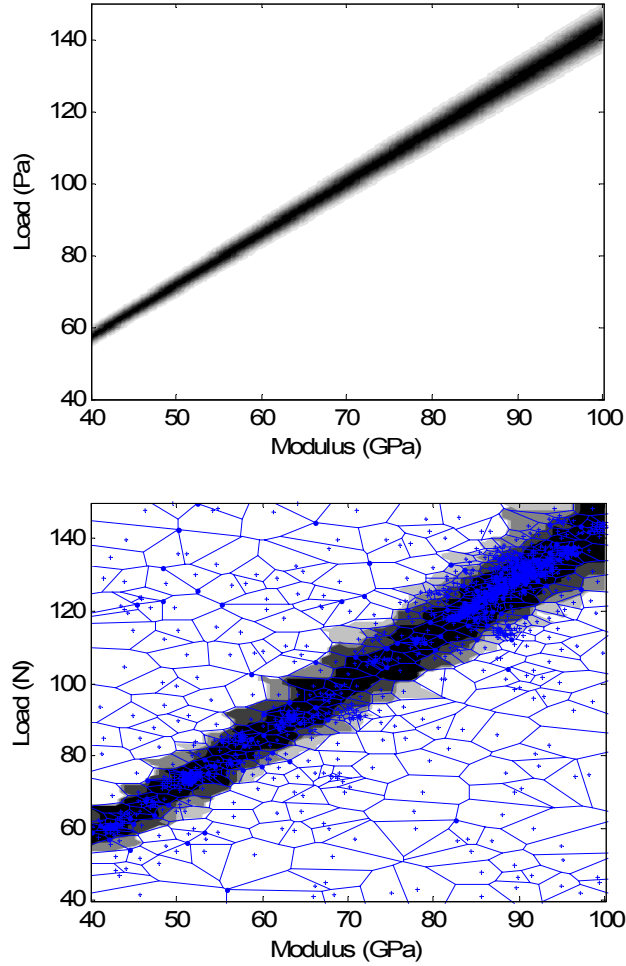


Figure 4-7 - Exact plot (top) and neighborhood approximation (bottom) of the likelihood function with 1000 models. Sampled models, as well as corresponding Voronoi diagram are also shown ($\Sigma_{\Delta} = 0.001 \text{ m}$).

Matlab® Application Program

To implement the outlined probabilistic approach, a user friendly Matlab® based application is prepared to evaluate the probabilistic solution with NA approximation. The application, which uses Matlab® scripts as inputs, is designed as a general purpose inversion tool for the solution of different inverse problems and is used for applications in the following chapters. A snapshot of the input window of this application is presented in Figure 4-10.

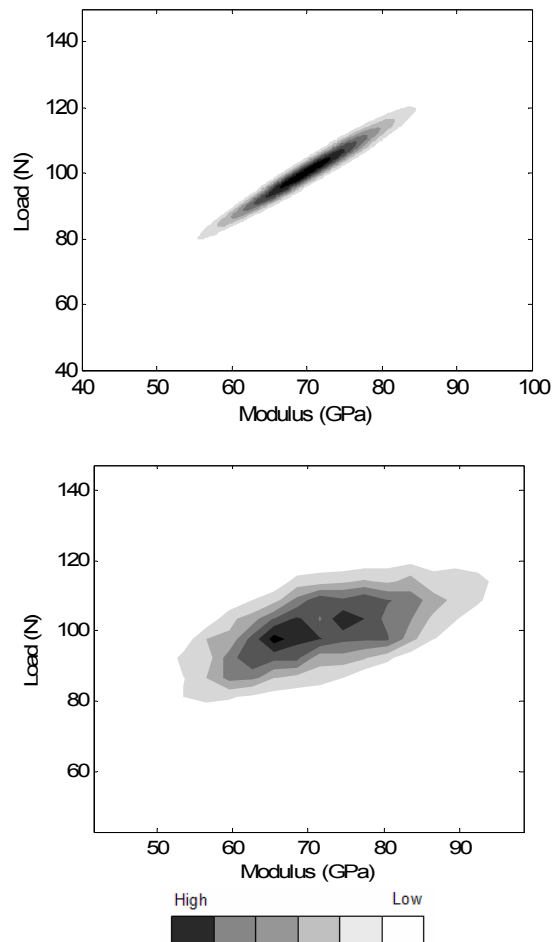


Figure 4-8 - Exact plot of $\sigma(E, P)$ (top) and MCMC solution using neighborhood approximation (bottom) of the modulus determination experiment

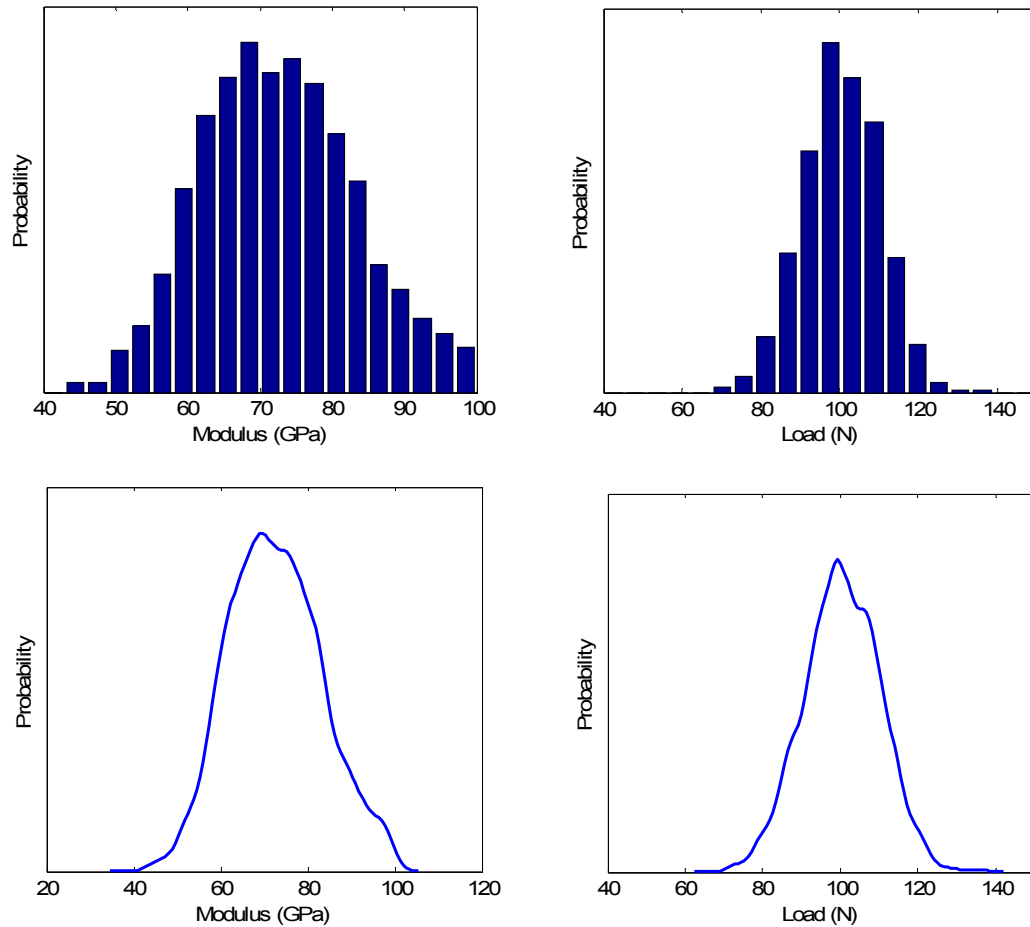


Figure 4-9 Histogram of 10000 samples of the one dimensional marginal a posteriori probabilities of (a) modulus and (b) load, and their corresponding kernel density estimates (c and d)

Summary

In this chapter, a number of techniques for quantitative evaluation of the probabilistic solution were presented. The techniques for direct analytical evaluation and numerical approximation of the probabilistic solution using Monte Carlo Markov Chains (MCMC), with and without Neighborhood Algorithm (NA) approximation, were introduced and explained. To demonstrate the advantages of the presented approach and to illustrate the concepts and techniques in more practical terms, a very simple modulus

determination experiment was presented. It has been shown that the major advantage of the probabilistic approach to inverse problem is its capability to evaluate the uncertainty measures for the solution. Additionally, it has been shown that the a priori information about the model parameters can be readily incorporated in the probabilistic solution process.

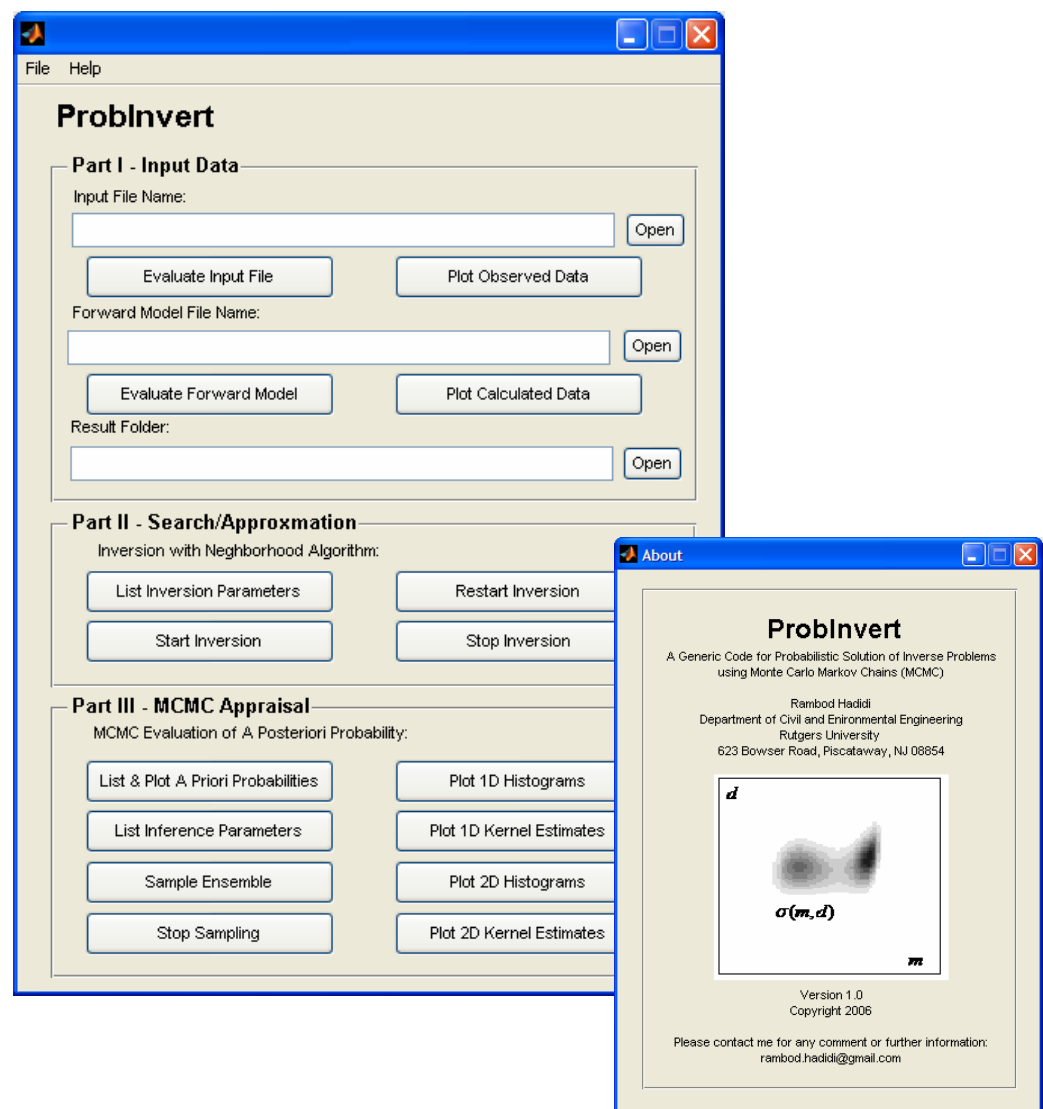


Figure 4-10 Snapshot of the input window of ProblInvert, the developed probabilistic inversion application.

References

- Bhat, U. N. and Miller, G. K. (2002), "Elements of Applied Stochastic Processes", John Wiley & Sons Inc., Hoboken, NJ.
- Bowman, A.W. and Azzalini A. (1997), "Applied Smoothing Techniques for Data Analysis: The Kernel Approach with S-PLUS Illustration", Clarendon Press, UK.
- Cowles, K. and Carlin P. (1996), "Markov Chain Monte Carlo Convergence Diagnostics: A Comprehensive Review", Journal of American Statistical Association, 91 (434), 883-904.
- Gelman, A. and Rubin, D.B. (1992), "Inference from Iterative Simulation Using Multiple Sequences", Statistical Science, 7, 457-511.
- Geweke, J. (1992), "Evaluation of the Accuracy of Sampling Based Approaches to Calculation of Posterior Moments", in Bayesian Statistics 4, eds. M. Bernardo, J. Berger, A. P. Dawid, and A. F. M. Smith, Oxford University Press, Oxford, UK.
- Hammersley, J. M. and Handscomb, D. C. (1964), "Monte Carlo Methods", Methuen and Co. Ltd, London, UK.
- Hastings W. K. (1970), "Monte Carlo sampling methods using Markov chains and their applications", Biometrika, 57:97-109.
- Metropolis, N., A. W. Rosenbluth, M. N. Rosenbluth, A. H. Teller, and E. Teller. (1953), "Equation of state calculations by fast computing machines", J. Chem. Phys. 21:1087-1092.
- Mosegaard K. and Tarantola, A. (1995), "Monte Carlo Sampling of Solution to Inverse Problems", Journal of Geophysical Research, Vol.100, No. B7, p 12,431-12,447.
- Raftery, A. E. and Lewis, S. (1992), "How Many Iterations in Gibbs Sample?", in Bayesian Statistics 4, eds. M. Bernardo, J. Berger, A. P. Dawid, and A. F. M. Smith, Oxford University Press, Oxford, UK.
- Robert, C. P., and Casella, G. (1999), "Monte Carlo statistical methods", Springer-Verlag, New York, NY.
- Roberts, G. O. (1992), "Convergence Diagnostics of Gibbs Sampler", in Bayesian Statistics 4, eds. M. Bernardo, J. Berger, A. P. Dawid, and A. F. M. Smith, Oxford University Press, Oxford, UK.
- Ritter, C. and Tanner, M. A. (1992), "Facilitating the Gibbs Sampler: The Gibbs Stopper and the Griddy-Gibbs Sampler", Journal of American Statistical Association, 87, 861-868.
- Sambridge, M. (1999), "Geophysical Inversion with Neighborhood Algorithm – II. Appraising the Ensemble", Geophysical Journal International, 138, 727-746.
- Sambridge, M. (1999), "Geophysical Inversion with Neighborhood Algorithm – I. Searching the Parameter Space", Geophysical Journal International, 138, 479-494.
- Sambridge, M. and Mosegaard K. (2002), "Monte Carlo Methods in Geophysical Inverse Problems", Reviews of Geophysics, 40,3.
- Tarantola, A. (2005), "Inverse Problem Theory", SIAM, Philadelphia, PA.
- Tanner, M. (1996), "Tools for Statistical Inference", Springer-Verlag, New York, NY.
- Tierney, L. (1994), "Markov Chains for Exploring Posterior Distributions", Annals of Statistics, 22, 1701-1728.

- Zellner, A. and Min, C. K. (1995), “Gibbs Sampler Convergence Criteria”, Journal of American Statistical Association, 90, 921-927.

5 Application One: Falling Weight Deflectometer Backcalculation

Introduction

Falling weight deflectometer test, commonly referred to as FWD test, is the most widely accepted, used, and studied technique for in-situ non-destructive evaluation of pavements. The objective of the test is to excite and measure the pavement response under the load levels equivalent to those applied on pavements by truck traffic. The measured pavement response is then analyzed or backcalculated to infer elastic moduli of pavement layers. FWD test is a very important tool for evaluation, design, and maintenance of transportation infrastructure. The test is routinely used by pavement engineers to backcalculate and estimate the in-situ pavement layer moduli, design overlays, estimate remaining life of pavements, evaluate load transfer capability, and perform network level monitoring.

In this chapter the probabilistic backcalculation of FWD test results is introduced as the first example of the application of the probabilistic solution of inverse problems in civil engineering. Introduction of limited probabilistic concepts in FWD backcalculation has been previously suggested by others [*e.g. Zaghoul et al, 2004*]. However, to the author's knowledge, the presented approach in this chapter is the most comprehensive and structured treatment of probabilistic backcalculation of FWD test results. Following

the introduction, a review of the FWD test procedure and current backcalculation techniques are provided. The backcalculation problem is then formulated from a probabilistic point of view and the results of the probabilistic backcalculation of synthetic test data are presented. To compare different methods of FWD backcalculation, such as static vs. dynamic and deflection bowl vs. time history backcalculation, the same set of synthetic test data are backcalculated using different methods and the results are compared. To illustrate the applicability of the developed backcalculation approach to actual field data, a set of experimental FWD test results are backcalculated using the probabilistic approach and the results are presented. The chapter concludes with a discussion of the importance of considering the frequency dependence of layer moduli on backcalculation results. This effect is evaluated using a spectral element model, which simulates the pavement response in the frequency domain. The developed spectral element model is used to backcalculate the same set of synthetic test results used previously. The results of the backcalculation are presented and compared to other results.

Background

Review of FWD Test Procedure

FWD test is conducted by dropping a weight on a guided system from a series of predetermined heights and monitoring the ensuing pavement response. The test procedure with FWD is documented in ASTM 4694-96 [ASTM, 1996] and ASTM D4695-03 [ASTM, 2003]. Schematics of the test setup and one of the trailers developed commercially for its implementation are depicted in Figure 5-1.

During each drop, an approximately a half sine transient impulse force is applied to the pavement. Currently available FWD trailers can apply loads ranging from 13600 to over 227000 N (3000 to over 50000 lb). The equipment has a relatively low preload so its influence on the pavement response is relatively negligible. The falling weight is generally dropped on a composite loading plate with a 0.30 m (12 inch) diameter. The composite plate generally consists of a steel plate, a PVC plate, and a rubber pad placed on the lower surface of the plate, which rests on the pavement. The function of the composite plate is to distribute the impact force, transferred to the plate via rubber buffers attached to the bottom of the weight, rather uniformly over the pavement surface. However, numerical studies have shown that for flexible pavements with a low paving layer modulus, the interaction between the pavement and the loading plate during the test might be significant enough to influence the stress distribution over the pavement surface and produce a non uniform distribution [*Boddapati and Nazarian 1994*].

The FWD loading cycle is about 30 to 40 msec long. The transferred load to pavement and pavement response during the test is generally monitored for 60 msec by transducers resting at different radial offsets from the impact location. A typical loading history and corresponding deflection time history records measured during FWD test are depicted in Figure 5-2. The transferred load is commonly recorded by a load cell and pavement response is monitored by geophones. It is common practice to measure the pavement response at offset distances recommended by Federal Highway Administration (FHWA) for Long Term Pavement Performance (LTPP) study. These offsets are 0, 0.20, 0.30, 0.45, 0.60, 0.90, 1.20 and 1.50 m (0, 8, 12, 18, 24, 36, 48 and 60 inch respectively). During an FWD test, after dropping the weight and completion of initial loading and

unloading cycle, the weight loses contact with the plate for a time period after which the contact takes place again. Previous studies have indicated that for the most conservative lower drop heights the time interval between two contacts is about 180 msec. Consequently, considering the duration of initial FWD impulse, the initial pavement response during the FWD test can be considered independent of the subsequent rebounds and impacts of the weight [Sebaaly, Davies and Mamlouk, 1985].

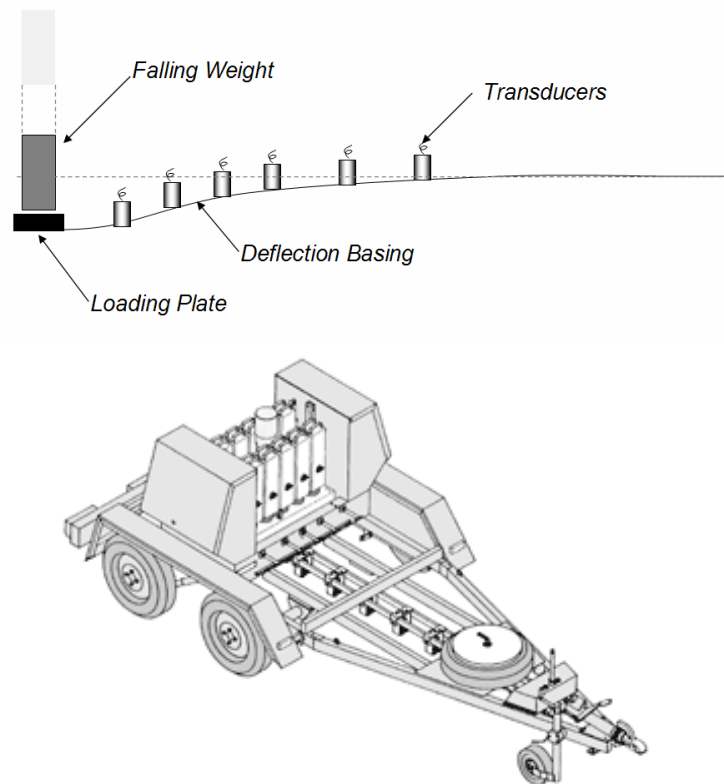


Figure 5-1 - Schematics of FWD test setup (top) and Dynatest® model 8000 FWD trailer (bottom).

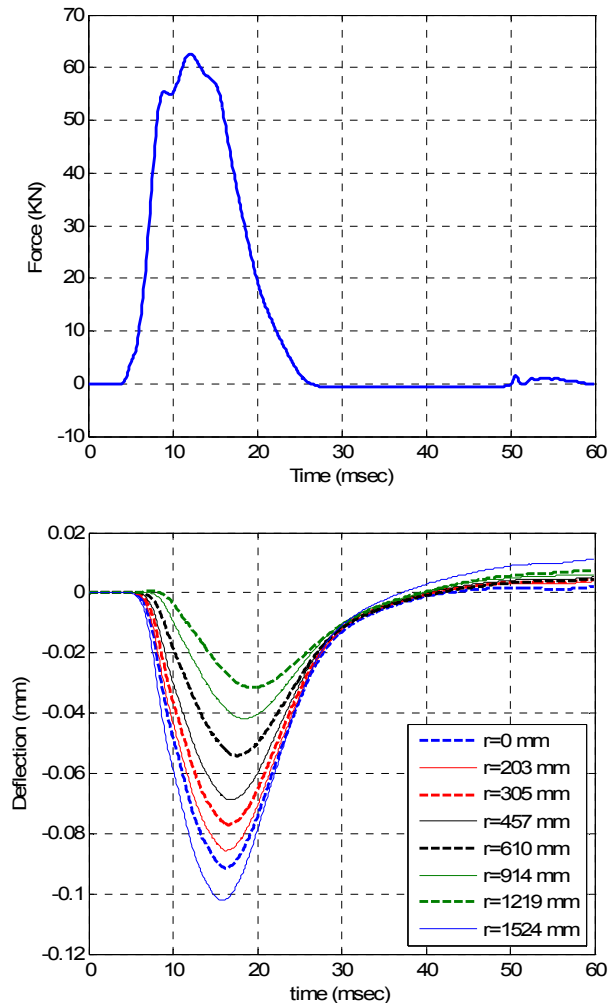


Figure 5-2 - Typical measured loading history (top) and pavement response during FWD test at different offsets (bottom).

Review of Current FWD Backcalculation Procedures

Over the past few decades, there has been a considerable number of publications addressing different aspects of interpretation and backcalculation of FWD test results with many of the important findings presented in several volumes of American Society for Testing and Material (ASTM) special technical publications [Bush and Baladi, 1989, Von Quintus, Bush, and Baladi 1994, Tayabji and Lukanen, 2000]. The review of currently available backcalculation procedures indicates that the available procedures use

a deterministic approach to the solution of the problem. These procedures can be divided into several categories based on the degree of complexity of the forward model used [Uzan 1994], such as:

- Static linear elastic procedures,
- Static nonlinear elastic procedures,
- Dynamic linear procedures using either time or frequency domain fitting, and
- Dynamic nonlinear procedures.

In static linear elastic procedures, the theoretical static response of an elastic pavement model under the maximum applied load is matched to the maximum measured deflection of the pavement at each transducer location. The maximum deflection of the pavement at each receiver is collectively referred to as the deflection bowl. Due to simplicity and speed of calculation, static linear backcalculation procedures are widely used in the current engineering practice. There are several programs available that implement this approach, such as MODCOMP [Irwin, 1993], Modulus [Michalak and Scullion, 1995] and ELMOD [ELMOD, 2001].

In static non-linear backcalculation schemes, a nonlinear static model is used to generate a theoretical pavement response that matches the observed deflection bowl. The main premise of the static non-linear backcalculation scheme is that by considering the nonlinear effects, a more realistic theoretical model of pavement is used, which consequently provides a better backcalculated estimates of pavement material properties. The non-linear forward model is generally developed and analyzed using Finite Element

(FE) programs. There have been also attempts to include nonlinear effects in linear static analysis by using empirically or theoretically generated relationships. Static non-linear models in theory can provide a better representation of pavement response, however, since the static model does not consider the dynamic nature of the FWD test, the validity and accuracy of the static non-linear backcalculation approach are questionable.

The FWD loading cycle can not be in any sense considered as a static loading, as is assumed in static procedures. There have been several studies against using static pavement models in the FWD backcalculation [Mamlouk 1987, Uzan 1994, Alkhoury *et al* 2001]. However, there is a general notion that in absence of a shallow bedrock (<3m) and stiff and thick surface layer, the results of static linear backcalculation are reliable [Uzan 1994].

In the dynamic linear analysis the theoretical dynamic pavement response is matched to the observed deflection bowl or time histories. The calculation of forward model can be implemented either in the time domain using either finite element or finite difference techniques [Loizos and Scarpas 2005] or in the frequency domain using analytical techniques, such as the transfer matrix approach suggested by Thomson [1950] and Haskell [1953], which was further developed by Kausel and Roesset [1981], or the spectral element technique [Doyle, 1997]. The studies by Uzan [1994] and Alkhoury *et al.* [2001 *a,b*] are examples of successful application of dynamic linear forward model in the FWD backcalculation. Although dynamic modeling of a pavement for generation of the theoretical response is fundamentally a more appropriate approach to FWD backcalculation [Zaghloul *et al.* 1994], due to a restrictive computational cost, its application is currently very limited. However, with ever increasing computational power

available to practitioners, it is expected that dynamic modeling for backcalculation will be used more extensively in future.

As partially outlined above, there have been a few decades of effort by engineers and researchers to improve the FWD backcalculation procedures. Despite the extensive research on FWD backcalculation and significant advances in this area, the current backcalculation procedures still use a deterministic approach, which lacks uncertainty measures. Adoption of the probabilistic approach in FWD backcalculation would improve the current backcalculation procedures by evaluation of uncertainties in the analysis, especially in the following areas:

- *Evaluation of uncertainties in backcalculation results due to uncertainties in the layer thickness input:* Probably the most restrictive aspect of the FWD test is that it requires knowledge of the pavement layer thickness as an input to backcalculation routines. Such information is rarely available for every location and should be estimated from other data. The uncertainty in the thickness estimates used in the backcalculation translates to uncertainty in obtained results, which is not possible to evaluate with current backcalculation procedures. In the probabilistic approach, such estimates can be obtained.
- *Evaluation of uncertainties due to selection of backcalculation variables:* The backcalculation results may vary depending on how the pavement model is developed and the model parameters, such as the number and thickness of pavement layers, are selected. Inappropriate selection of the model parameters may produce poor backcalculation results. For example, it is generally

accepted that when a thin paving layer (<80mm) exists, its modulus can not be reliably backcalculated. In the current backcalculation procedures, if such a layer is selected as one of the parameters, there is no measure that determines the uncertainty of the obtained results. In the probabilistic approach, uncertainty measures are obtained as a part of the solution.

- *Evaluation of uncertainties due to uncertainty in evaluation of the depth to shallow bedrock:* The presence of a shallow bedrock affects the results of FWD test. Current practice relies on the analyst to detect presence of the bedrock from the recorded data and estimate the depth to the bedrock from a separate analysis and include it in the backcalculation analysis [Roesset et al. 1995]. The inaccuracy in determination of the depth to bedrock affects the analysis results and increases uncertainties. In the probabilistic approach, these uncertainties can be quantified.

Furthermore, since the probabilistic approach presented here uses a global search algorithm, the obtained results are repeatable, which is not generally the case for some of the available backcalculation procedures [Uzan 1994]. Using the probabilistic approach, also allows exploration of the possibility of simultaneous backcalculation of the layer moduli, depth to bedrock, and layer thicknesses as a part of the backcalculation analysis along with associated uncertainty measures.

Probabilistic Formulation of FWD Backcalculation

Using the notion of generalized measurement presented in the previous chapters, the FWD test and the associated backcalculation can be considered as a generalized measurement of pavement layer properties using surface deflection measurements. The notion of a generalized measurement combined with tools developed in the previous chapters will be used here to backcalculate the pavement layer properties and obtain uncertainty measures.

As presented in the review section, there are different approaches to the modeling of the pavement response in backcalculation of FWD test results, such as static or dynamic modeling. Similar to the deterministic formulation of FWD backcalculation, the probabilistic approach can also be formulated using different types of forward models. In this study, two general types of forward models are considered and probabilistic backcalculation is formulated using each of those:

- *Probabilistic formulation using static linear elastic forward model:* Although the nature of the FWD test is obviously dynamic, due to their simplicity and computational savings, historically, static forward models have been used to model FWD test in backcalculation procedures. Since the static backcalculation routines are still very popular with practicing engineers, this class of backcalculation procedures is reformulated probabilistically to investigate the uncertainties in the obtained results from this approach.
- *Probabilistic formulation using dynamic linear elastic forward model:* Intuitively, the dynamic backcalculation approach should provide a more realistic estimate of the pavement layer properties. The deterministic dynamic

backcalculation routines based on complete time history records of the pavement deflection have been previously proposed for FWD backcalculation [e.g. Alkhoury, 2001]. The probabilistic approach, in addition to more realistic modeling of the pavement response, provides the required tools to investigate the information carried by recorded data to backcalculate the layer moduli, obtain uncertainty measures, and consider the possibility of directly backcalculating other pavement properties, such as the depth to bedrock or even pavement layer thicknesses.

The probabilistic formulation of a FWD backcalculation in terms of the a priori information and the forward model operator is presented below and its application is illustrated by backcalculation of synthetic and experimental FWD test data.

Model a Priori Information

In the probabilistic formulation, the model a priori information, represented by probability density $\rho_M(m)$, presents the knowledge about the value of the model parameters prior to the solution of the problem. For pavement layer properties, most often, there is no information available other than possible limits of the value of the parameters. The information about the limits of the value of the parameter of interest is presented by a homogenous probability density. Since this type of a priori information is the most common type encountered in practice, it is the only a priori information considered here. Homogenous a priori probability densities considered for all pavement layer properties in this chapter can be presented by:

$$\rho_M(m) = \begin{cases} \frac{1}{m_{\max} - m_{\min}} & m_{\max} < m < m_{\min} \\ 0 & \text{otherwise} \end{cases} \quad (5-1)$$

where m_{\max} and m_{\min} are respectively the maximum and minimum limits of the value of the parameter of interest, m . The choice of limits of m generally depends on the problem and the experience and judgment of the analyst. However, when in doubt, a larger interval should be selected.

Data a Priori Information

Data a priori information, represented by probability $\rho_D(d)$, expresses the uncertainties in the measurement of the observed parameters, which for a FWD test are simply deflections at transducer locations.

The uncertainties in deflection measurement can be divided into two categories according to guidelines of United States National Institute of Standards and Technology (NIST): uncertainties of “Type A” and “Type B” [Taylor and Kuyatt, 1994]. The uncertainties in deflection measurement of the transducers are usually evaluated as a “Type A” uncertainty by the transducer manufacturer. For example, for Dynatest 8081 FWD/HWD system, these uncertainties are quantified in the owner’s manual as, “The deflections are measured with an absolute accuracy of better than 2%±2 microns, and with typical, relative accuracy of 1%±1. The resolution of the equipment (in terms of deflection) is one micron” [Dynatest, 1995]. However, in addition to uncertainties associated with instrument measurements, there are generally other uncertainties in FWD measurements that should be considered, such as the uncertainties in positioning and appropriate contact of the transducers, uncertainties in instrument readings due to

vibrations sources other than the FWD impact, and uncertainties due to presence of surface cracks. Ideally, each component of uncertainty should be evaluated statistically and combined with other components to obtain the standard combined uncertainty. However, in absence of such an evaluation, a reasonable estimate of uncertainty can be obtained from repeatability studies reported in literature. The repeatability of FWD measurements for several commercially available trailers is presented in Figure 5-3. Based on these studies data a priori probability distribution, $\rho_D(d)$, will be considered to be a Gaussian distribution with a mean equal to the observed value and a coefficient of variation of two percent.

It should be mentioned that in a repeatability study each reading of the device is compared to previous readings of the same device, not to the actual value of the measurand. So, there is a difference between the result of repeatability studies and uncertainties. However, in absence of any measure of uncertainty, the repeatability results are used here as a rough estimate of the uncertainty in FWD measurements. Obviously, a more thorough evaluation of the uncertainty of FWD measurements in the probabilistic context would be required for more accurate estimates.

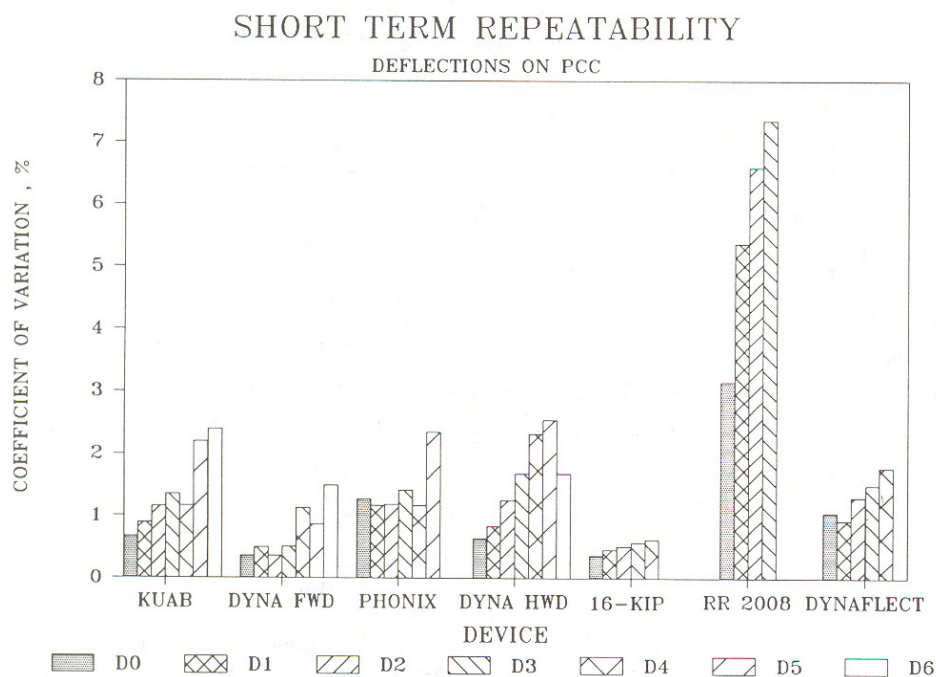
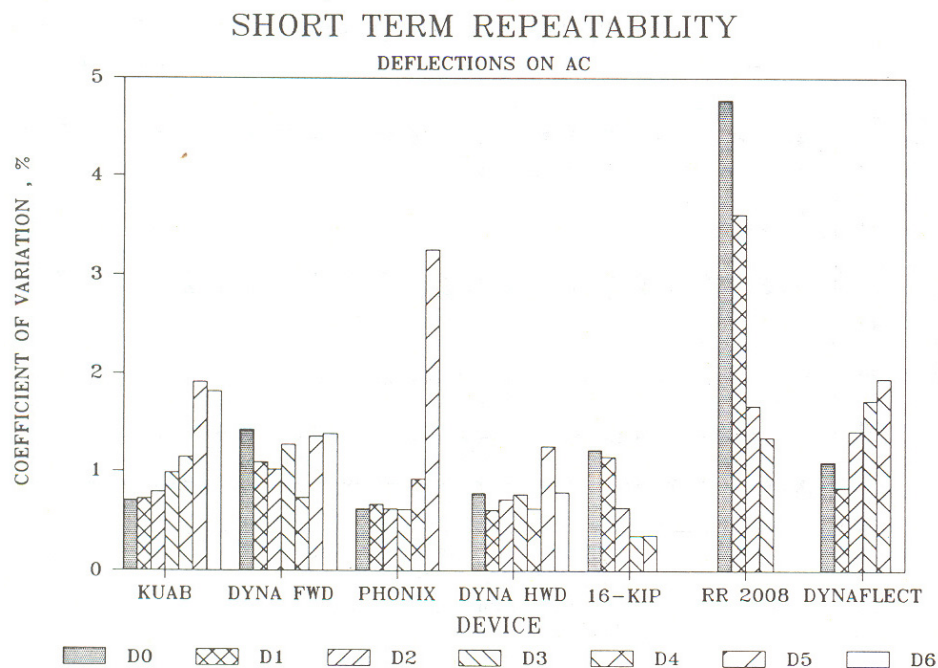


Figure 5-3 - Coefficient of variation of deflection from short term repeatability experiments [Benson, Nazarian and Harrison, 1994]. D1 thru D6 indicates different deflection sensors.

Forward Model

There are several approaches towards the modeling of the FWD test. The choice of the model depends on many factors, such as the type of analysis, required degree of complexity, computational requirements, and availability of resources. For this research a finite element model was selected as the forward model. In finite element analysis, the pavement response is generally calculated in the time domain. The main benefit of the finite element model is its generality and the ease of modeling different geometries, boundary conditions, and material models using commercially available and verified codes. Finite element analysis can also be used to obtain the static response of the system for a comparison to conventional backcalculation methods. The main disadvantage of the finite element analysis is its computational cost.

The finite element forward model for this study was developed using ABAQUS® program [ABAQUS, 2005]. The developed finite element mesh is presented in Figure 5-4. The same mesh was used for both static and dynamic analyses.

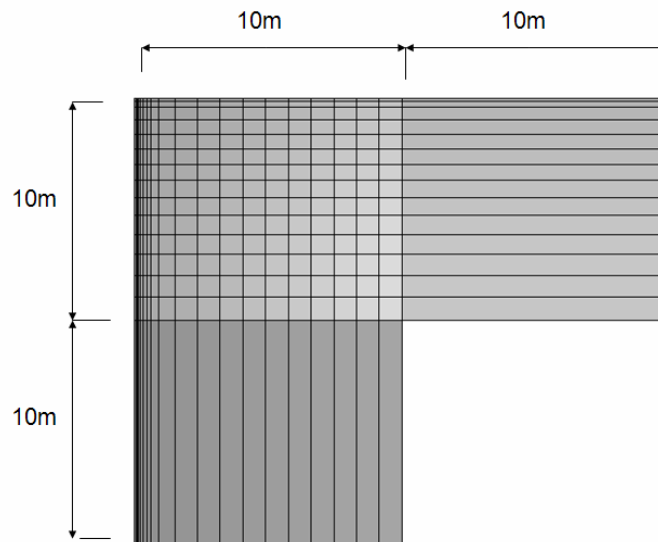


Figure 5-4 – Axisymmetric ABAQUS® Finite Element mesh with absorbing boundary elements for theoretical modeling of FWD test.

There were several considerations in the development and analysis of the finite element model, including:

- *Loading Wavelet:* The FWD load pulse is modeled as a time varying, spatially uniform load on the 0.15 m radius loading plate. An idealized loading wavelet of the FWD test and its frequency spectrum resulting from a maximum load of 50000 N are depicted in Figure 5-5. This wavelet is used in the numerical simulation of FWD tests. As presented, most of the energy of the FWD excitation is below 100 Hz.
- *Element Size and Type:* The FWD test can be modeled as an axisymmetric problem. Consequently, the finite element model was developed using two dimensional axisymmetric elements. The size of the elements is very important in the finite element analysis, especially in the dynamic analysis. The element size generally depends on the material properties and characteristics of the impact loading wavelet. The approximate element size, e , can be estimated from the relationship $e < \chi \times V_R / f_{\max}$ [Zerwer, Cascante, and Hutchinson 2002], where V_R is the Rayleigh wave velocity, f_{\max} is the highest frequency of interest, and χ is a constant less than 0.5 because of the Nyquist limit considerations. Since the FWD excitation frequency is relatively low (<100 Hz), the element size near the impact location was dictated by the location of the transducers rather than element size e , as defined above. To minimize the number of model elements and consequently reduce the

computational time of the forward model, the element size was increased towards the boundaries of the model.

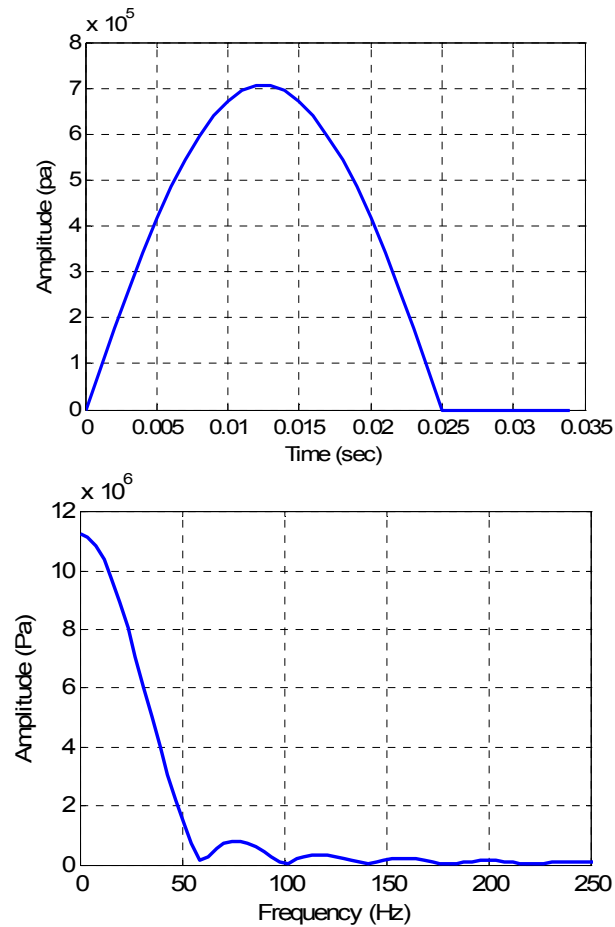


Figure 5-5 - Time history (top) and frequency spectrum (bottom) of idealized time history wavelet.

- *Overall Dimensions of the Model:* To ensure the accuracy of the static finite element analysis, consistent with the recommendations of previous studies, the model boundaries were established at 10 m from the impact location. Additionally, to ensure the accuracy of the dynamic analysis, infinite non-reflecting boundaries were used at the perimeter of model. The relatively large dimension of the model and non-reflecting infinite boundaries reduce the effect of reflected waves from the boundaries and result in a more accurate

dynamic analysis. It should be mentioned that the infinite boundary elements are also formulated to model far field response in a static analysis.

- *Dynamic Analysis Time Step:* The dynamic analysis of the FWD test was performed using an explicit time integration method. The explicit dynamic analysis procedure is based on the implementation of an explicit central difference time integration rule. Unlike implicit dynamic analysis methods that are unconditionally stable, the explicit dynamic analysis is only conditionally stable. The time step in this type of analysis should be small enough to prevent instability of the solution, which in simple terms means that the time step should be small enough to prevent information to propagate over more than one element per time step. This condition, which is sometimes referred to as Courant, Friedrichs, and Lewy (CFL) condition, requires selection of a time step Δt such that: $\Delta t < L/V_p$, where V_p is the compressional wave velocity and L is the smallest distance between two nodes in the model [Cook, Malkus, and Plesha, 1989].

Using the presented finite element model, the surface deflection time histories from the dynamic linear elastic analysis by ABAQUS® due to the presented loading wavelet are calculated and presented in Figure 5- 6. The material properties used in the definition of the model are presented in Table 5-1. The presented pavement profile was selected to be identical to the profiles considered in previous research studies, so that the theoretical accuracy of finite element model can be further verified through a comparison with the published deflection histories [Alkoughry et al, 2001]. The analysis was restricted

to 0.06 second because during the FWD test, pavement response is generally monitored for this period of time. ABAQUS® automatically adjusts analysis time step to satisfy CFL condition, however, the calculation results were reported at 0.001 second intervals.

As mentioned, the response of the presented pavement system under the idealized loading wavelet, has been also previously studied by other researchers. To verify the numerical accuracy of the developed finite element model, the model predictions were compared to the published results. The published pavement deflection histories [Alkhoury, 2001] for the same pavement model, as presented in Table 5-1, are presented in Figure 5-7. These results are in close agreement with the obtained finite element results presented in Figure 5-6. The predictions of dynamic models have been also compared to actual field measurements in general. In a recent study Loizos and Scarpas [2005] have verified that the predictions of dynamic finite element models are in fact in very good agreement with actual field measured values. Similar results were also published by Zaghloul et al. [1994].

Table 5-1 - Geometrical and material properties used for definition of finite element model.

Material Type	Thickness (m)	Elastic Modulus (MPa)	Rayleigh Damping Ratio	Poisson's Ratio	Mass Density (kg/m ³)
Asphalt Concrete	0.15	1000	0.001	0.35	2300
Aggregate Base Course	0.25	200	0.001	0.35	2000
Subgrade	infinity	100	0.001	0.35	1500

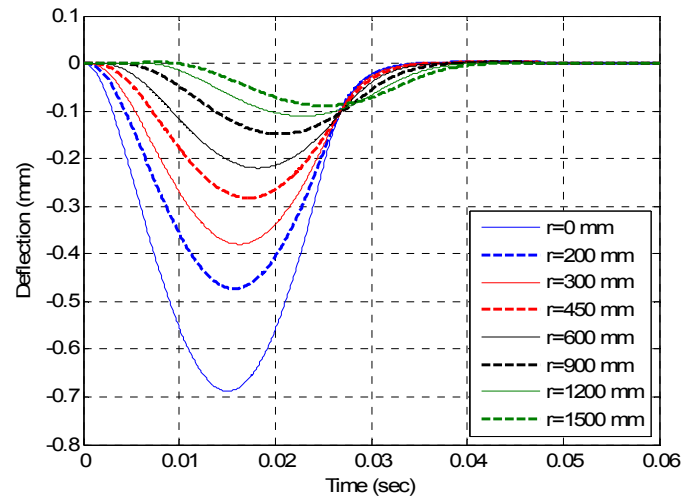


Figure 5-6 - Predicted pavement surface deflection time histories from ABAQUS® finite element model.

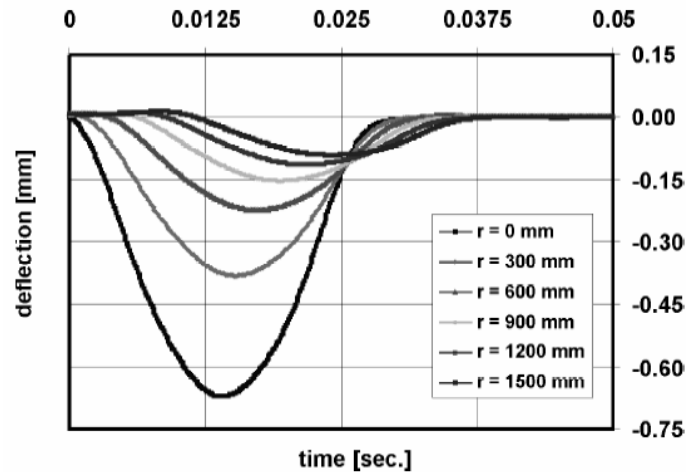


Figure 5-7 - Response of pavement surface deflection time histories [Alkhoury, 2001].

To be able to evaluate the probabilistic solution, modeling uncertainties should also be defined. In general, evaluation of modeling uncertainties is a complex task and further research is required to quantify such uncertainties. For examples presented in this chapter, based on the experience, nominal modeling uncertainties were assigned for each analysis.

Probabilistic Solution

It was shown in previous chapters that the probabilistic solution of the inverse problem is the a posteriori probability, which can be presented as:

$$\sigma_M(m) = \rho_M(m)\lambda(m) \quad (5-2)$$

where $\lambda(m)$ is the likelihood function:

$$\lambda(m) = k \exp\left(-\frac{1}{2}(d_{obs} - g(m))^T (C_T^{-1} + C_d^{-1})(d_{obs} - (g(m)))\right) \quad (5-3)$$

In these equations, the model parameter(s) m is the parameter(s) of interest in the problem, C_d is the covariance of the data a priori information (assumed Gaussian) and C_T is the uncertainty in prediction of forward model $g(m)$ (assumed Gaussian as well). In this chapter, this problem is solved using the Monte Carlo solution scheme with neighborhood approximation, as presented in Chapter 4. For backcalculation analysis presented in this study the data were considered to be a single vector formed by combining the data from individual receives.

Computational Time

The computational time for backcalculation analysis is directly proportional to the number of forward model runs. In the probabilistic approach, the number of the forward model runs depends on many factors, such as the number of model parameters, accuracy required in defining the probabilities and accuracy in identifying the maximum point of probabilities. The NA algorithm provides two variables to control the search effort and define accuracy of the results. For FWD backcalculation using a three layer pavement model, depending on the value of control parameters, the number of forward model runs can vary significantly (approximately from 50 runs to 500 runs). Obviously, the higher

the required accuracy or the number of the model parameters, the higher the number of forward model runs.

Backcalculation of Synthetic Test Data

Synthetic FWD Test Data

To be able to evaluate the performance of the probabilistic backcalculation approach, the approach is initially implemented on a set of synthetic FWD test results, where the material properties used for generation of the synthetic data are known. These data sets were generated using the described dynamic finite element model above. The material and geometric properties used in the generation of the synthetic data are the ones presented in Table 5-1.

The presence of the shallow bedrock affects the FWD test results. Therefore, in addition to the presented finite element model, where no bedrock was considered in development of the model (i.e. deep bedrock), another set of synthetic data with the similar finite element model was also generated, except that it was assumed that the bedrock is at 2 m below the surface (i.e. shallow bedrock). Deflection time histories for both these cases are depicted in Figure 5-8. Artificial, normally distributed random noise with a maximum amplitude of one micron, which is a typical resolution of the FWD displacement measurement [*Dynatest, 1995*], was added to these records to simulate environmental noise in actual FWD test data and to avoid potential numerical problems. The deflection bowls for the simulations with and without bedrock are also shown in Figure 5-9. It should be emphasized that the deflection bowls are obtained from time

histories of dynamic model. The presented deflection bowls as well as the time histories are used here as the synthetic FWD test results for input to the backcalculation routine.

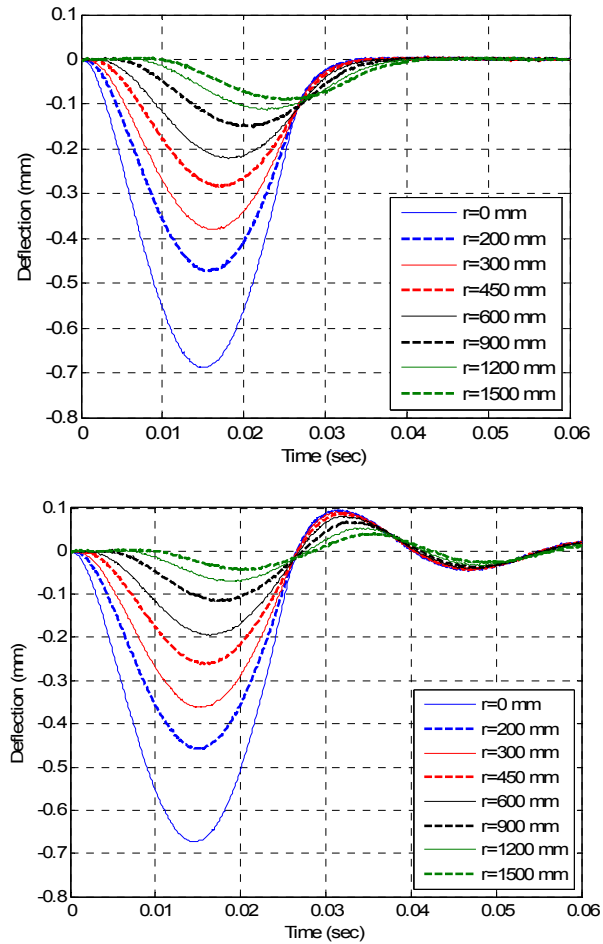


Figure 5-8 - Synthetic FWD data for no bedrock (top) and shallow bedrock at 2 m below the surface (bottom).

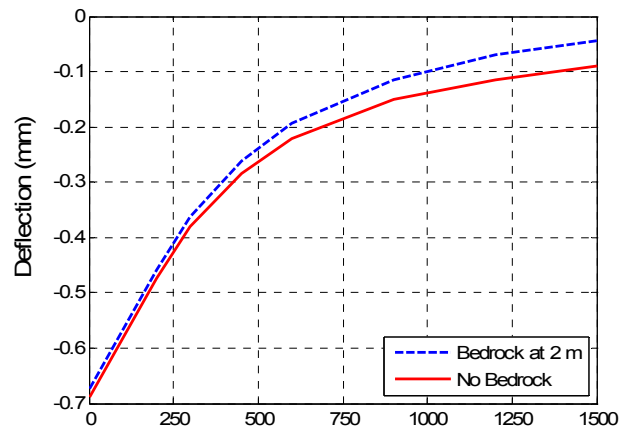


Figure 5-9 - Deflection bowls for synthetic FWD data.

Backcalculation of Layer Modulus based on Deflection Bowl Using Linear Static Forward Model

The first set of backcalculation analysis consists of backcalculation of layer moduli based on the deflection bowl measurements for the pavement section with a deep bedrock. The forward model in this backcalculation analyses was the static linear finite element model presented previously. The data uncertainty was considered to follow a Gaussian distribution with the mean equal to the observed value and a coefficient of variation of two percent. Although present, no modeling uncertainty was considered for this analysis.

One-dimensional kernel density estimates of marginal probability densities of the layer moduli from the backcalculation analysis are presented in Figure 5-10. A comparison between the observed deflection bowl and the deflection bowl corresponding to the most probable moduli values is also presented in the same figure. It can be observed that, although there is a reasonably good match between the observed and backcalculated deflection bowls, the backcalculated layer moduli are very different from the values used in the generation of the synthetic data. This discrepancy is basically due to modeling uncertainties that are not included in the backcalculation analysis. In other words, the synthetic observed deflection bowl, as presented in Figure 5-9, was generated using a linear dynamic finite element model. However, the backcalculation routine uses a static model to backcalculate for layer moduli. Unless this discrepancy in modeling is explicitly considered in the backcalculation, the final results would not be close to the target values used in the generation of the deflection bowl. It should be mentioned that

this approach to backcalculation is similar to the current dominant practice of FWD backcalculation, where the results of the FWD test (a dynamic test) are summarized in terms of the deflection bowl and are backcalculated using a static forward model. Based on this analysis, it can be observed that the static backcalculation, without an explicit consideration of modeling uncertainty, results in incorrect backcalculated values.

The fact that the static backcalculation may produce incorrect results has been previously acknowledged by other researchers. However, it is the general assumption that the difference in the obtained results is relatively small. Obviously, for the example presented here, this is not the case and this assumption should be further evaluated.

In the probabilistic backcalculation, the modeling uncertainties, can be explicitly considered in the analysis. To illustrate such an approach, the modeling uncertainty for this analysis has been evaluated by comparing the deflection bowls from static and dynamic analyses of the same pavement model for a range of layer modulus values, as presented in Table 5-2. The kernel density estimates of the absolute difference between calculated deflections from dynamic and static analyses for each receiver are depicted in Figure 5-11. The calculated histograms of the this absolute difference are also presented in this figure.

Table 5-2 – Range of layer moduli values used for evaluation of modeling uncertainties using deflection bowls from static analysis.

Material Type	Elastic Modulus Range (MPa)
Asphalt Concrete	500~4000
Aggregate Base Course	50~400
Subgrade	50~400

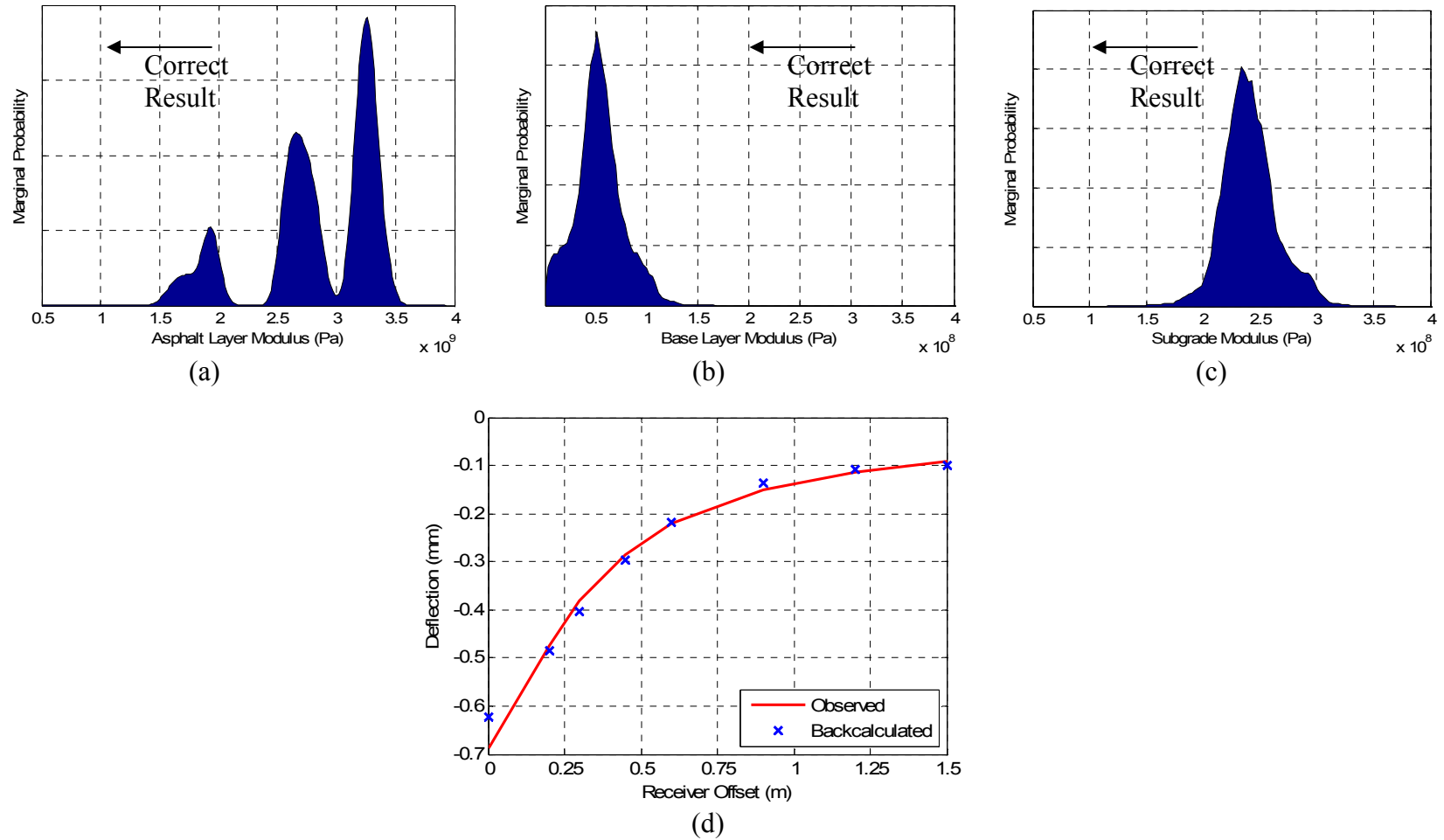


Figure 5-10 - (a, b and c) Kernel density estimates of marginal a posteriori probabilities for the layer moduli obtained from the probabilistic backcalculation of the deflection bowl with the static forward model without considering modeling uncertainties and (d) comparison of the backcalculated deflection bowls for the pavement section with the most probable layer moduli and the observed data.

The modeling uncertainty at each receiver for input in the backcalculation procedure can be evaluated by calculating the covariance of the difference between calculated deflections from dynamic and static analyses for each receiver. Based on this analysis, as a first estimate, a Gaussian distribution with a standard deviation of 0.1 mm will be used to represent the modeling uncertainty for all receivers. It can be observed that the evaluated modeling uncertainty is significantly higher than the data uncertainty. The uncertainty in data was shown to be small, with a coefficient of variation of about 2 percent, where the coefficient of variation for modeling uncertainty ranges from 20 to about 170 percent.

In the probabilistic approach with Gaussian data and model uncertainties, the covariance representing the modeling uncertainties can be added to the data uncertainty covariance. Using this approach, a new set of analysis was performed, which includes the combined effect of data and modeling uncertainties. One-dimensional marginal probability densities of the layer moduli from the backcalculation analysis are presented in Figure 5-12. It can be observed that the obtained probabilities have significant spreads, which indicated low reliability of the results. Based on these results, it can be concluded that due to high modeling uncertainties, the backcalculation of modulus using a static model is very unreliable.

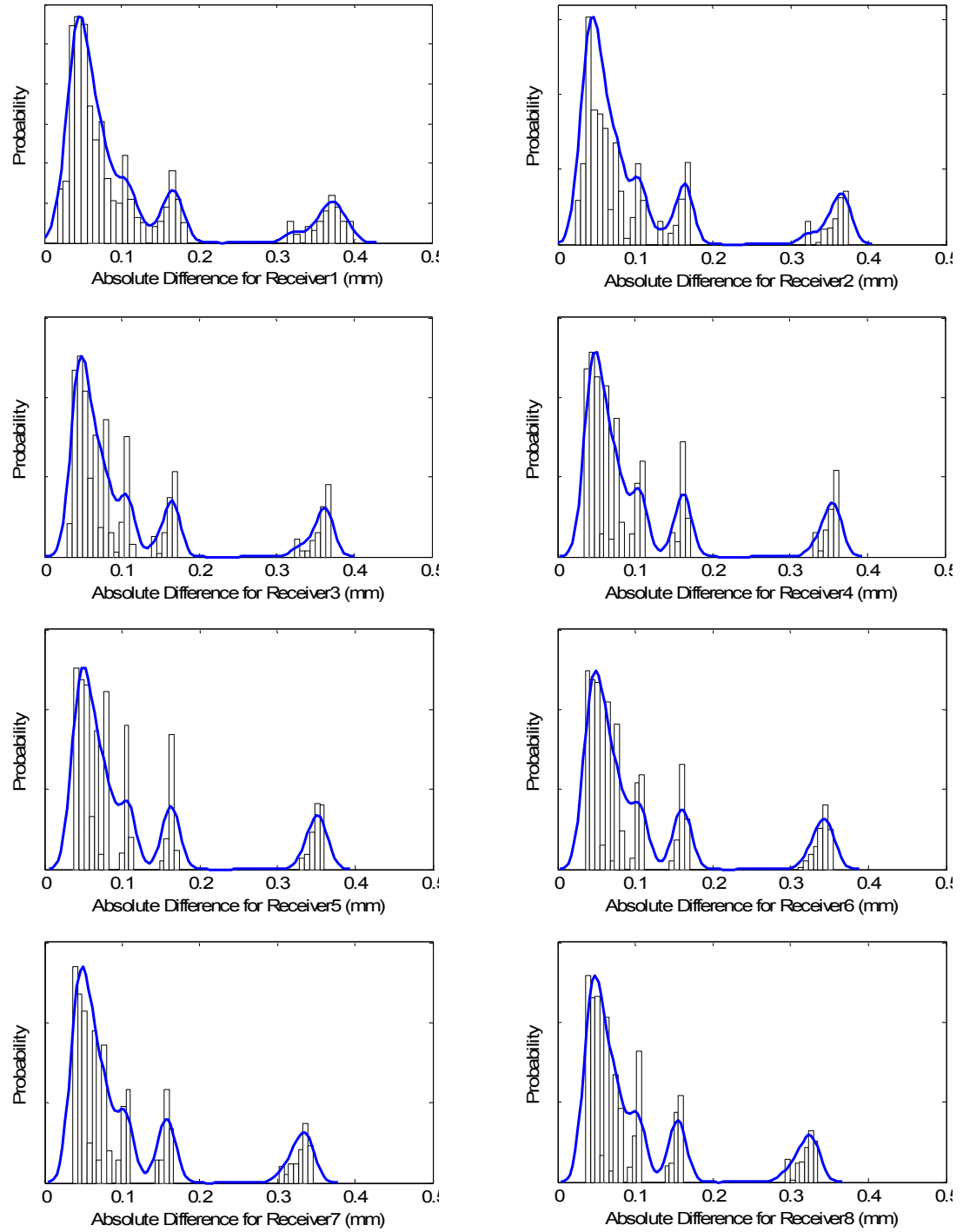
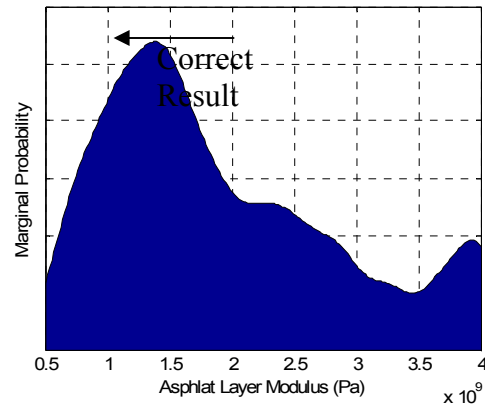
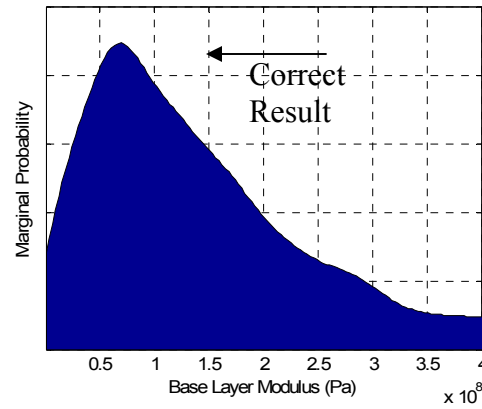


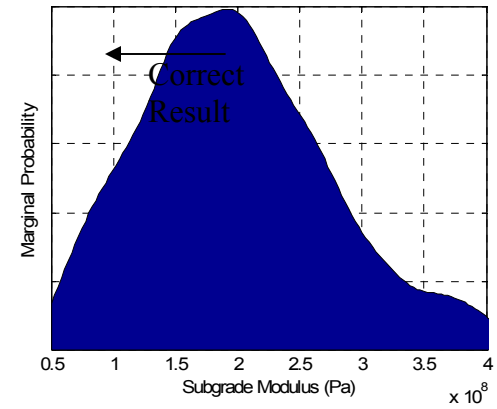
Figure 5-11 – Histograms and kernel density estimate of the absolute difference between the calculated maximum deflections from dynamic and static analyses at each receiver location and . The area under each density estimate is equal to one unit. The histograms are scaled to fit in the same figure.



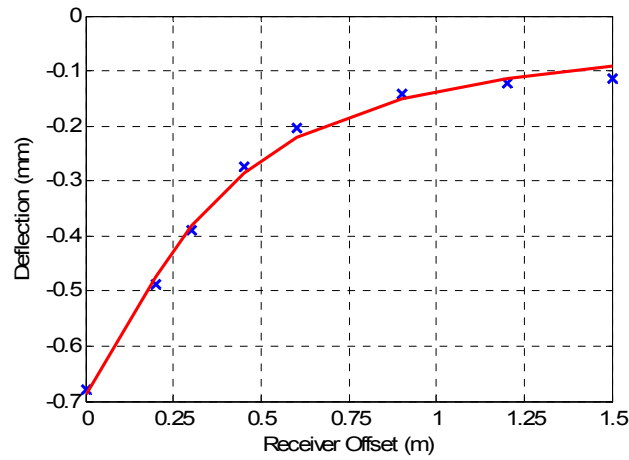
(a)



(b)



(c)



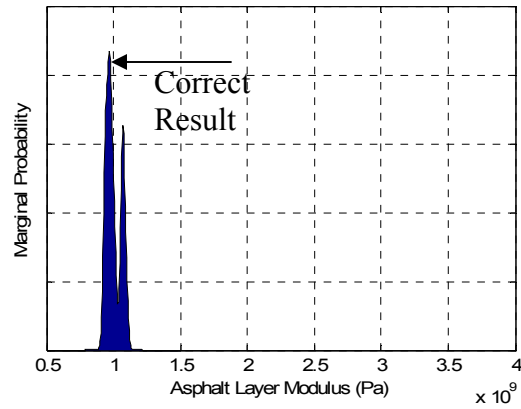
(d)

Figure 5-12 - (a, b and c) Kernel density estimates of marginal a posteriori probabilities for the layer moduli obtained from the probabilistic backcalculation of the deflection bowl with the static forward model, which includes the modeling uncertainties, and (d) comparison of the backcalculated deflection bowls for the pavement section with the most probable layer moduli and the observed data.

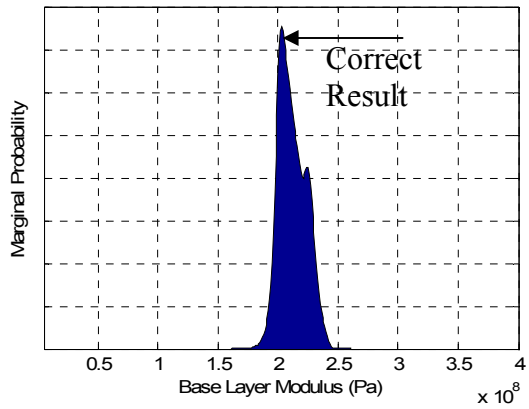
Backcalculation of Layer Moduli Based on Deflection Bowl Using Linear Dynamic Forward Model

It was shown that due to significant modeling uncertainties, the results of FWD deflection bowl backcalculation using static forward model are very unreliable. If instead of a static model, a dynamic model is used, the discrepancy and uncertainty in the modeling will be eliminated, and it is reasonable to expect that the analysis would recover the correct layer moduli. This expectation is in fact verified by the analysis results. Kernel density estimates of marginal probability densities for the layer moduli obtained from the probabilistic deflection bowl backcalculation with a dynamic forward model are presented in Figure 5-13. For this analysis, data uncertainty was considered to follow a Gaussian distribution with the mean equal to the observed value and a coefficient of variation of two percent. No modeling uncertainty was considered, because the same model was used to generate both theoretical and observed deflection bowls. As depicted, the backcalculation results have peaks at the correct modulus values. A comparison of the observed and backcalculated deflection bowls are also presented in the same figure.

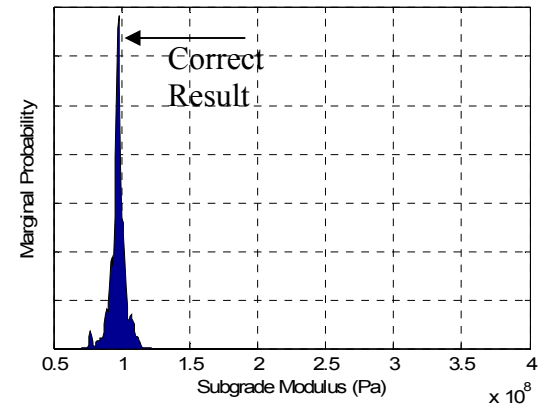
By review of the presented results, it can be observed that, even though the data uncertainty is very small (a coefficient of variation of two percent was used as presented previously) and there is no modeling uncertainty (the same model was used in the generation of theoretical and synthetic data), the backcalculated values have a relatively large spread and display several peaks. This spread and multiple peaks can be related to the sensitivity of the deflection bowl data to the layer modulus values.



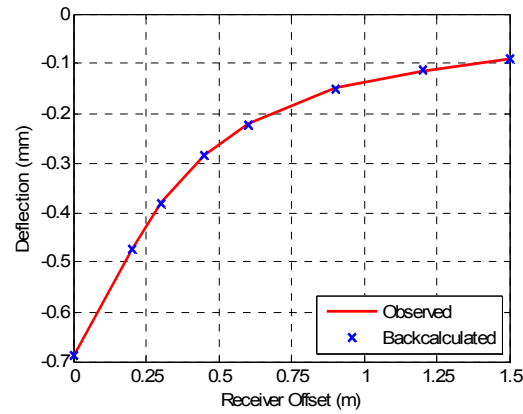
(a)



(b)



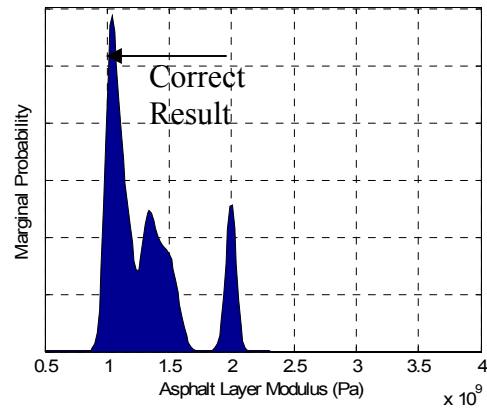
(c)



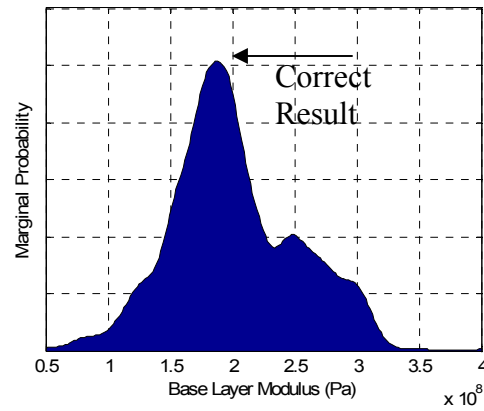
(d)

Figure 5-13 - (a, b and c) Kernel density estimates of marginal a posteriori probabilities for the layer moduli obtained from the probabilistic backcalculation of the deflection bowl with the dynamic forward model and (d) comparison of the backcalculated deflection bowls for the pavement section with the most probable layer moduli and the observed data.

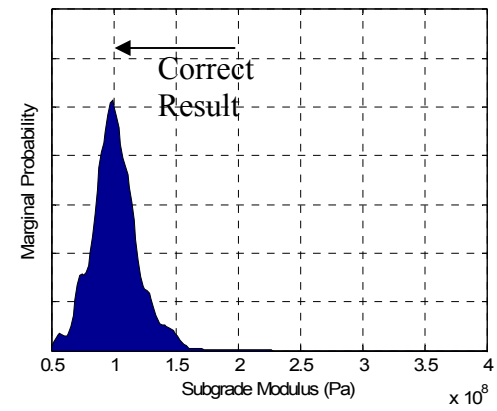
Deflection bowl backcalculation procedures rely heavily on deflection measurements at discrete points. For the specific analysis presented here, eight discrete deflection measurements were used to backcalculate three unknown modulus values. So, it should be expected that any uncertainty in the deflection measurement and/or theoretical modeling would translate into a relatively significant variation of backcalculated moduli. This statement can be demonstrated in the probabilistic approach by increasing the uncertainty in data. Figure 5-14 depicts the kernel density estimates of marginal probabilities for the same problem with a combined data and modeling uncertainty coefficient of variation of eight percent. It can be observed that the spread of the backcalculated moduli has increased significantly. The increase in the spread indicates that, if for any reason the uncertainty in data or model increases, the reliability of backcalculation results based on the deflection bowl would decrease significantly.



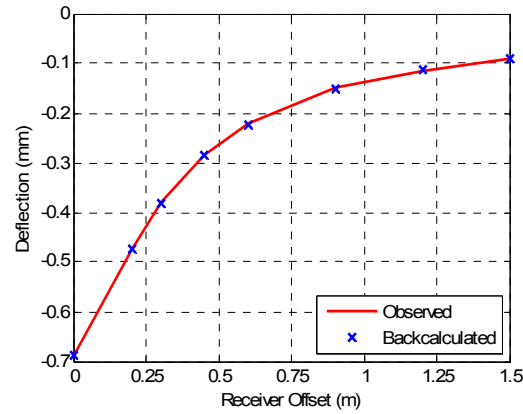
(a)



(b)



(c)



(d)

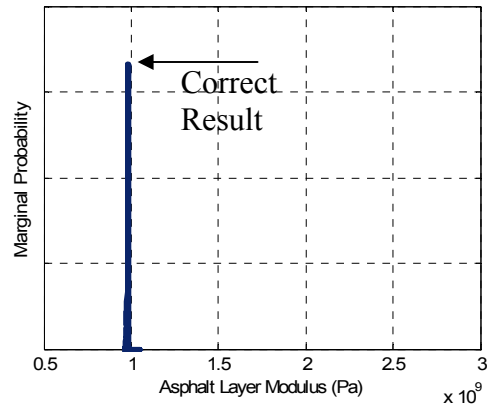
Figure 5-14 -(a, b and c) Kernel density estimates of marginal a posteriori probabilities for the layer moduli obtained from the probabilistic backcalculation of the deflection bowl with the dynamic forward model with high model and data uncertainty and (d) comparison of the backcalculated deflection bowls for the pavement section with the most probable layer moduli and the observed data.

The heavy reliance of the deflection bowl backcalculation on a very small set of data has resulted in difficulties in the deterministic backcalculation procedures, such as inconsistency of the results from different programs and analysts for the identical a set of data. As it has been shown, the a posteriori probabilities may have multiple peaks. In the deterministic backcalculation procedures, presence of several peaks means that the deterministic procedures can be trapped in any of the peaks and report the corresponding value as the backcalculation result. This means that there is chance that the reported values are not the correct values. This is a very serious problem, especially when the uncertainty in data increases. Such an increase should be expected for actual FWD test data, because for the experimental data, in addition to data uncertainty, there is always a modeling uncertainty component. Therefore, it can be concluded that, although the deflection bowl backcalculation using dynamic models can be used to correctly backcalculate the moduli, the relatively low sensitivity of the moduli to data (or in other words low information content of data) may produce a rather large uncertainty in the backcalculated result.

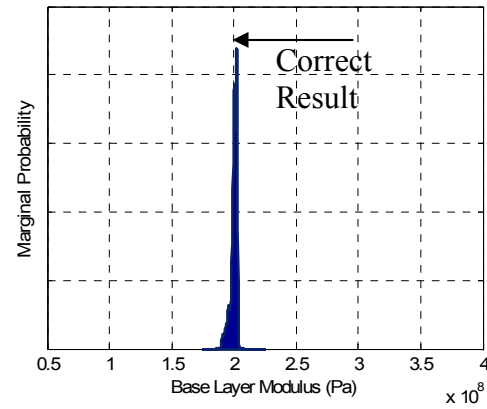
Backcalculation of Layer Moduli Based on Deflection Time History Using Linear Dynamic Time Domain Forward Model

Intuitively, deflection time histories of the FWD test carry significantly more information regarding the pavement than the discrete deflection bowl measurements. So, it is expected that the backcalculation procedures that use time histories should provide more reliable results. This in fact can be observed from the backcalculation of the synthetic test result on the pavement section with a deep bedrock using the dynamic

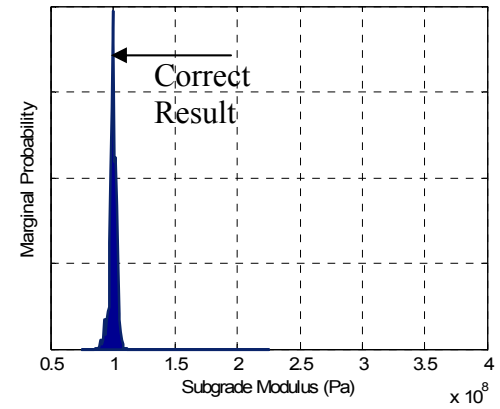
forward model. For this backcalculation analysis, the data uncertainty coefficient of variation was selected to be two percent and no modeling uncertainty was considered, because the same model was used in the generation of synthetic results, as well as theoretical data. Kernel density estimates of marginal a posteriori probability densities for the layer moduli obtained from the probabilistic backcalculation are presented in Figure 5-15. A comparison of the backcalculated deflection time histories for the pavement section with the most probable layer moduli and the observed data are also presented in the same figure. As presented, these results have much sharper peaks at the correct moduli values. So, it can be concluded that using the complete deflection time history as the data is a much more reliable approach in the FWD backcalculation. The main practical problem in using this approach is its computational cost in terms of calculating the dynamic response of the pavement. However, with a rapid increase in the available computational power and availability of faster forward modeling approaches, the additional computational cost should not be considered as a major obstacle.



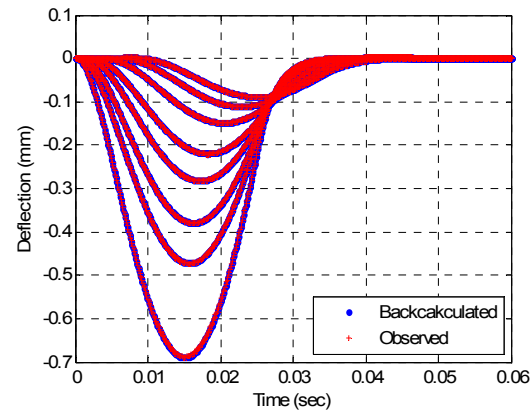
(a)



(b)



(c)



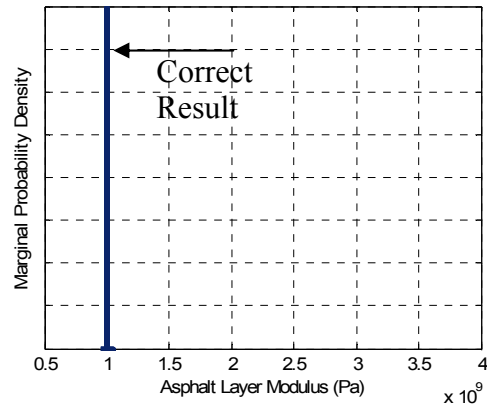
(d)

Figure 5-15 - (a, b and c) Kernel density estimates of marginal a posteriori probabilities for the layer moduli obtained from the probabilistic backcalculation of the deflection time history with the dynamic forward model and (d) comparison of the backcalculated deflection time histories for the pavement section with the most probable layer moduli and the observed data. The two time histories are overlapping.

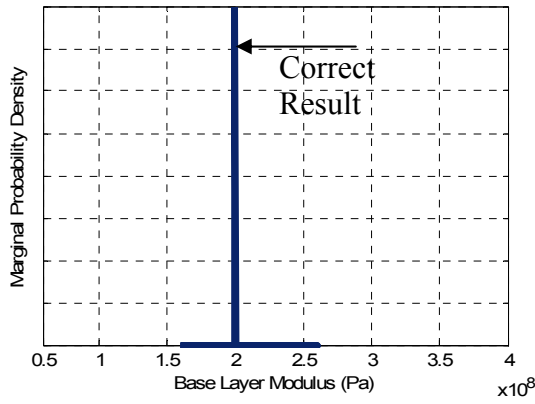
Backcalculation of Layer Moduli and Depth to Bedrock Based on Deflection Time History Using Linear Dynamic Forward Model

The pavement response to FWD impact is remarkably different when a shallow bedrock is present, compared to when it is not. Consequently, the backcalculation of moduli should consider the effect of the bedrock. There is no direct indication of the presence of a shallow bedrock in deflection bowl measurements. However, presence of a shallow bedrock can be recognized by low amplitude reflections present at the later part of a time record. Currently, available backcalculation procedures rely on the ability and experience of the analyst to recognize presence of a shallow bedrock, estimate its depth, and include its effect in the analysis.

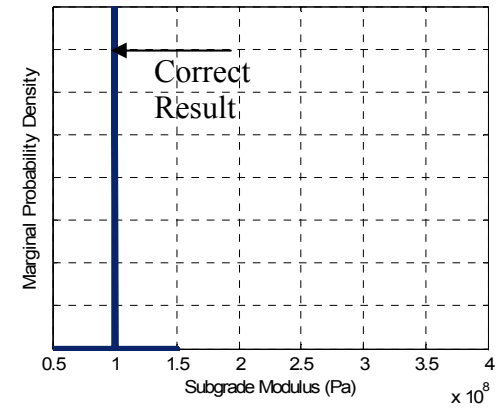
Conceptually, the depth to bedrock can be considered as one of the model parameters that should be resolved from the backcalculation analysis. Any prior estimates of the depth to bedrock, if available, can also be included as a priori information. Using this method, the solution of the backcalculation problem simultaneously provides the backcalculated values of the depth to bedrock, as well as pavement layer moduli. To evaluate such an approach, the backcalculation of time histories of the synthetic test with a shallow bedrock was performed, where the depth to bedrock was considered to be one of the model parameters. Marginal a posteriori probability densities for the layer moduli and depth to bedrock obtained from the probabilistic backcalculation are presented in Figure 5-16. A comparison of the backcalculated deflection time histories for the pavement section with the most probable layer moduli and the observed data are also presented in this figure.



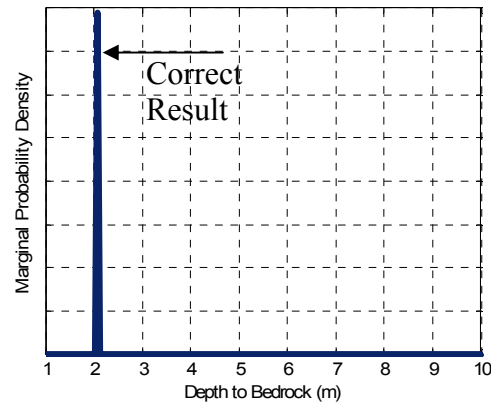
(a)



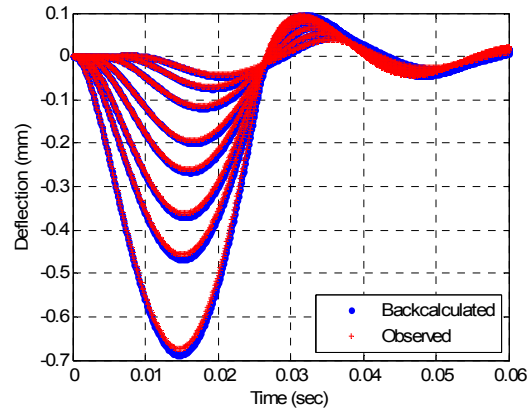
(b)



(c)



(d)



(e)

Figure 5-16 - (a, b, c and d) Kernel density estimates of marginal a posteriori probabilities for the layer moduli and depth to bedrock obtained from the probabilistic backcalculation of the deflection time histories with the dynamic forward model and (e) comparison of the backcalculated deflection time histories for the pavement section with the most probable layer moduli and the observed data.

As presented, these results have sharp peaks at the correct moduli and depth to bedrock values, confirming the possibility of simultaneously backcalculating moduli and depth to bedrock with low levels of uncertainty. However, the additional information (i.e. the depth to bedrock) is obtained at the expense of additional computational cost required to search a higher dimension model space and locate the “good” regions of the space. This analysis demonstrates that the dynamic deflection time histories carry much more information than deflection bowls and, thus, confirms that using time histories as the input data is a much more reliable approach in the FWD backcalculation.

Backcalculation of Layer Moduli and Thickness Based on Deflection Time History Using Linear Dynamic Forward Model

Theoretically, the thickness and moduli of pavement layers can be both considered as the model parameters in a backcalculation analysis. Including the thickness in backcalculation analysis increases the number of model parameters, which in turn would require more computational effort in the search stage. Limited backcalculation analyses performed as part of this research were not successful in recovering the correct thickness and moduli and further work is required to investigate the possibility of backcalculation of thickness and moduli from time history data.

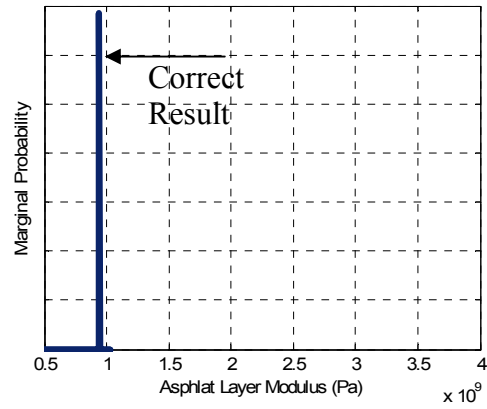
Backcalculation Based on Velocity Time History

Most often, the transducers used in FWD testing do not directly measure the pavement deflection. These transducers generally measure the particle velocity of the

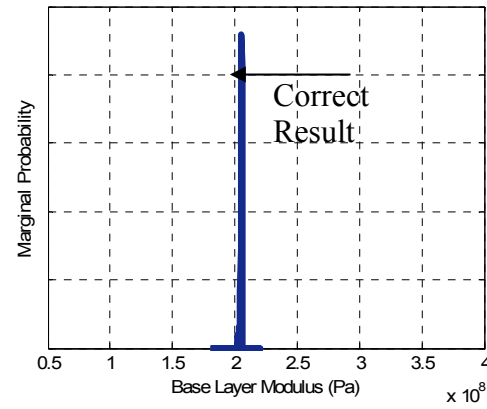
pavement motion following the impact. The measured velocity history is then integrated to evaluate the pavement deflection history. The integration introduces additional uncertainties in the analysis. If the resolution of the transducers is low or the noise level is high, such uncertainties can be significant. To reduce such uncertainties, the backcalculation analysis can be performed using the velocity time histories as data.

For the backcalculation analysis presented in this research, there is no fundamental difference between using the velocity time histories or the deflection time histories. The deflection data has been historically used in FWD backcalculation mainly because it is more tangible. However, if using the deflection data introduces additional uncertainties; the backcalculation can be performed on the velocity level.

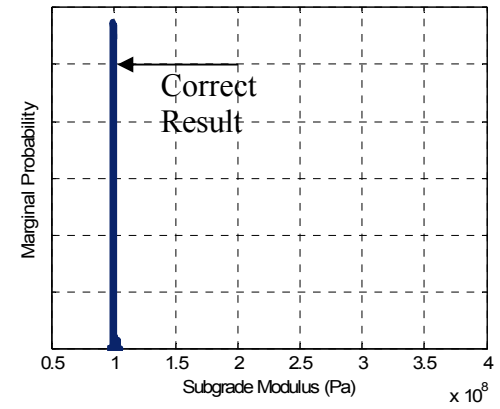
The feasibility of such analysis is illustrated here by the backcalculation of velocity time histories of pavement during the synthetic FWD test. For this analysis, similar to the previous analyses, the data uncertainty coefficient of variation was chosen to be two percent. Marginal a posteriori probability densities for the layer moduli obtained from the probabilistic backcalculation are presented in Figure 5-17. A comparison of the backcalculated velocity time histories for the pavement section with the most probable layer moduli and the observed data are also presented in the figure. Based on the presented results, it can be observed that the velocity backcalculation can be used to backcalculate the correct layer moduli with small uncertainty.



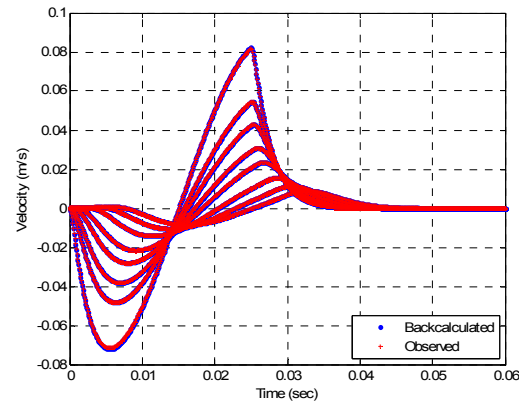
(a)



(b)



(c)



(d)

Figure 5-17 - (a, b, and c) Kernel density estimates of marginal a posteriori probabilities for the layer moduli obtained from the probabilistic backcalculation of the velocity time histories with the dynamic forward model and (d) comparison of the backcalculated velocity time histories for the pavement section with the most probable layer moduli and the observed data.

Backcalculation of FWD Test Data

The objective of the analysis presented in this section is to demonstrate the applicability of the presented probabilistic approach for backcalculation of the actual FWD test results. To achieve this objective, time records of the actual tests are backcalculated using a dynamic forward model to obtain the layer moduli. Details of the analysis are presented in this section.

FWD Test Results

The test results used in this section were collected as a part of the FWD monitoring program performed in the course of a research project on pavement material characterization and seasonal variation of properties conducted jointly by Rutgers University and Stantec, Inc. The details of the project and its results have been published in a number of reports and papers [Zaghloul *et al.* 2006, Gucunski *et al.* 2004]. For the analysis in this section, the results from the section No. 340507 of SPS-5 test site are used. The load and deflection records for this test are shown in Figure 5-18. Inspection of the recovered core at this section indicates that the thickness of the paving layer is about 0.36 m and it is underlain by a base layer of about 0.275 m thick. The presented data are used as the input to the backcalculation analysis to obtain the layer moduli and corresponding uncertainty measures based on the deflection time histories.

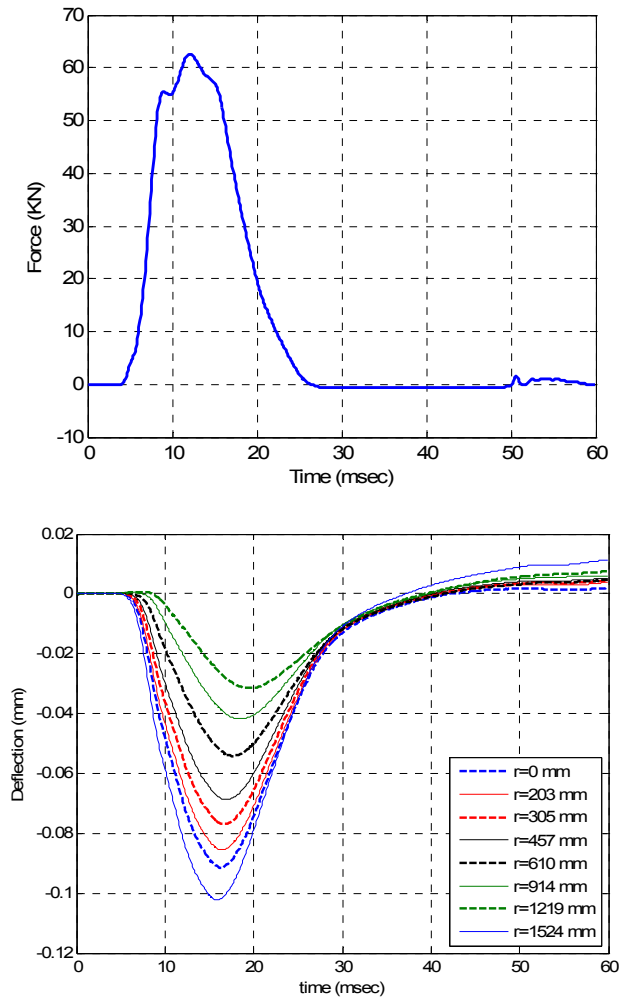


Figure 5-18 - Measured loading history (top) and pavement response for FWD test.

Backcalculation Results

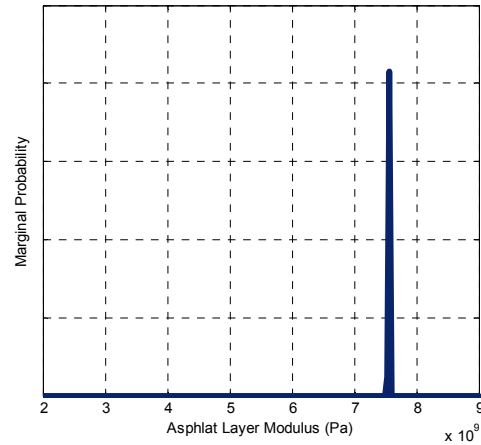
For this backcalculation analysis, the presented loading history was used as an input to the analysis to model the test. The data uncertainty coefficient of variation for the presented analysis was selected to be two percent and modeling uncertainty was considered to be negligible. Both these assumptions will be examined in the next section. Kernel density estimates of marginal a posteriori probability densities for the layer moduli obtained from the probabilistic backcalculation are presented in Figure 5-19. A

comparison of the backcalculated deflection time histories for the pavement section with the most probable layer moduli and the observed data are also presented in the same figure. As presented, these results have sharp peaks at the moduli values. So, it can be concluded that using the complete deflection time history as the data it is possible to backcalculate the experimental FWD data for layer moduli. It should be mentioned that the accuracy of these results should be further validated with a more extensive study.

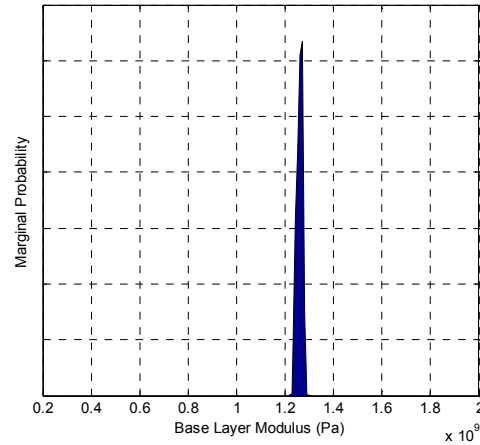
A Discussion on Data and Modeling Uncertainties

For the presented analysis of experimental data, it was assumed that modeling uncertainty is negligible and the data uncertainty coefficient of variation was selected to be two percent. Due to many factors, there are modeling uncertainties in predictions of forward models. An evaluation of such uncertainties is required before routine application of the presented approach for backcalculation of experimental FWD measurements. Some sources of uncertainty are discussed below.

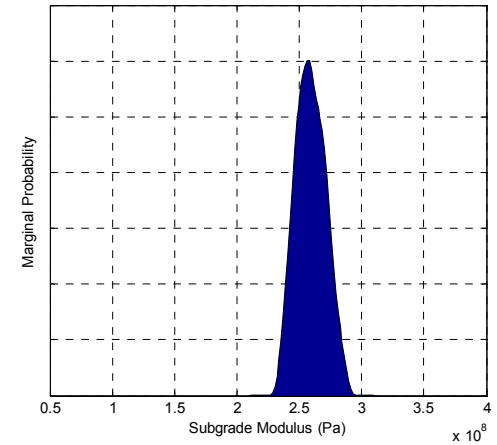
Based on the presented time history records, the data uncertainties seem to be much higher than assumed two percent. As presented in Figure 5-17, there are residual deflections at the end of the record, which is not present in theoretical results. A possible explanation for these residual displacements at the end of the record is that they are numerical artifact produced as a result of a poor transducer resolution. As mentioned previously, the response of the pavement during a FWD test is measured by geophones, which measure the velocity. To obtain displacement records, the velocity records are numerically integrated. Consequently, the poor resolution of the velocity records and/or presence of noise, would translate to a poor quality of deflection records.



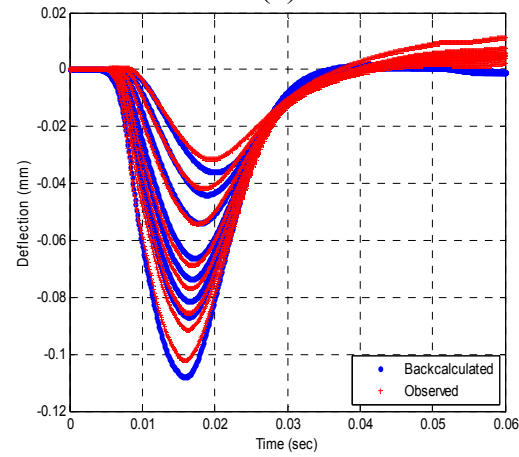
(a)



(b)



(c)



(d)

Figure 5-19 -(a, b, and c) Kernel density estimates of marginal a posteriori probabilities for the layer moduli obtained from the probabilistic backcalculation of the experimental deflection time histories with the dynamic forward model and (d) comparison of the backcalculated deflection time histories for the pavement section with the most probable layer moduli and the observed data.

For the set of the data presented in Figure 5-17, the velocity time histories can be calculated by differentiating the time history records. The velocity time history record for the receiver at a zero offset distance is presented in Figure 5-20 as a typical result. The poor resolution of the velocity record is evident from the jumps in the data. Such poor quality may explain residual displacements in the deflection records, which ultimately would affect the backcalculation results and increase the uncertainties. An alternative explanation for the residual displacements can be the low frequency vibration of the frame supporting the test apparatus. A thought understanding of the sources of uncertainty requires a more detailed study. However, this brief discussion highlights the necessity of quantifying the magnitude of the uncertainties in the data so that they can be appropriately represented in probabilistic backcalculation.

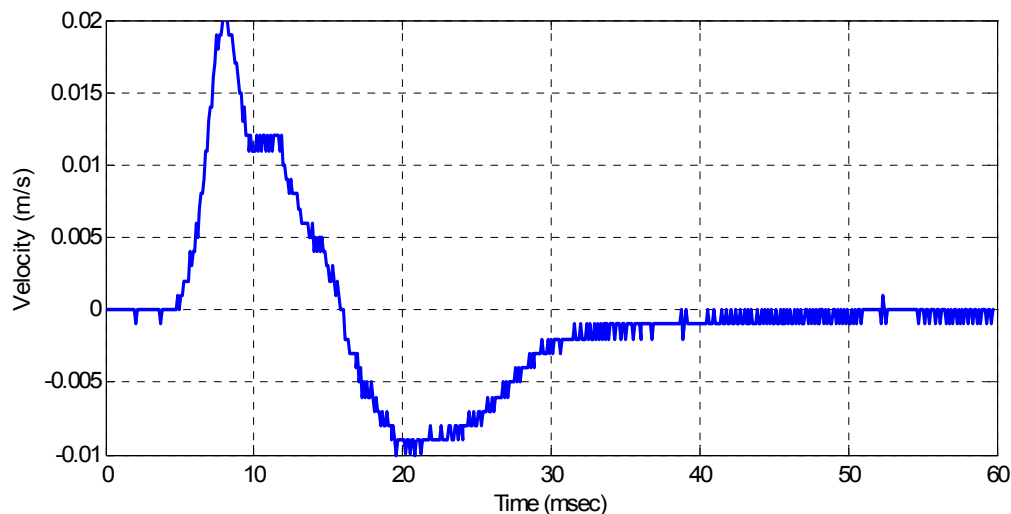


Figure 5-20 - Measured velocity time history record at receiver at zero offset.

Effect of Considering Dynamic Material Properties of Pavement Layers on Backcalculation Results

Dynamic Moduli and Damping of Pavement Layers

In FWD backcalculations, the pavement system is generally modeled as a layered elastic system, where the layer thicknesses and moduli are the model parameters. In the current practice, the layer thicknesses are often evaluated prior to the tests and are considered as a given input for backcalculation. So, pavement layer moduli are the only model parameters that should be evaluated in the backcalculation.

Since the FWD test is in principle a dynamic test, the evaluated pavement moduli can not be treated as static elastic moduli of pavement layers. Furthermore, the dynamic pavement response is affected by internal or material damping of pavement layers, which should be included in the analysis.

Moduli of pavement layers vary considerably throughout the year based on environmental factors and the type of pavement layers. However, for backcalculation purposes, the moduli of the pavement layers are assumed constant during the very short period of the test. The validity of this assumption is investigated here.

Granular Layers

Among the factors that affect the moduli of granular layers during the short period of FWD test, strain level is the only important factor that can not be considered constant. From the field experience, for good pavements, the strain levels during the FWD test are generally below 0.1% for the paving layer and are in the order of 0.01% for granular layers [Lozios, *et. al.* 2003]. The variation of modulus and damping of sands with strain

is presented in Figure 5-21 as representative of the typical behavior of granular layers. Based on these graphs, for strain levels encountered during the FWD test, the modulus and damping of the soil layers can essentially be considered constant and very close to the low strain static modulus. Additionally, based on these results, a hysteretic damping ratio of two to six percent is a good representative of the damping of granular pavement layers.

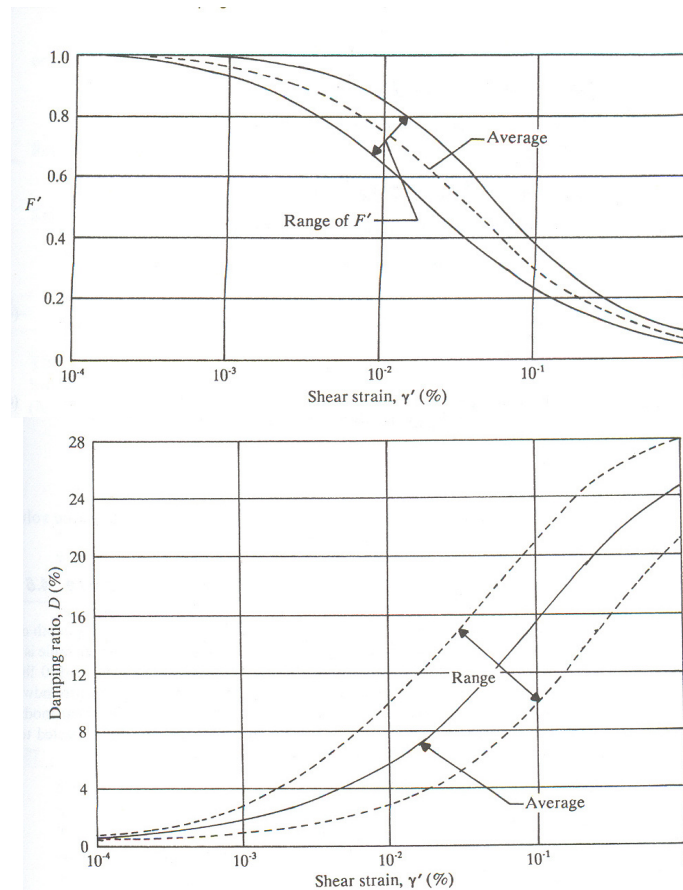


Figure 5-21 - Variation of modulus (top) and damping (bottom) with shear strain for sands [Seed et. al. 1986]. F' indicates the ratio of the modulus at each frequency to the static modulus.

Asphalt Layer

The most important factor during the short period of FWD test that affects the modulus of the asphalt layer is the excitation frequency. The variation of the pavement dynamic modulus with frequency is quantified by the modulus master curve [NCHRP 9-19, 1999]. The master curve of a specific asphalt mixture allows evaluation and comparison of the asphalt modulus over an extended range of frequencies and temperatures. In the definition of the master curve, the modulus is defined as a complex modulus, where the absolute value represents the modulus value and the phase angle can be translated into damping. Master curves are generated based on the time-temperature superposition principle. This principle allows for test data collected at different temperatures and frequencies to be shifted horizontally relative to a reference temperature or frequency. Typical modulus master curve for an asphalt mixture is presented in Figure 5-22.

The master curve is defined by a nonlinear sigmoidal function of the following form [NCHRP 9-19, 1999]:

$$\log|E^*| = \delta + \frac{\alpha}{1 + e^{\beta + \gamma(\log(f) + s_T)}} \quad (5-4)$$

where, E^* is the complex modulus, δ is the minimum value of the modulus, $\delta + \alpha$ is the maximum value of modulus, β and γ are parameters describing the shape of function, s_T is the temperature shift factor, and f is the load frequency.

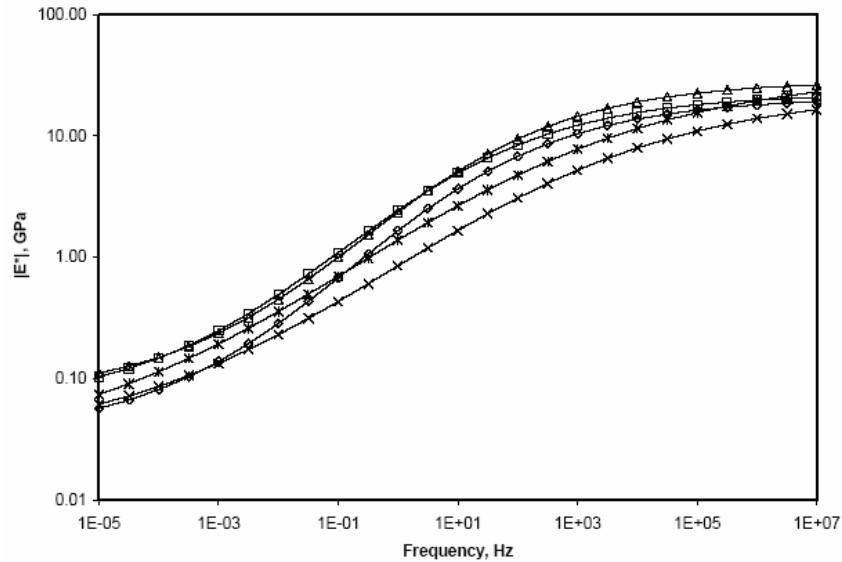


Figure 5-22 - Typical modulus master curves for different asphalt mixtures [Clyne et. al. 2003].

The dominant portion of the excitation frequency of the FWD loading pulse is generally below 100 Hz. As presented in the sample curves, for this range of frequencies, the modulus can not be considered constant. Consequently, the assumption of constant modulus during the backcalculation is not accurate, and effect of changes in modulus in forward modeling and backcalculation should be studied and, if necessary, included in the modeling and backcalculation.

The variation of internal damping of asphalt is much less than the variation of modulus. Considering the small range of the damping ratios encountered, a constant hysteresis damping ratio of two to five percent is representative of the damping of an asphalt layer.

Concrete Layer

It is generally accepted that the modulus and damping of the cured concrete is constant for the range of frequency and strain levels encountered during the FWD test.

Numerical Modeling of Dynamic Moduli and Damping

It has been shown that changes in frequency of excitation are the most important factor affecting the pavement layer material properties during the short period of a FWD test. So far, the moduli of pavement layers in presented backcalculation analysis were considered to be independent of frequency and constant. This is the assumption generally used in the current backcalculation procedures. However, as illustrated, the modulus of asphalt is dependent on the frequency of excitation. Furthermore, the material damping in finite element analysis was modeled as Rayleigh damping, which is a frequency dependent damping. In other words, the damping ratio varies for different excitation frequencies. However, as shown, the damping of pavement layers is generally constant. The constant, frequency independent damping is modeled more appropriately using a hysteresis damping model.

Modeling frequency dependent material properties in time domain is not straight forward. The most convenient approach to include frequency dependent material properties in the analysis is to use a frequency domain modeling approach. In the frequency domain modeling, the response of the pavement system is obtained by a synthesis of waveforms of many frequency components. In this research, a recently developed frequency modeling technique, referred to as spectral element method, is used to model the pavement response in the frequency domain. A general description of a

typical spectral element model of a pavement section and sample results are presented below.

Frequency Domain Forward Model using Spectral Element Method

Spectral element method is a modeling approach for evaluation of the dynamic response of horizontally layered media, such as pavements. Computationally, spectral element method is a much more efficient method than the finite element modeling. In this technique the solution is obtained by a synthesis of waveforms of many frequency components, which are in part are obtained analytically. An overview of the mathematical derivation and numerical implementation of this method is provided in Appendix A. A more comprehensive explanation of this technique can be found in cited references [Alkhoury, 2001, Rizzi and Doyle, 1992, Doyle, 1997].

For this study, a Matlab® code was developed to implement the spectral element approach. The predicted surface deflection time histories evaluated by spectral element method due to an idealized loading wavelet, presented previously, are shown in Figure 5-23. Except for the damping ratios, the material properties used in the numerical evaluation of the presented histories are similar to those used for the finite element model. These properties are also listed in Table 5-3.

Table 5-3 - Geometrical and material properties used for development of spectral element results.

Material Type	Thickness (m)	Elastic Modulus (MPa)	Hysteresis Damping Ratio	Poisson's Ratio	Mass Density (kg/m ³)
Asphalt Concrete	0.15	1000	0.05	0.35	2300
Aggregate Base Course	0.25	200	0.02	0.35	2000
Subgrade	infinity	100	0.02	0.35	1500

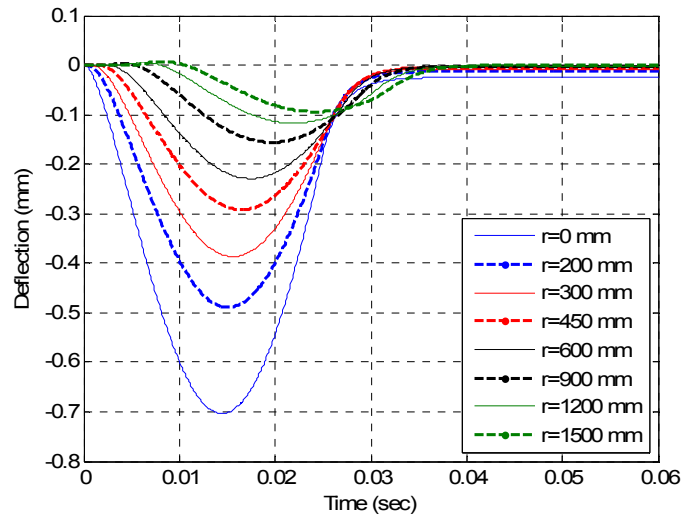


Figure 5-23 - Predicted pavement surface deflection time histories from linear spectral element analysis.

Comparison of Time and Frequency Domain Models

The predicted surface deflections from time domain and frequency domain models for the pavement system in previous sections are compared in Figure 5-24. Since tow models use different damping models, the results were not expected to match and no attempt was made to vary the damping ratio to match them. However, the results are a qualitative verification of the modeling approaches. As presented, the two results are in a very good agreement. The slight difference in the predicted response is due to the difference in the formulation of damping in time and frequency domain analyses, as discussed previously. In the time domain, damping is modeled as Rayleigh damping, where as in the frequency domain, damping is modeled as hysteresis damping. The hysteresis damping is constant through out the analysis, but Rayleigh damping varies depending on the frequency of excitation. Effects of this difference on the backcalculation results are investigated in the next section.

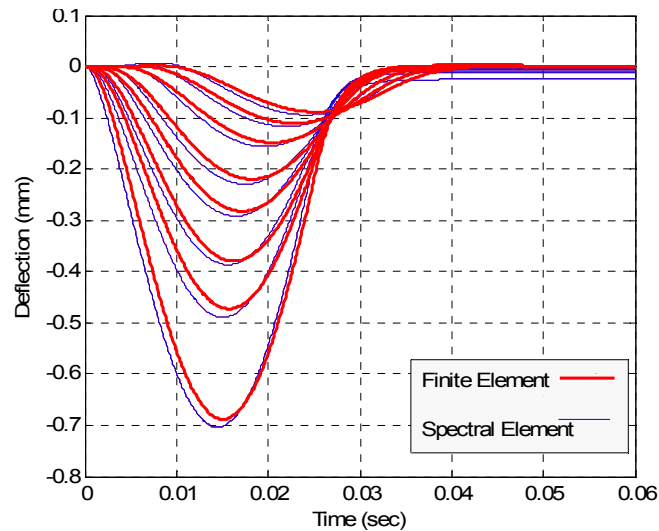


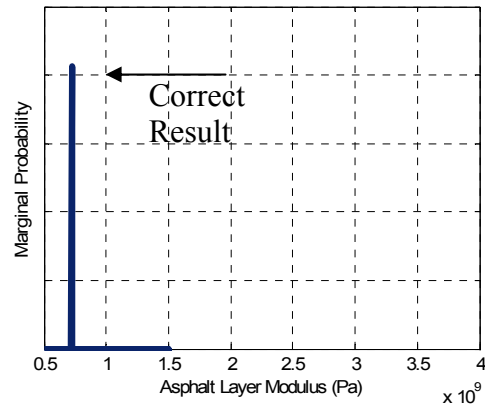
Figure 5-24 - Comparison of predicted surface deflections at different receiver location from time domain and frequency domain models.

Backcalculation of Layer Moduli Based on Deflection Time History Using Linear Dynamic Frequency Domain Forward Model

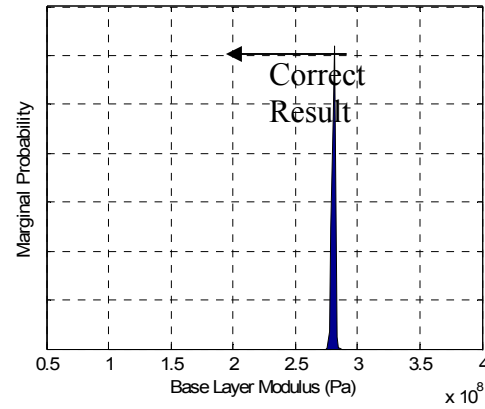
It has been shown that due to the difference in the damping model, there will be differences in the analysis results for the same pavement system using time or frequency domain models. The general assumption in the backcalculation analysis presented so far was that due to low sensitivity of the pavement response to damping ratios, the difference in the damping model is not expected to be a major source of discrepancy in backcalculation results. To evaluate this assumption, a backcalculation analysis was performed, where the pavement deflection time histories obtained from the finite element analysis were used as synthetic data and the backcalculation was done using a spectral element forward model. The synthetic data was presented previously in Figure 5-8. In this analysis, it has been assumed that the modeling uncertainty is negligible. In other words, it has been assumed that the spectral element results are comparable to finite element results. Marginal a posteriori probability densities for the layer moduli obtained

from the probabilistic backcalculation are presented in Figure 5-25. A comparison of the backcalculated deflection time histories for the pavement section with the most probable layer moduli and the observed data are also presented in the figure.

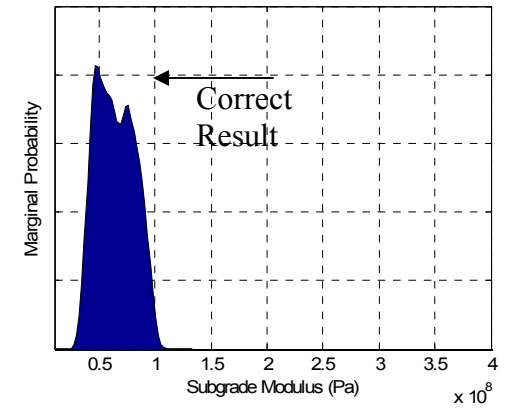
It can be observed that, even though there is good match between the observed and backcalculated time histories, the backcalculated layer moduli are not correct. This result can be explained by the difference between the spectral element and finite element time history results. Consequently, the modeling uncertainties should be included in the analysis. This result is important because it highlights the importance of considering the modeling uncertainties in the analysis.



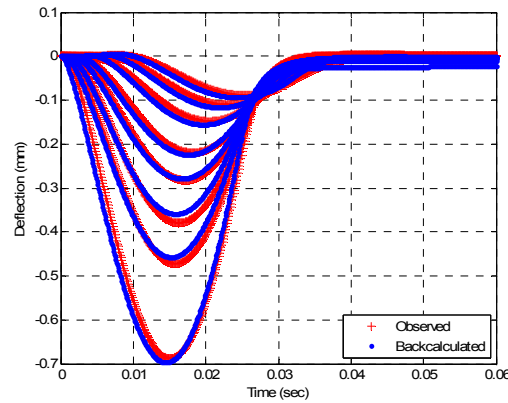
(a)



(b)



(c)



(d)

Figure 5-25 - (a, b and c) Kernel density estimates of marginal a posteriori probabilities for the layer moduli obtained from the probabilistic backcalculation of the deflection time history with the spectral element forward model and (d) comparison of the backcalculated deflection time histories for the pavement section with the most probable layer moduli and the observed data.

Pavement Response with Dynamic Moduli

For the FWD test, modulus and damping of granular and cement concrete layers, and damping of on asphalt layer can be considered constant in forward modeling and backcalculation of pavement layer moduli. However, the asphalt layer modulus is strongly dependent on frequency of excitation for the frequency range of interest in FWD tests. To study the effect of variable moduli on the analysis results, a dynamic analysis using spectral element method was performed, where the frequency modulus master curve were used to model the frequency dependent asphalt modulus. Except for damping and modulus values, the geometry and material properties used in the analysis are basically the same properties used in the finite element and spectral element analyses presented. The modulus and damping values used in this analysis are presented in Table 5-4. For this analysis, the asphalt modulus was calculated at each frequency based on the sample modulus master curve presented in Figure 5-26. The predicted surface deflection time histories due to an idealized loading wavelet are shown in Figure 5-27.

Table 5-4 – Modulus and damping values used for numerical evaluation of spectral element analysis.

Material Type	Elastic Modulus (MPa)	Damping Ratio
Asphalt Concrete	See Master Curve in Figure 5-26	0.05
Aggregate Base Course	200	0.02
Subgrade	100	0.02

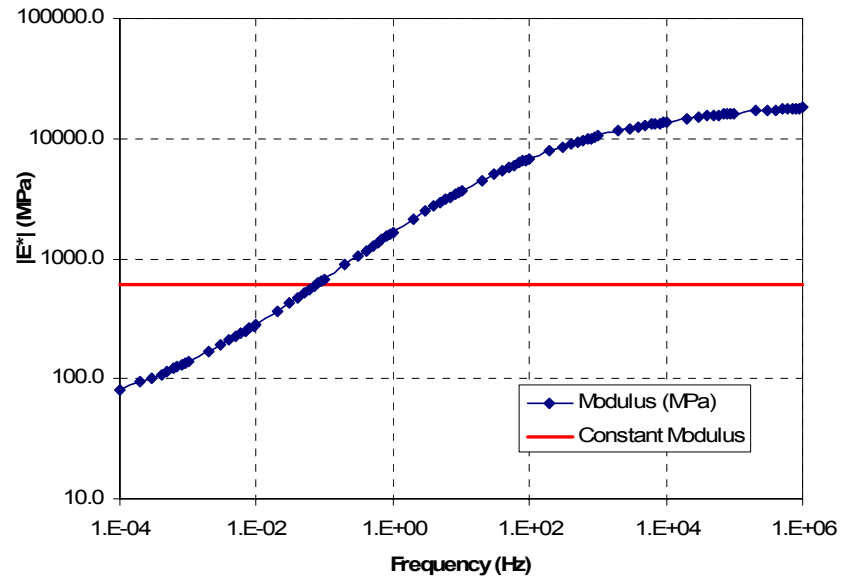


Figure 5-26 – Sample modulus curve and constant modulus line used for numerical evaluation of the pavement response with spectral element approach. The curve parameters are $\alpha = 2.8$, $\beta = -0.44$, $\delta = -1.48$, $\gamma = -0.56$ and $S_T = 0$ (See equation 5-4).

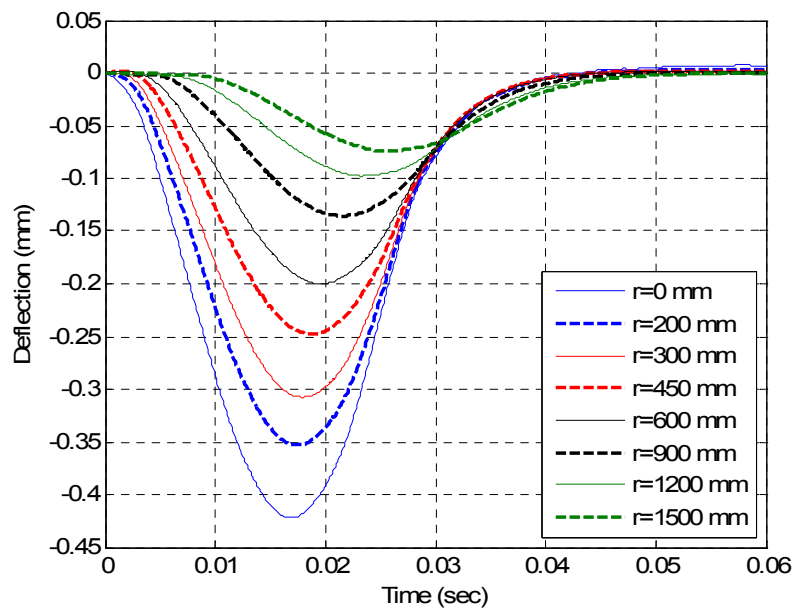


Figure 5-27 - Predicted pavement surface deflection time histories from spectral element analysis with dynamic asphalt layer modulus.

To evaluate the effect of dynamic moduli, response of the pavement system with a constant asphalt modulus is compared to the response obtained from the analysis with dynamic moduli. The properties of the pavement system with constant moduli are similar to the one used in the analysis with variable moduli, except that the value of the asphalt modulus is considered constant and selected such that the maximum deflections of the two systems are similar. This constant modulus value and the modulus master curve are depicted in Figure 5-26. The results of the comparison of the two systems are presented in Figure 5-28. It can be observed that, although the maximum deflections are similar, the time histories are quite different.

Based on this preliminary simulation, it can be observed that the backcalculated asphalt modulus using the assumption of a constant modulus is at best some sort of an average modulus over the frequency range of interest. So, for more accurate backcalculation results, the frequency dependent modulus should be considered in the analysis.

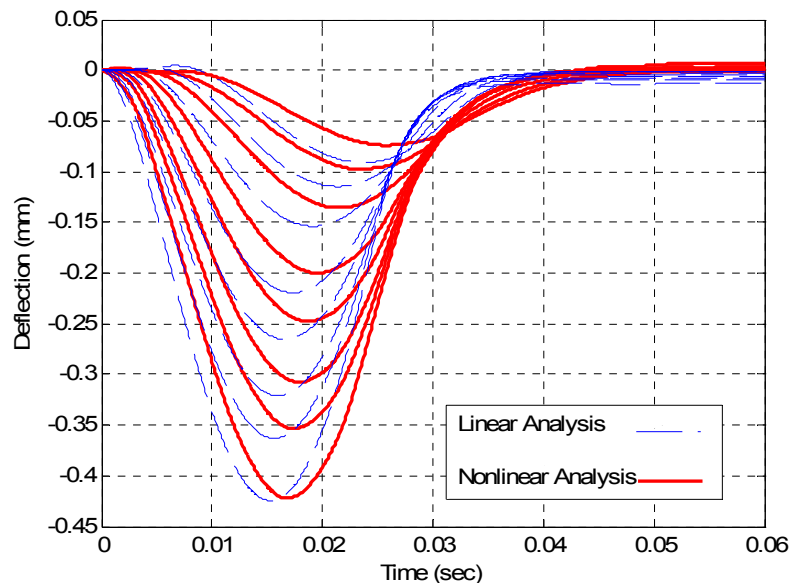


Figure 5-28 - Predicted pavement surface deflection time histories from nonlinear spectral element analysis.

Finally, for the modeling and backcalculation of FWD test results it has been assumed throughout this study that the material response is elastic and there is no plastic deformation during the test. This is certainly a reasonable assumption for the level of FWD loading. However, under the combination of heavy loads, weak pavement system and/or high temperatures, plastic deformations of pavement layers may occur, which invalidate this assumption. These extreme cases were not considered in this study.

Summary

In this chapter, the probabilistic backcalculation of FWD test results was introduced, formulated and the results of the probabilistic backcalculation of synthetic test data using different backcalculation methods were presented as a better approach to the FWD backcalculation. The probabilistic backcalculation was then applied to different methods of backcalculation, such as static and dynamic backcalculation and the results were compared. Based on the presented results, it was shown that, although very popular, the static backcalculation procedures fail to capture the essential dynamic nature of the test and consequently can not be relied upon for accurate backcalculation. Through the comparison of two different sets of deflection bowl backcalculation using the dynamic forward model, it was also demonstrated that there is little redundancy in dynamic deflection bowl backcalculation procedures, which can produce large uncertainties in the obtained backcalculation results. It was also shown that the dynamic deflection time history backcalculation offers the best and most reliable approach in FWD backcalculation. The application of this approach was illustrated both on synthetic and

experimental test data. It was also shown that, at least in the case of synthetic data, the deflection time histories carry enough information to simultaneously backcalculate layer moduli and the depth to bedrock. However, such additional information is obtained at a higher computational cost required for a more thorough search of the model space. Finally, the effect of frequency dependent layer material properties on the predicted deflection time histories was investigated. It was shown that such effects can be significant and produce discrepancies in the backcalculation results. A complete understanding of these effects and techniques to include them in the backcalculation analysis requires further research.

References

- ABAQUS (2005), Hibbitt, Karlsson, and Sorensen, Providence, RI.
- Al-khoury, R., Scarpas, A., Kasbergen, C., Blaauwendraad, J. (2001a), “Spectral Element Technique for Efficient Parameter Identification of Layered Media: Part I: Forward Model”, *International Journal of Solids and Structures*, Vol. 38.
- Al-khoury, R., Scarpas, A., Kasbergen, C., Blaauwendraad, J. (2001b), “Spectral Element Technique for Efficient Parameter Identification of Layered Media: Part II: Inverse Calculations”, *International Journal of Solids and Structures*, Vol. 38.
- ASTM International, (1996), “ASTM D4694-96, Standard Test Method for Deflections with a Falling-weight-type Impulse Load Device”, American Society for Testing and Material (ASTM), Philadelphia, PA.
- ASTM International, (2003), “ASTM D4695-03, Standard Guide for General Pavement Deflection Measurements”, American Society for Testing and Material (ASTM), Philadelphia, PA.
- Bentson, R.A., Nazarian, S., Harrison, A. (1989), “Reliability of Seven Nondestructive Pavement Testing Devices”, *Nondestructive testing of pavement and Backcalculation of moduli*, American Society for Testing and Material (ASTM) Special Technical Publication 1198, ASTM, Philadelphia, PA.
- Boddapati, K.M., and Nazarian, S. (1994), “Effects of Pavement-Falling Weight Deflectometer Interaction on Measured Pavement Response”, *Nondestructive testing of pavement and Backcalculation of moduli – Second Volume*, American Society for Testing and Material (ASTM) Special Technical Publication 1198, ASTM, Philadelphia, PA.

- Bush, A. J. III, and Baladi, G.Y. (Editors) (1989), “Nondestructive testing of pavement and Backcalculation of moduli”, American Society for Testing and Material (ASTM) Special Technical Publication 1026, ASTM, Philadelphia, PA.
- Cook R., Malkus D., Plesha M. (1989), “Concepts and Application of Finite Element Analysis” John Wiley & Sons, New York, NY.
- Clyne R., Li, X., Marasteanu, M. O., Skok E. L. (2003), “ Dynamic and Resilient Modulus of MN/DOT Asphalt Mixtures” Report No. MN/RC-2003-09, Minnesota Department of Transportation, St. Paul, MN.
- Doyle, J.M. (1997), “Wave Propagation in Structures”, Springer-Verlag, New York, NY.
- Dynatest, (1995), “Dynatest 8081 HWD Test System – Owners Manual”, Dynatest Consulting Inc., Starke, FL.
- ELMOD, (2001), “ELMOD Pavement Evaluation Manual (Version 4.5)”, Dynatest, Denmark.
- Foinquinos, R., Roesset, J. M., and Stokoe, K.H. (1995), “Response of pavement systems to dynamic loads imposed by nondestructive tests” Transportation Research Record, n 1504, p 57-67.
- Gucunski, N., Hadidi, R., Maher, A., and Vitillo, N. (2004), “Seismic Pavement Evaluation in Development of Seasonal Variation Models of Pavement Properties”, 5th International Conference on Case Histories in Geotechnical Engineering, New York, NY.
- Haskell, N.A. (1953), “The Dispersion of Surface Waves on Multilayered Media”, Bulletin of Seismological Society of America, Vol. 43, 17-34.
- Kausel, E. and Roesset, J. M. (1981), “Stiffness Matrices for Layered Soils”, Bulletin of Seismological Society of America, Vol. 71, 1743-1761.
- Mamlouk, M.S. (1987), “Dynamic Analysis of Multilayered Pavement Structures – Theory, Significance and Verification”, Proceedings of 6th International Conference on Structural Design of Asphalt Pavements, Ann Arbor, Michigan.
- Michalak, C.H., and Scullion, T., (1995), “MODULUS 5.0: User Manual”, Research Report 1987-1, Texas Transportation Institute, Texas A&M University, College Station, TX.
- Lozios A., Boukovalas, G., and Karlaftis, A. (2003), “Dynamic Stiffness Modulus for Pavement Subgrade Evaluation” Journal of Transportation Engineering, Vol 129, No. 4.
- Lozios, A., and Scarpas, T., (2005), “Verification of Falling Weight Deflectometer Backanalysis Using Dynamic Finite Elements Simulation”, The International Journal of Pavement Engineering, Vol. 6, No. 2.
- National Cooperative Highway Research Program (NCHRP) (1999), “NCHRP 9-19, superpave support and performance models management, advanced AC mixture material characterization models framework and laboratory test plan.,” Final Report, submitted by Superpave Models Team, Dr. M. W. Witzak, Project Principal Investigator, Arizona State University, Tucson, AZ.
- Rizzi, S.A. and Doyle, J.F. (1992), “Spectral Analysis of Wave Motion in Plane Solids with Boundaries”, Trans. of ASME, Journal of Vibration and Acoustics, Vol 114, No. 2, pp. 133-140.

- Roesset, J. M., Stokoe, K. H. II, Send, C.R. (1995), "Determination of Depth to Bedrock from Falling Weight Deflectometer Test Data", Transportation Research Record, Vol. 1504.
- Seed, H. B., Wong, R. M., Idriss, I. M., and Tokimatsu, K. (1986), "Moduli and Damping Factors for Dynamic Analysis of Cohesionless Soils", Journal of the Soil Mechanics and Foundation Division, Vol. 112, pp. 1016-1032.
- Sebaaly, B. E., Davies, T. G., Mamlouk, M. S. (1985) "Dynamics of Falling Weight Deflectometer", Journal of Transportation Engineering, ASCE, Vol. 3, No. 6.
- Tayabji, S.D., and Lukanen, E.O. (Editors) (2000), "Nondestructive testing of pavement and Backcalculation of moduli – Third Volume", American Society for Testing and Material (ASTM) Special Technical Publication 1375, ASTM, Philadelphia, PA.
- Taylor B. N. and Kuyatt C. E. (1994), "Guidelines for Evaluation and Expressing Uncertainty of NIST Measurement Results", Technical Note 1297, United States National Institute of Standards and Technology (NIST), United States Department of Commerce, Washington, DC.
- Thomson, W.T., (1950), "Transmission of Elastic Waves through a Stratified Solid Media", Journal of Applied Physics, Vol. 21, p. 89-93.
- Uzan, J. (1994), "Advanced Backcalculation Techniques", Nondestructive testing of pavement and Backcalculation of moduli – Second Volume, American Society for Testing and Material (ASTM) Special Technical Publication 1198, ASTM, Philadelphia, PA.
- Von Quintus, H.L., Bush, A. J. III, and Baladi, G.Y. (Editors) (1994), "Nondestructive testing of pavement and Backcalculation of moduli – Second Volume", American Society for Testing and Material (ASTM) Special Technical Publication 1198, ASTM, Philadelphia, PA.
- Zaghoul, S.M., White, T.D. Drenevich, V.P., and Coree, B., (1994), "Dynamic Analysis of FWD Loading and Pavement Response Using a Three Dimensional Dynamic Finite Element Program", Nondestructive testing of pavement and Backcalculation of moduli – Second Volume, American Society for Testing and Material (ASTM) Special Technical Publication 1198, ASTM, Philadelphia, PA.
- Zaghoul, S.M., Gucunski, N., Jackson, H., and Hadidi, R. (2006), "Material Characterization and Seasonal Variation in Material Properties", Report No. FHWA-NJ-2005-024, New Jersey Department of Transportation, Trenton, NJ.
- Zaghoul S. M., Hoover, T., Swan, D. J., Vitilli, N., Sauber, R., and Jumikis, A. (2004), "Enhancing Backcalculation Procedures Through Consideration of Thickness Variability" Transportation Research Record, No. 1869, pp. 80-87.
- Zerwer, A., Cascante, G., and Hutchinson, J. (2002), "Parameter Estimation in Finite Element Simulation of Raleigh Waves", Journal of Geotechnical and Environmental Engineering, ASCE, 128(3).

6 Application Two: Model Calibration Based On Geotechnical Instrument Measurements

Introduction

In design and construction problems in geotechnical engineering, there are always elements of uncertainty due to different factors, such as the uncertainty in soil parameters and/or construction sequence. To reduce the potential risk from the uncertainties that are not included in the design, many important geotechnical engineering projects use an observational method towards design and management of the project. The observational method, which its development is generally attributed to Terzaghi [*Casagrande, 1965, Peck, 1969*], can be described by the following steps:

- Assess probable and adverse outcomes for the design,
- Establish key parameters for observation,
- Calculate observational parameters under probable and adverse conditions using predictive models,
- Measure observational parameters and compare them to calculations,
- Calibrate the predictive model based on the measured observational parameters, and

- Change the design as needed.

Implementing the observational method is not a trivial task due to many limitations in the ability to predict the ground response and/or monitor the desired parameter. This is especially important for the projects, where the complexity of the factors involved limits the ability of an engineer to evaluate the monitoring results and outcomes without the help of predictive models. So, the development of a representative model and its calibration is one of the important steps in implementing the observational approach.

Model calibration is a classical example of an inverse problem, which can be solved using the probabilistic approach. This chapter introduces the probabilistic approach to the solution of inverse problems as a tool in calibration of the predictive models and implementation of the observational method. Model calibration has been historically performed by comparison between the observed and predicted model responses and adjustment of the model parameters to obtain a reasonable match. Once there is a good match between the observed and predicted responses, the model parameters are considered to represent the true ground parameters, and the model is considered calibrated. However, in this approach to calibration, effects of uncertainties in observations and model predictions are not included in the analysis. This affects the calibration analysis and consequently the model predictions for future measurements. Using the probabilistic approach, uncertainties in the calibration process can be quantified and their effects on the model predictions can be studied.

In this chapter, a landfill redevelopment project is used as an example to demonstrate how the probabilistic approach to the solution of inverse problems can be used to calibrate a predictive model and complement the application of the observational method in geotechnical engineering. Although the main focus of this chapter is on calibration based on the settlement data, the same approach can be used in different contexts and for different problems with different types of measurements. Following this introduction, an overview of the mentioned landfill redevelopment project is presented and the need for model calibration and implementation of the observational method is highlighted. The calibration of a settlement prediction model using the probabilistic approach is then outlined and formulated. Finally, the results of the analysis are presented and discussed.

Background

Project Overview

In a large scale landfill redevelopment project on several landfills in Northern New Jersey, it was decided early on that some development features, including some of the light structures, would be supported on shallow foundations over the landfill material, which is underlain by a peat, organic silt, and deep varved clay strata. This decision was justified because the costs for relocating landfill materials would be prohibitive and the depth to competent bearing material makes deep foundation systems uneconomical. This type of construction is in contrast to common practice of landfill development, which relies on deep foundations to support structures planned for the project. Generally, due to expected long term biodegradation settlement of landfill materials, most of the landfill

development projects to date are limited to types of construction that are not very sensitive to settlement of the landfill materials, such as golf courses and parks. However, the feasibility of shallow foundation construction for this project was justified by considering the limited thickness of the landfill, the significant age of the landfill materials, and the limited amount of gas being generated.

To limit the long term settlements from the compression of the landfill material and underlying peat, organic silt, and varved clay strata, in addition to implementation of an extensive environmental remediation program to address environmental concerns, implementation of an intensive ground improvement program was anticipated. The ground improvement program consisted of dynamic compaction of the landfill material, a surcharge program to pre-compress the landfill material and the underlying peat, organic silt, and varved clay strata, and the placement of controlled compacted fill of sufficient thickness to provide a significant separation between the bottom of the proposed footings and the top of the improved waste layer. Further details about the project and ground improvement program can be found in the published literature [*Lifrieri, et al. 2006a, Lifrieri et al., 2006b*].

At this time, the initial phase of this project, which consists of the development of a 10 acre parcel of the project site, is completed. However, other phases of the project are currently underway. The focus of this chapter is on the initial 10 acre parcel of the project. The envisioned development plan for this landfill parcel consists of construction of mid-rise residential and commercial real estate. The portion of the development that will not be pile supported generally consists of parking areas, roadways, and settlement sensitive landscaping features. To avoid future settlement related issues for these

features, a settlement criterion for the design of the ground improvement program was adopted, which specifies limiting the long term total site settlement in 10 years to a maximum of three inches.

Site Conditions

The soil borings performed within the project site indicated that the landfill material, nine to 12 feet thick, is covered with a two to three foot layer of fill material of various types. This waste layer is underlain by a peat and organic silt stratum with an average thickness of five to ten feet. However, at limited portions of the project site, this stratum is as thick as 25 feet. This organic stratum lie on top of a 110 to 140 feet thick deposit of varved clay, which in turn rests on top of the glacial till and bedrock. Geotechnical laboratory test results indicate that, except for the top desiccated portion of the varved clay stratum of about five to ten foot thick, the varved clay is normally consolidated and is very soft. A sketch of the generalized subsurface profile is depicted in Figure 6-1.

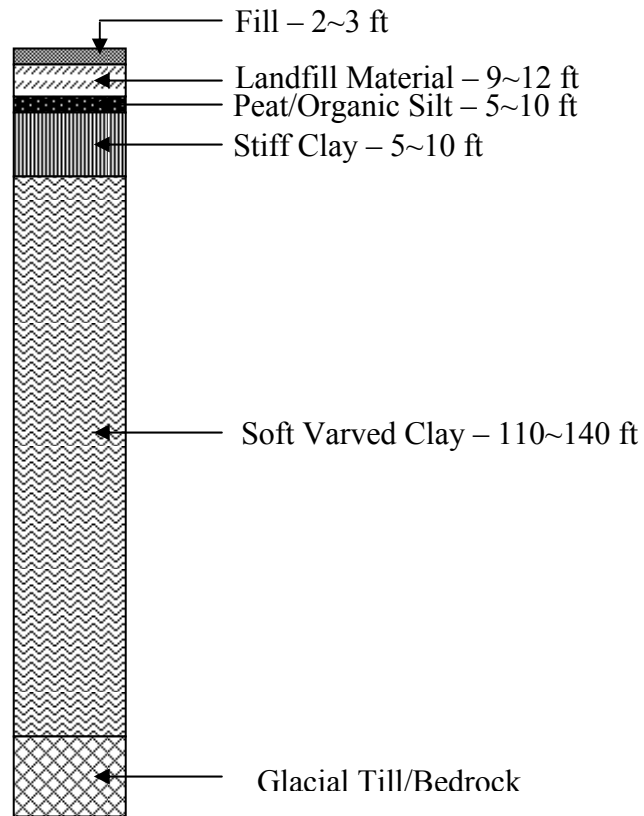


Figure 6-1 – Sketch of the generalized subsurface profile

Ground Improvement Program

The ground improvement program consists of dynamic compaction (DC) to improve the compression characteristics of the existing waste layer, followed by the placement of 12 feet of surcharge fill over the proposed site grades to improve the strength of the underlying peat, organic silt, and soft clay strata and to reduce post construction long term settlements resulting from the settlement of these strata. To monitor and verify the performance of the surcharge program, an instrumentation program was designed for the project site. The instrumentation program included installation and monitoring of magnetic extensometers, borros anchors, settlement plates, vibrating wire piezometers, stand pipe piezometers, and inclinometers.

To predict the future site response both during and after the construction and validate the satisfactory performance of the surcharge loads, a predictive model was developed and the ground settlement response was used to calibrate it. The calibrated model was then used to predict the long term settlement of the site. The following section presents the basic elements used in the analysis, formulates the probabilistic approach to the problem, and demonstrates how the probabilistic approach offers advantages in model calibration.

Development of Predictive Model and Calibration Measurements

Development of Predictive Model

A plan of the site along with the location of the borings and installed monitoring instruments is presented in Figure 6-2. To evaluate the settlement and verify the performance of the surcharge, a two dimensional predictive model of the site was developed using Plaxis® software. The model geometry was developed based on the borings performed at the project site along the cross section shown in Figure 6-2. The developed model geometry is depicted in Figure 6-3.

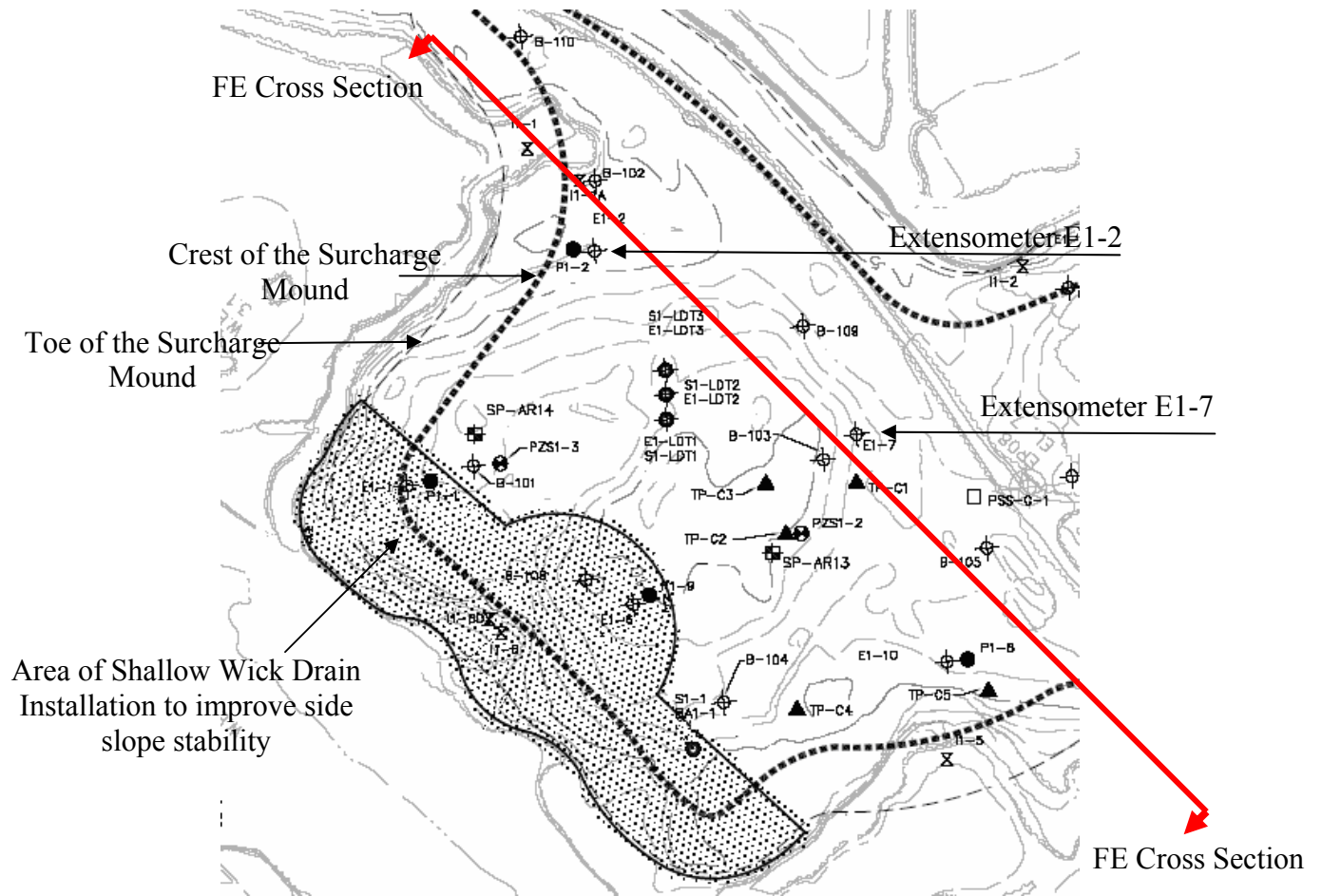


Figure 6-2 – Total layer settlement for waste, organic site/peat and clay strata. E1-7 and E1-2 are the installed extensometers along the modeled cross section.

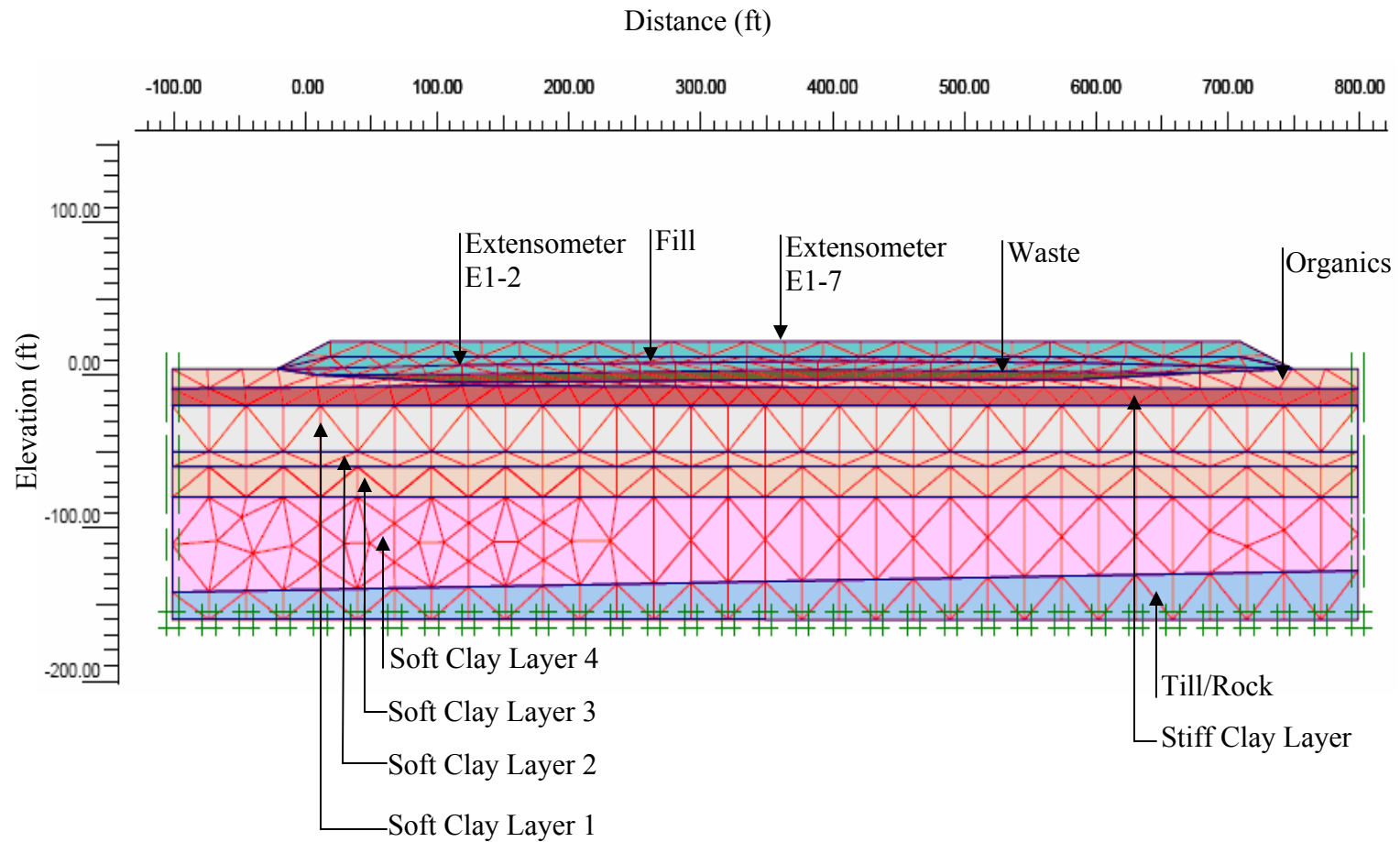


Figure 6-3 – Geometry of developed finite element predictive.

To model the fill placement activities, the stage construction analysis option in Plaxis® was used. Fill placement at different locations along the cross section took place at slightly different schedules. The loading history at two points along the cross section is presented in Figure 6-4. This loading sequence was idealized for the development of the model. The idealized loading sequence used in the model development is also presented in Figure 6-4. A close up of the loading stages in the finite element model is shown in Figure 6-5.

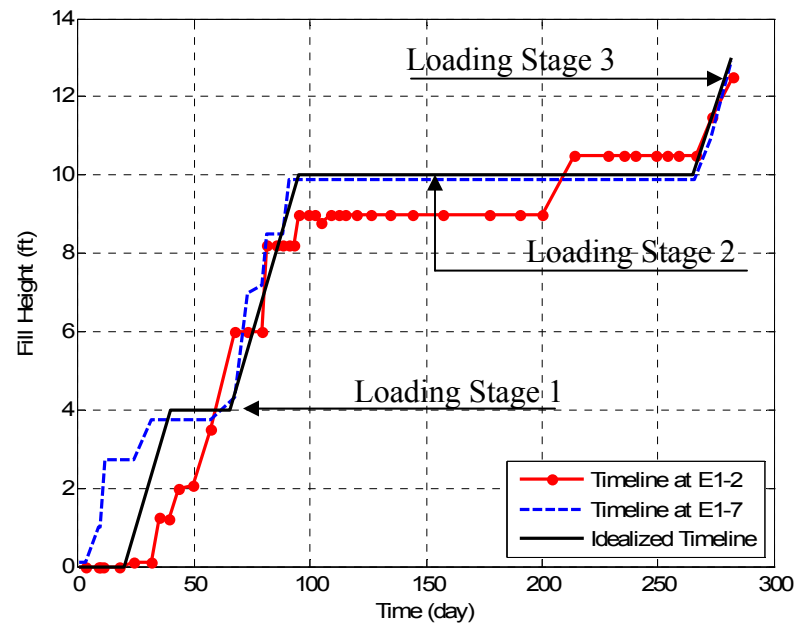


Figure 6-4 – Fill placement timeline at two points along the cross section and idealized fill placement timeline and stages used for model development.

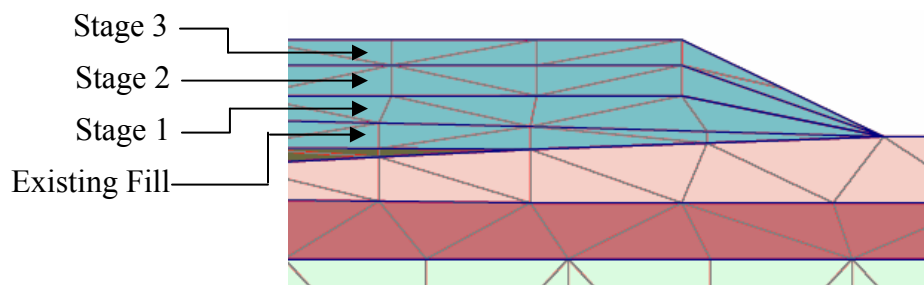


Figure 6-5 – Close up view of idealized loading stages.

Material properties for the initial development of the predictive model were selected based on the available site specific laboratory test results and published literature pertaining to the type of soils encountered at the project site. The initial material properties are listed in Table 6-1.

Measurement Results

The observed settlement of the waste, organics, and clay strata from monitoring of extensometers E1-2 and E1-7 along the modeled section are presented in Figure 6-6. The location of these extensometers is also indicated on the developed model presented in Figure 6-2. The presented ground settlement response will be used to calibrate the predictive model. Once the model is calibrated it was used to predict the future response of the site under the applied loads.

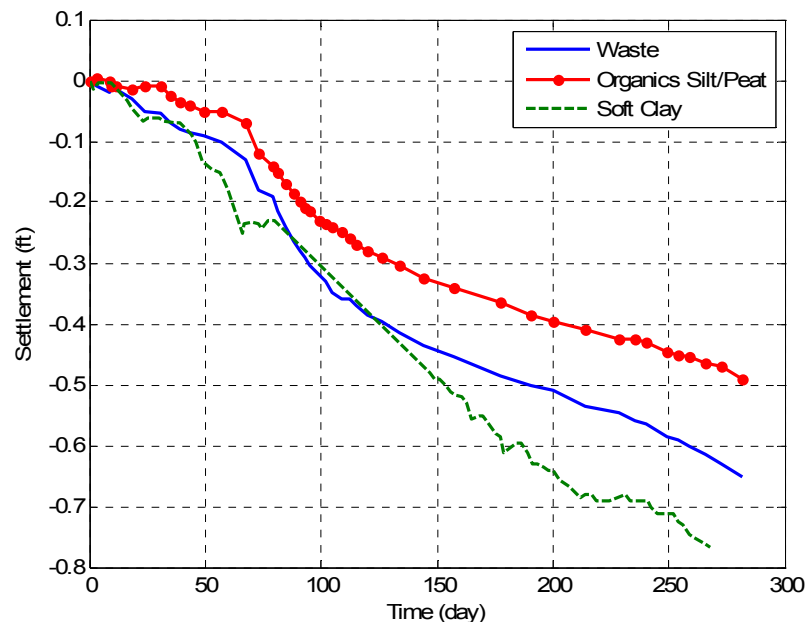


Figure 6-6 – Total layer settlement for waste, organic silt/peat and clay strata from extensometer measurements along the modeled cross section (Extensometer E1-2 and E1-7).

Table 6-1 – Initial material properties used for development of predictive model.

	(A)	(B)	(C)	(D)	(E)	(F)	(G)	(H)	(I)	(J)	(K)	(L)	(M)
Material	Model	γ_{unsat} kg/m3 (pcf)	γ_{sat} kg/m3 (pcf)	k_y m/sec (ft/d)	k_y / k_x	ν	V_s m/s (ft/s)	c KPa (psf)	ϕ	OCR	C'_c	C'_r	C'_α
Fill	MC	1922 (120)	2002 (125)	3.52E-6 (1)	1	0.3	225 (750)	4.8 (100)	34	-	-	-	-
Waste	SSC	1041 (65)	1521 (95)	10.6E-9 (3E-3)	1	-	-	9.6 (200)	30	1	0.14	0.014	0.0014
Organics	SSC	961 (60)	1441 (90)	1.06E-9 (3E-4)	1	-	-	19.2 (400)	20	1	0.34	0.034	0.017
Stiff Clay	MC	1762 (110)	1922 (120)	2.12E-9 (6E-4)	3	0.3	150 (500)	71.8 (1500)	23	-	-	-	-
Soft Clay 1	SSC	1601 (100)	1762 (110)	2.12E-9 (6E-4)	3	-	-	14.4 (300)	23	1	0.1	0.01	0.004
Soft Clay 2	SSC	1601 (100)	1762 (110)	1.76E-9 (5E-4)	3	-	-	23.9 (500)	23	1	0.2	0.02	0.008
Soft Clay 3	SSC	1601 (100)	1762 (110)	3.18E-9 (9E-4)	3	-	-	33.5 (700)	23	1	0.3	0.03	0.012
Soft Clay 4	SSC	1601 (100)	1762 (110)	1.06E-9 (3E-4)	3	-	-	43.1 (900)	23	1	0.2	0.02	0.008

Table Legend:

Independent Model Parameter for Calibration

Dependent Model Parameter for Calibration

(A) Material Model: MC –Mohr-Coulomb Material Model, SSC–Soft Soil Creep Material Model (Plaxis, 2005), (B) Unit weight, (C) Saturated unit weight, (D) Permeability in vertical direction (E) Ratio of vertical to horizontal permeability, (F) Poisson's ration, (G) Shear wave velocity, (H) Cohesion, (I) Friction angle, (J) Over consolidation ratio, (K) Strain based compression index, (L) Strain based recompression index, (M) Strain based secondary compression index.

Initial Model Predictions

The predicted model response using initial material properties at E1-2 and E1-7 extensometer locations is depicted in Figure 6-7. For a comparison, the measured response of the site at the same locations is depicted in the same figure. It can be observed that, even though the material properties for the model are obtained from the site specific laboratory test results, the predicted site response is very different than the observed response, which highlights the need for model calibration.

Model Parameters

A fundamental step in the solution of any inverse problem, including the calibration problem presented, is the selection of model parameters or parameterization. Due to a relatively short span of settlement monitoring used for model calibration, the presented site response can be considered to be essentially representative of the primary consolidation of subsurface strata. Therefore, it is logical to expect that the response can be adequately described by the compression indices and permeability coefficients of subsurface strata. Based on this logic, the compression indices and permeability coefficients of waste, organics, and first sublayer of soft clay strata were selected as the model parameters. Since all four soft clay sublayers represent one single geologic unit, the compression indices and permeability coefficients of other soft clay sublayers were not selected as independent model parameter. Instead, these were calculated based on the values of the first soft clay sublayer in such a way to keep the ratios between the

compression indices and permeability coefficients equal to the ratios in the original model.

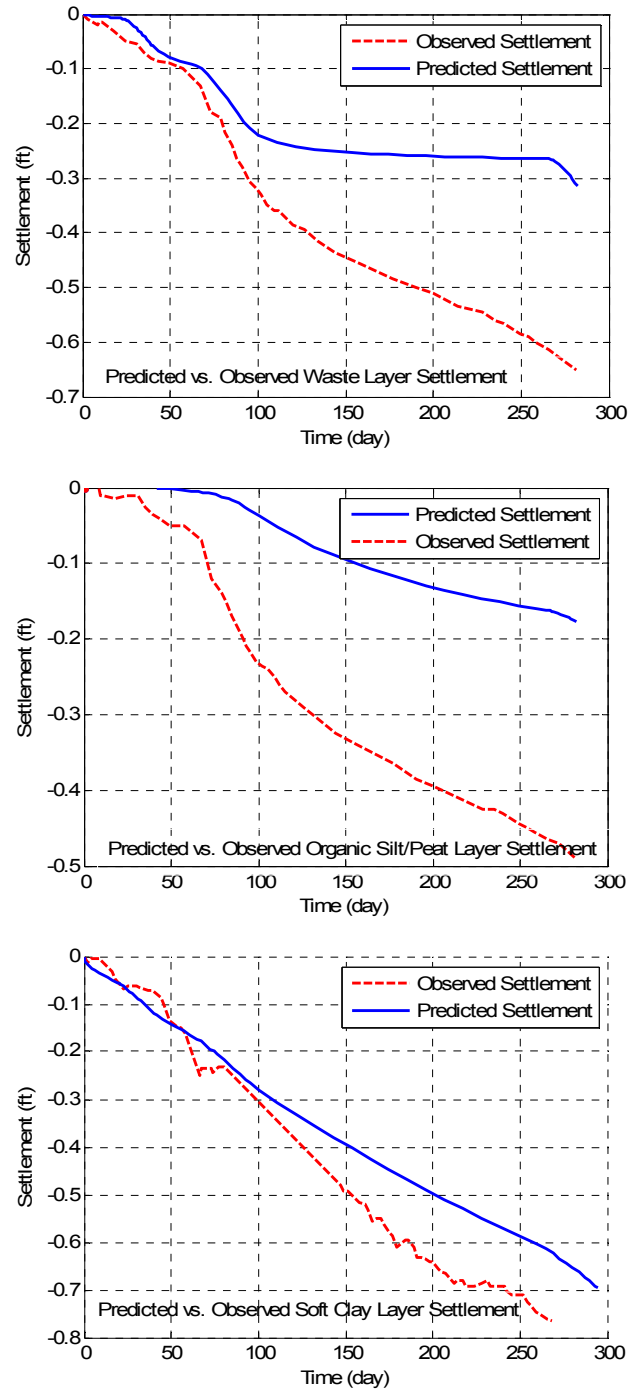


Figure 6-7 – Comparison of observed vs. calculated total layer settlement based on initial layer properties for waste, organic silt/peat and clay strata.

The settlement response of the material is also affected by the value of recompression and secondary compression indices. Logically, these can not be considered constant while the compression index varies as a model parameter. Therefore, for the calibration problem presented, these parameters were determined using the established and verified correlations [Terzaghi, Mesri, and Peck 1995]. These correlations are presented below:

$$\begin{aligned}
 &\text{For all layers: } C'_r = 0.01C'_c \\
 &\text{For waste layer: } C'_\alpha = 0.01C'_c \\
 &\text{For organic silt/peat layer: } C'_\alpha = 0.05C'_c \\
 &\text{For soft varved clay layer: } C'_\alpha = 0.04C'_c
 \end{aligned} \tag{6-1}$$

where C'_c is the strain based compression index, C'_r is the strain based recompression index, and C'_α is the strain based secondary compression index. The independent and dependent model parameters are highlighted in Table 6-1

Probabilistic Formulation

Using the notion of the generalized measurement presented in previous chapters, the model calibration problem can be considered as a generalized measurement of the subsurface consolidation properties using surface settlement measurements. The notion of the generalized measurement, combined with the tools developed in the previous chapters, is used here to calibrate the predictive model, obtain the layer consolidation properties, and obtain associated uncertainty measures. It should be reiterated that the uncertainty measures can only be obtained using a probabilistic approach. Such estimates are not available in the traditional deterministic approach.

Model a Priori Information

Homogeneous a priori probability densities were considered here for all model parameters. This probability density reflects the general information about the limits of the value of the parameter and can be presented by:

$$\rho_M(m) = \begin{cases} \frac{1}{m_{\max} - m_{\min}} & m_{\max} < m < m_{\min} \\ 0 & \text{otherwise} \end{cases} \quad (6-2)$$

where m_{\max} and m_{\min} are respectively the maximum and minimum limits of the value of the parameter of interest, m .

Data a Priori Information

In the probabilistic approach, the uncertainties in observations are represented by data a priori probability, denoted by $\rho_D(d)$. For the settlement calibration problem presented, the data are basically the individual extensometer settlement measurements. For the extensometers used in this project, these uncertainties are quantified by the instrument manufacturer to be on the order of 0.25 to 0.5 cm (0.1 to 0.2 in). However, in addition to uncertainties associated with the extensometer measurements, there are other uncertainties in settlement measurements that should be considered, such as uncertainties due to a change of the observer, or due to a deviation of the line of extensometer casing from the vertical line. The evaluation of the magnitude of these uncertainties is not trivial and the best approach for their evaluation is to assign uncertainties to them based on the experience [ISO 1993, Taylor and Kuyatt 1994]. In this work, based on the available data and field experience, the data a priori probability $\rho_D(d)$, which combines all uncertainty

sources, was considered to be a Gaussian distribution with the mean equal to the observed value and a standard deviation of 0.75 cm (0.3 in).

Forward Model

The forward model used in the calibration was presented earlier. In the calibration analysis presented here, it is considered that the developed model is representative of the physical phenomenon that is being modeled. Consequently, the modeling uncertainties were considered to be negligible in comparison to the data uncertainties. In general, evaluation of modeling uncertainties is a complex task and further research is required to quantify such uncertainties.

Probabilistic Formulation and Solution

It was shown in the previous chapters that the probabilistic solution of the inverse problem, or simply the results of a generalized measurement, is the a posteriori probability, which can be presented as:

$$\sigma_M(m) = \rho_M(m)\lambda(m) \quad (6-3)$$

where $\lambda(m)$ is the likelihood function:

$$\lambda(m) = k \exp\left(-\frac{1}{2}(d_{obs} - g(m))^T (C_T^{-1} + C_d^{-1})(d_{obs} - (g(m)))\right) \quad (6-4)$$

In these equations, model parameter m is the parameter of interest in the problem, C_d is the covariance of the data a priori information (assumed Gaussian) and C_T is the uncertainty in predictions of the forward model $g(m)$. In this chapter, this

problem is solved using the Monte Carlo solution scheme with neighborhood approximation presented in Chapter 4.

Calibration Results

Based on the presented probabilistic formulation, a calibration analysis was performed to find the best model parameters, which can replicate the observed data, and obtain the corresponding uncertainty measures. The final result of the analysis, in terms of a comparison between the observed settlements of the waste, organics, and clay strata and the theoretically predicted site response for the obtained best fit model parameters, are presented in Figure 6-8. The model parameters corresponding to the best fit model are also presented in Table 6-2.

Table 6-2 – Numerical values of the best fit model obtained from calibration analysis.

Material	(A) k_y m/sec (ft/d)	(B) C'_c	(C) C'_r	(D) C'_α
Waste	16.1E-9 (4.6E-3)	0.26	0.026	0.0026
Organics	16.6E-9 (4.7E-3)	0.40	0.040	0.020
Stiff Clay	2.12E-9 (6E-4)	-	-	-
Soft Clay 1	2.12E-9 (6E-4)	0.07	0.007	0.0028
Soft Clay 2	1.76E-9 (5E-4)	0.14	0.014	0.0056
Soft Clay 3	3.18E-9 (9E-4)	0.21	0.021	0.0084
Soft Clay 4	1.06E-9 (3E-4)	0.14	0.014	0.0056

To evaluate the uncertainty of the obtained results, one-dimensional kernel density estimates of marginal probability densities of model parameters from the calibration analysis are also calculated and presented in Figure 6-9. The densities are basically the probabilistic solution of the problem, which not only contain information about the best fit model, they also reflect information about the uncertainties of the

obtained results. In other words, they provide the complete picture of the solution, which is not available in the deterministic approach. Based on these results, it can be observed that the calibration analysis has identified the compression indices of the layers with low levels of uncertainty (i.e. low spread of the probabilities). However, the uncertainties of the permeability coefficients of layers are relatively high. These results suggest that the settlement time histories carry adequate information to identify the compression indices of layers rather accurately. However, within the considered range, the sensitivity of the data to permeability values is much less and permeability coefficients can not be identified with confidence based on the used data. This simply points to the fact that additional data, such as pore pressure dissipation measurement should be included in the analysis. In general, a high uncertainty in observational method is simply an indication that it is necessary to obtain additional information from other available data to reduce the uncertainty of the results. In some cases, this means including more data in the calibration analysis or simply using a different type of analysis.

The ability of the probabilistic approach to evaluate data uncertainties provides an engineer with the understanding of the limitations of the results and consequently enables him/her to devise a more appropriate course of action. In the deterministic approach, the results of the calibration analysis are simply the optimum values of the model parameters and no uncertainty measures are stated. Such a presentation of results does not provide the complete picture and in some cases may be misleading.

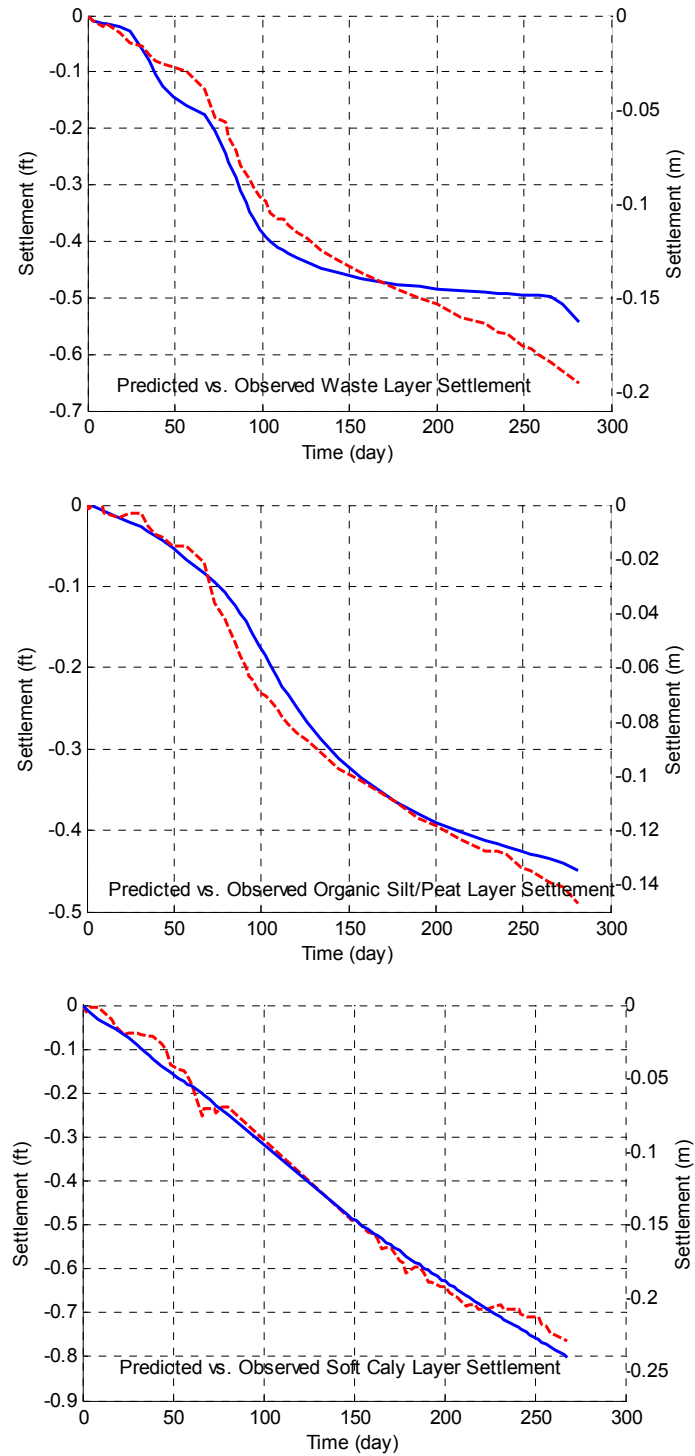


Figure 6-8 - Comparison of observed vs. calculated total layer settlement based on calibrated layer properties for waste (top), organic silt/peat (middle) and clay (bottom) strata.

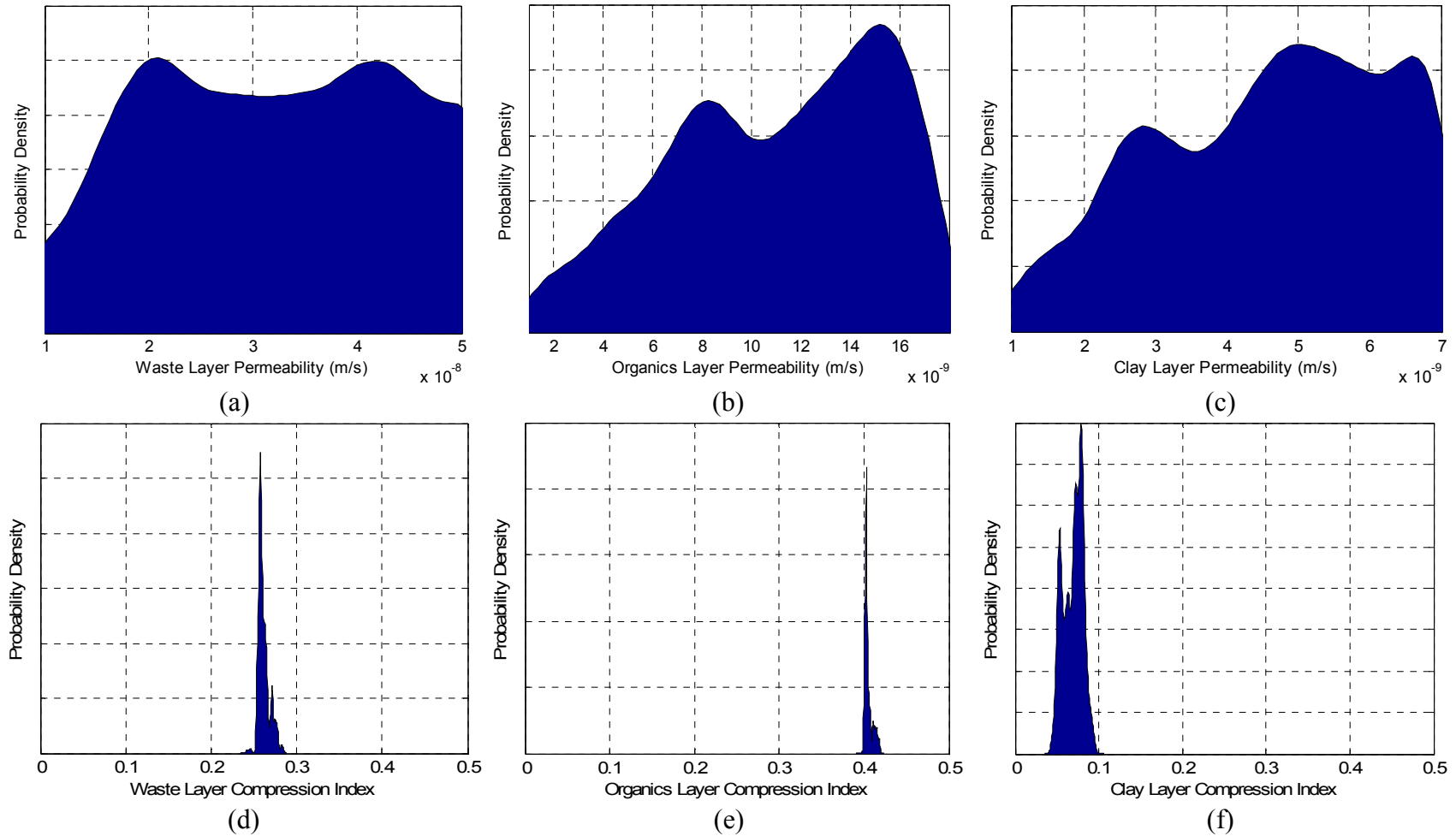


Figure 6-9 - One-dimensional kernel density estimates of marginal probability densities of model parameters for permeability of waste (a), organic sit/peat (b), and clay (c) layer. Similar information is also presented for the compression index of waste (d), organic sit/peat (e), and clay (f) layer.

Summary

In this chapter, calibration of a finite element settlement prediction model for a landfill redevelopment project was presented to demonstrate how the probabilistic approach to the solution of inverse problems can be used to complement the application of the observational method in geotechnical engineering. The basic formulation of the probabilistic solution of inverse problems was introduced and a numerical technique for evaluation of the solution was presented. The calibration of the settlement prediction model using the probabilistic approach was then outlined and formulated, and the results of the analysis were presented. Using the presented example, it was illustrated that the ability of the probabilistic approach to evaluate the uncertainties of the obtained analysis results provides an engineer with very valuable information regarding the limitations of the data and results and consequently assists him/her to devise an appropriate course of action.

References

- Casagrande, A. (1965), "Role of the calculated risk in earthwork and foundation engineering" *Journal of Soil Mechanics and Foundation Division, American Society of Civil Engineers*, 91(SM4): 1-40.
- Lifrieri, J. J., Hadidi, R., Burke, W. W., and Desai, M. B. (2006a), "Compression Characteristics of Solid Waste After Dynamic Compaction", *Proceedings of the 21st International Conference on Solid Waste Technology and Management*, Philadelphia, PA.
- Lifrieri, J. J., Hadidi, R., Burke, W. W., and Desai, M. B. (2006b), "Ground Improvement to Support Shallow Foundation Development over Landfills and Soft Natural Deposits", *Proceedings of the 22nd Central Pennsylvania Geotechnical Conference*, Hershey, PA.
- Peck, R. B. (1969), "Advantages and Limitations of the Observational Method in Applied Soil Mechanics", *Geot.*, 19, No. 1, pp. 171-187.
- Plaxis reference Manual, (2005), PLAXIS B. V., the Netherlands.
- Terzaghi, K., Peck, R. B., Mesri, G. (1995), "Soil Mechanics in Engineering Practice", John Wiley and Sons, New York, NY.

7 Application Three: Seismic Waveform Inversion

Introduction

Elastic waves carry substantial information about the characteristics of the media they propagate in. The seismic evaluation techniques use the information carried by elastic waves to infer information about the properties of the media. These techniques are generally nondestructive and they are being used increasingly in engineering applications, such as in determination of stiffness and integrity of structural elements, evaluation of the elastic moduli of soil deposits and pavement systems, void detection and sizing in geotechnical engineering, and crack detection. There are several techniques that are routinely used for shallow subsurface investigations namely; spectral analysis of surface waves (SASW) [Nazarian *et al.* 1993, Nazarian, 1984, Gucunski and Woods 1991], impulse response (IR) [Reddy, 1992], impact echo (IE) [Sansalone, 1997] and multi-channel analysis of surface waves (MASW) [Park, Miller and Xia, 1999]. However, these standard methods utilized in current engineering evaluations usually use a limited portion of the information carried by elastic waves, such as travel time, peak

return frequency, or wave velocity dispersion. Seismic waveform inversion seeks to use the full information content of the seismic waveform. The objective of the inversion is to find a reasonable model, consistent with a given a priori information, which its predicted waveforms match reasonably well the observed waveforms.

This chapter presents the probabilistic formulation of the seismic waveform inversion problem for evaluation of subsurface properties in civil engineering. Following this introduction, a synthetic seismic experiment is described that will be used as an illustrative example. The inversion problem is then formulated from a probabilistic point of view and the results of the probabilistic inversion of synthetic data are presented. The chapter concludes with the application of the probabilistic backcalculation to a set of experimental seismic data collected for pavement evaluation.

Probabilistic Formulation of Waveform Inversion Problem

Using the notion of a generalized measurement presented in the previous chapters, the inversion of seismic data in general and waveform inversion problem in particular can be considered as a generalized measurement of the subsurface properties, such as compressional wave velocities, using surface measurements. The notion of the generalized measurement combined with the tools developed in the previous chapters is used here to calculate layer properties and obtain uncertainty measures.

Model a Priori Information

Uniform probability density was considered for a priori probability density of all model parameters in this chapter. This probability density represents the information on the limits of the parameters. This probability density can be represented as:

$$\rho_m(m) = \begin{cases} \frac{1}{m_{\max} - m_{\min}} & m_{\max} < m < m_{\min} \\ 0 & \text{otherwise} \end{cases} \quad (7-1)$$

where $\rho_m(m)$ is the a priori probability density for the model parameter, and m_{\min} and m_{\max} are the lower and upper limits of the parameter, respectively.

Data a Priori Information

Data a priori, represented by probability $\rho_D(d)$, expresses the uncertainties in the measurement of the observed data. In seismic experiments, the data are often displacement, velocity, or acceleration time histories recorded by transducers. One technique that can be used in the evaluation of the data uncertainties is to use a noise record from transducers. This is especially a useful technique and is utilized in the numerical example presented later in this chapter, where an artificial Gaussian random noise is the only source of uncertainty in the problem and can be generated numerically. However, the technique can be used equally well if transducer noise is recorded and analyzed.

In the presented technique, it is assumed that uncertainties can be represented by a Gaussian distribution. Assuming that an ensemble of N noise waveforms s_i is available, the covariance matrix can be estimated by [Priestley, 1981]:

$$\hat{C}_D = \frac{1}{N} \sum_{i=1}^N s_i s_i^T \quad (7-2)$$

where \hat{C}_D represents the estimate of C_D based on N records.

Forward Model

In general, determination of the surface response to impact loads mathematically falls into the area of wave propagation theory. Numerical solutions are required to obtain the solutions in general. However, closed form solutions and/or simplified techniques exist when the problem boundary and geometry are simple. These simplifications, if possible, present considerable savings in terms of the computational effort.

For the analysis in this section, a finite element and a spectral element forward model are used to model the forward problem of wave propagation. A finite element models is selected as the forward model in inversion of synthetic data to conserve the generality of the presented procedure and provide a framework for considering other classes of problems. A spectral element model, as presented in Chapter 5 and Appendix A, is also considered, because it provides computational savings for simpler geometries. The spectral element model is used in the later part of this chapter for inversion of field seismic data.

To be able to evaluate the probabilistic solution, modeling uncertainties should also be defined. In general, evaluation of modeling uncertainties is a complex task and further research is required to quantify such uncertainties. For examples presented in this chapter, based on the experience, nominal modeling uncertainties were assigned for each analysis

Probabilistic Formulation and Solution

The probabilistic solution of inverse problem, or simply the results of a generalized measurement, is the a posteriori probability, which is presented as:

$$\sigma_M(m) = \rho_M(m)\lambda(m) \quad (7-3)$$

where $\lambda(m)$ is the likelihood function:

$$\lambda(m) = k \exp\left(-\frac{1}{2}(d_{obs} - g(m))^T (C_T^{-1} + C_d^{-1})(d_{obs} - (g(m)))\right) \quad (7-4)$$

In these equations, model parameter m is the parameter of interest in the problem, C_d is the covariance of the data a priori information (assumed Gaussian) and C_T is the uncertainty in prediction of the forward model $g(m)$ (assumed negligible). In this chapter, this problem is solved using the Monte Carlo solution scheme with neighborhood approximation presented in Chapter 4.

Synthetic Seismic Experiment

To illustrate the potential of the seismic waveform inversion, inversion of synthetic seismic test results is initially considered. The details of the test are presented in the following section.

Test Setup

Consider a hypothetical geological soil profile, as depicted in Figure 7-1. The profile consists of horizontal and inclined layers underlain by a half space or bedrock. Each layer is parameterized in terms of its thickness, T , compressional wave velocity, V_p , density, γ , and poisson's ratio ν . For the experiment presented in this

chapter, the objective of the seismic test is to quantify material properties of the subsurface layers, in terms of their compressional wave velocities, from the waveforms recorded at the surface. It is assumed that the layer thicknesses and dipping angle of layers are available from other information collected at the site, such as boring logs. To achieve the objective, a seismic test is performed by generating an elastic wave field using a known impact source and seismic waveforms are recorded at several locations along the surface. The recorded waveforms are then analyzed to infer/invert the unknown parameters of the model.

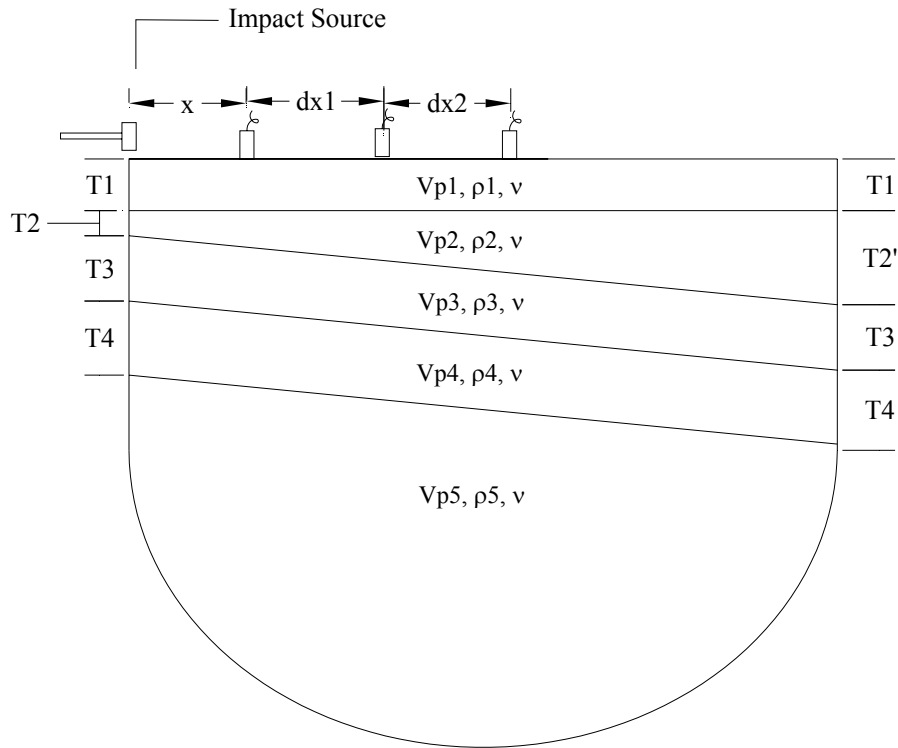


Figure 7-1 - Schematics of the synthetic seismic waveform inversion test setup

It should be mentioned that the waveform inversion, considered herein, is a relatively new technique for applications in civil engineering. This technique is a much

more versatile and powerful technique in comparison to the traditional techniques used in civil engineering, such as SASW, MASW, IR, IE, where their inherent assumptions limit their applicability. The traditional techniques generally assume that subsurface layers are horizontal, whereas the waveform inversion can invert virtually any type of geometry. The only theoretical limitation in the use of the waveform inversion would arise from the limitation in the parameterization and modeling of the test setup.

Synthetic Waveforms and Forward Model

To simulate the test and generate a set of synthetic data, the presented seismic test is modeled by finite elements using ABAQUS® [2005] software. Assuming that no lateral reflections occur, the test setup can be described as an axi-symmetric model with an impact loading at the center. Explicit time integration of the equation of motion is used to obtain the solution. Because the strain levels during the seismic tests are small, linear elastic material models were considered for all layers. To accurately model the wave propagation, several criteria were imposed during modeling to ensure accuracy of the simulation. The element size was selected relatively small to capture short wavelengths and the overall model was selected relatively large to allow propagation of large wavelengths and reduce the effects of boundaries. Infinite absorbing elements were used at the boundaries to further reduce the reflections from the boundaries. The developed finite element model is presented in Figure 7-2. Receiver locations, as well as boundaries of the layers, for a typical test setup are superimposed on the finite element model in this figure.

Using the developed model, a set of synthetic waveforms was generated at three receiver locations shown in Figure 7-2. The geometric and material properties used in the generation of synthetic data are presented in Table 7-1. To simulate field conditions and avoid numerical instabilities, artificial Gaussian random noise was added to the calculated waveforms. The waveform at each receiver is one second long and is sampled at 0.001 second intervals. These waveforms are depicted in Figure 7-3 and are used as the synthetic data for inversion.

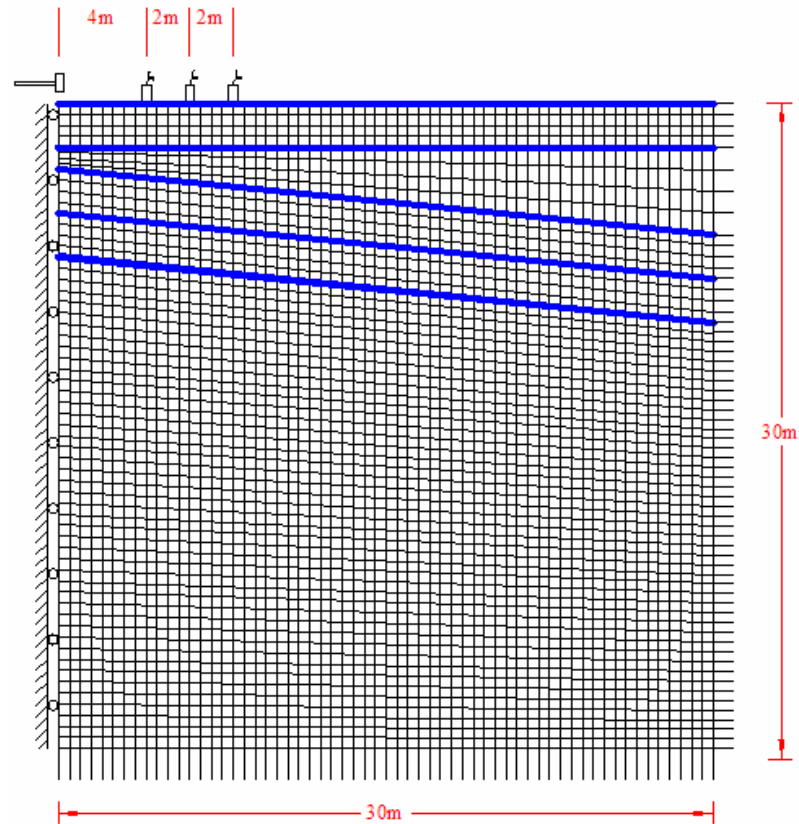


Figure 7-2 - Finite element model with the test setup superimposed on the mesh

Table 7-1- Subsurface profile parameters in the generation of synthetic waveform inversion example.

Parameter	Value	Unit
V_{p1}	80	m/s
V_{p2}	50	m/s
V_{p3}	70	m/s
V_{p4}	100	m/s
V_{p5}	60	m/s
T1	2	m
T2	1	m
T2'	4	m
T3	2	m
T4	2	m
ρ_1 thru ρ_5	1900	Kg/m ³
v	0.30	-
n	2	-
x	4	M
dx1	2	M
dx2	2	M

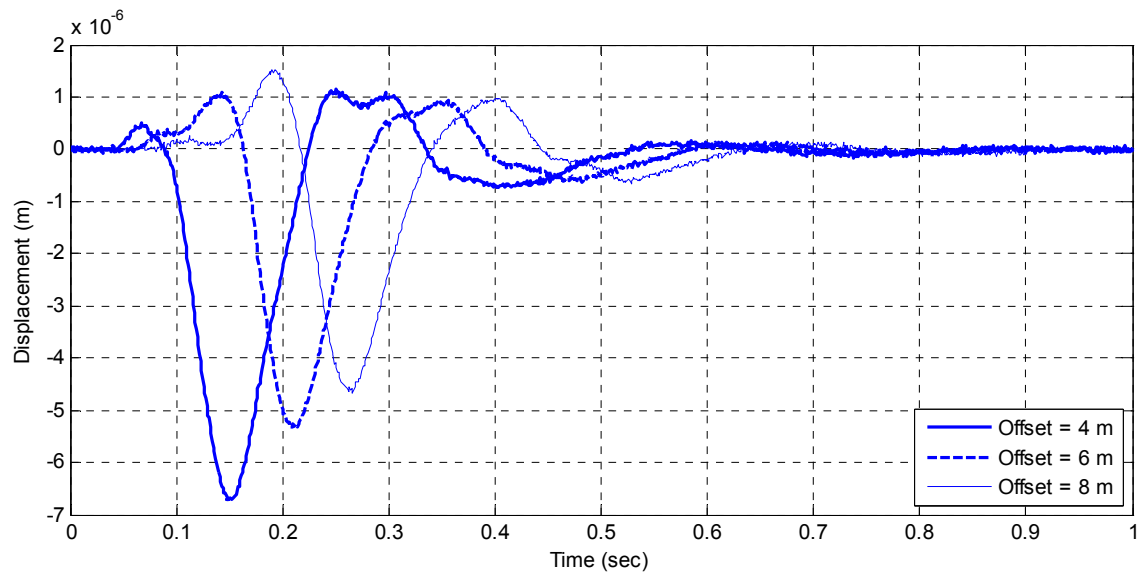


Figure 7-3 – Synthetic waveforms used in the inversion.

Results of Inversion of Synthetic Seismic Test

The presented synthetic data was analyzed to obtain the layer compressional wave velocities. Kernel density estimates of one-dimensional marginal a posteriori probability

densities for this example are presented in Figure 7-4. As presented, the inversion analysis results are very close to the target compressional wave velocities presented in Table 7-1. It can be observed that the inversion process has effectively inverted the profile and has clearly resolved the target compressional wave velocities. The calculated marginal a posteriori probability densities have clearly the peaks at the target compressional wave velocity values, which represent very low uncertainties of the wave velocities. In addition to the one-dimensional probabilities, for this case, estimates of some of the two dimensional joint marginal probabilities are also presented in Figure 7-5. These probabilities represent the joint marginal probability of two parameters. A review of these results indicates that the waveform inversion is a very effective tool in identification of model parameters from a seismic test. Additionally, it can be observed that the waveform inversion can solve problems where the assumptions of traditional seismic analysis techniques limit their application.

Inversion of Seismic Pavement Analyzer Data

To investigate the feasibility of implementation of the waveform inversion for shallow subsurface characterization, like pavement profiling, inversion of seismic waveforms from Seismic Pavement Analyzer (SPA) [Nazarian *et al.* 1993] is considered below as an example.

Test Setup

Seismic Pavement Analyzer (SPA) is a device for nondestructive evaluation of pavements developed under the Strategic Highway Research Program (SHRP). One of

the main objectives in the development of the SPA was to create a device that will allow measurement of onset of deterioration in pavements at their early stages. Primary applications of the SPA include pavement profiling, in terms of elastic moduli and layer thicknesses, detection of voids or loss of support under rigid pavements, delamination in rigid pavements and bridge decks, and subgrade evaluation. The SPA was originally designed to incorporate five seismic techniques: Ultrasonic Body-Wave (UBW), Ultrasonic Surface-Wave (USW), Impact Echo (IE), Impulse Response (IR), and Spectral Analysis of Surface Waves (SASW). Waveform inversion is an additional technique that is investigated here.

A schematic diagram of the SPA is depicted in Figure 7-6. The device includes a low frequency hammer (LFH), a high frequency hammer (HFH), five accelerometers (A1 thru A5), and three geophones (G1 thru G3) at different offset distances from the hammers, as depicted in the figure. The test with SPA is conducted by recording pavement vibrations generated by impact of the low and high frequency hammers.

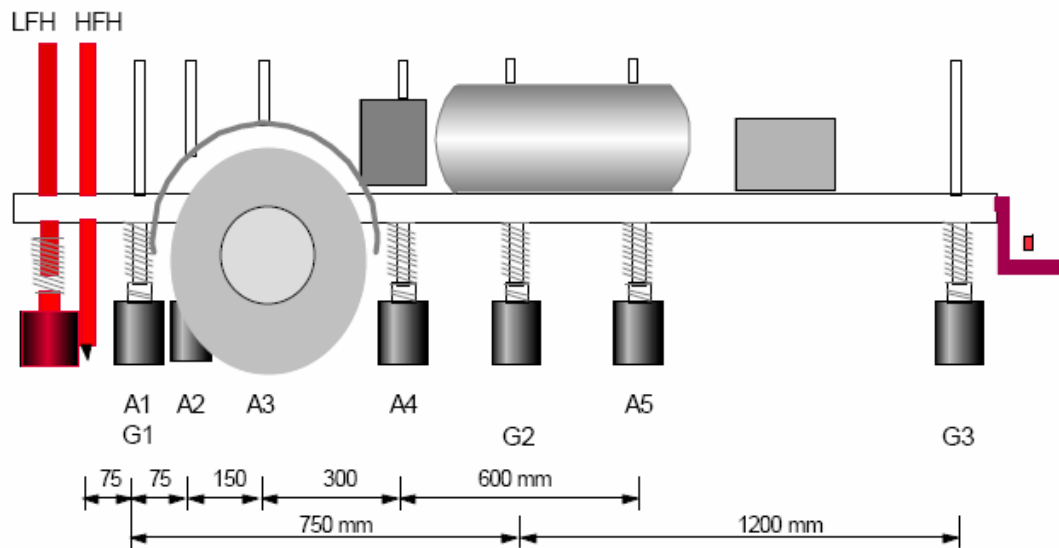
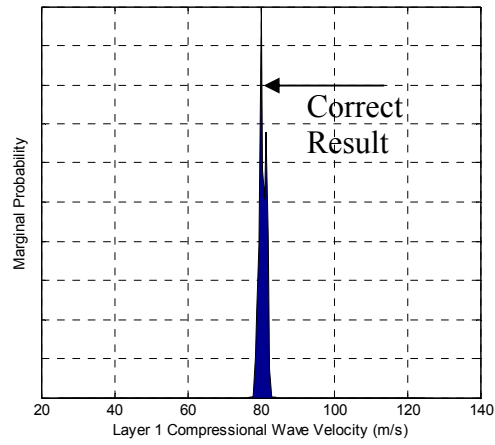
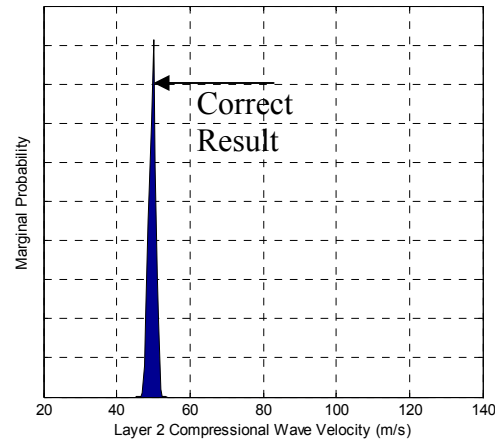


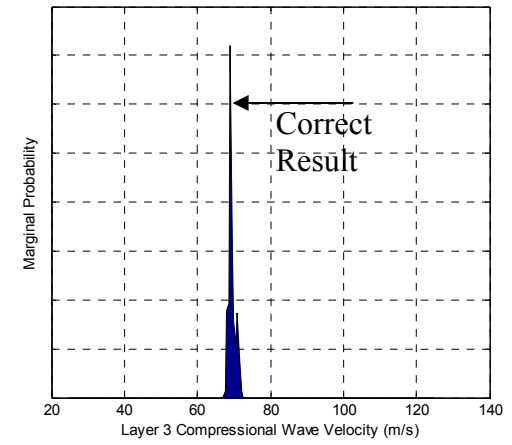
Figure 7-6 – Schematics of SPA.



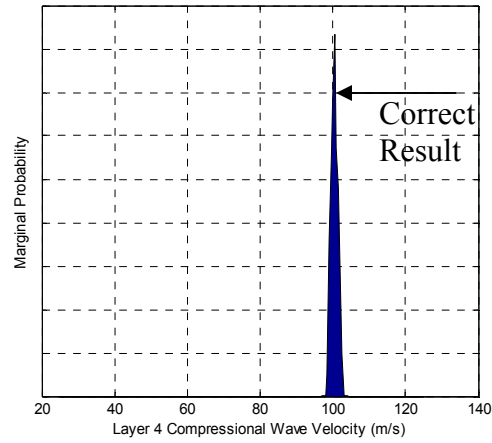
(a)



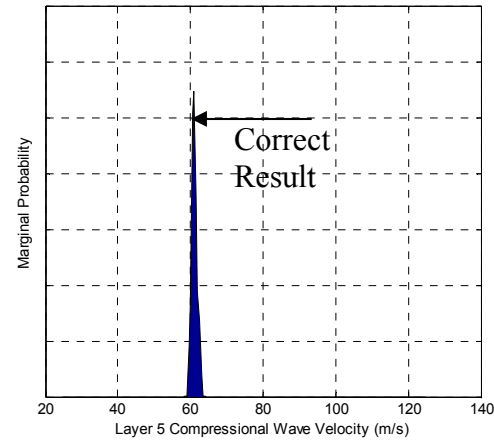
(b)



(c)

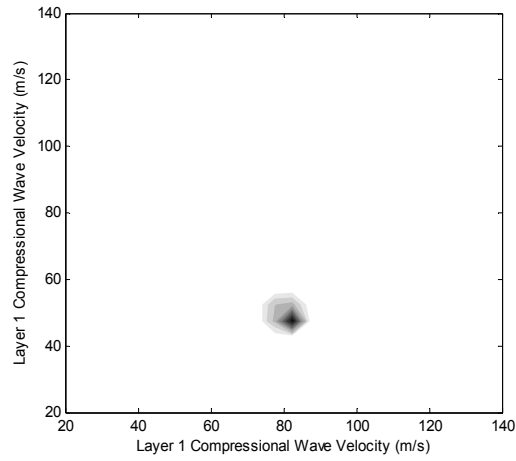


(d)

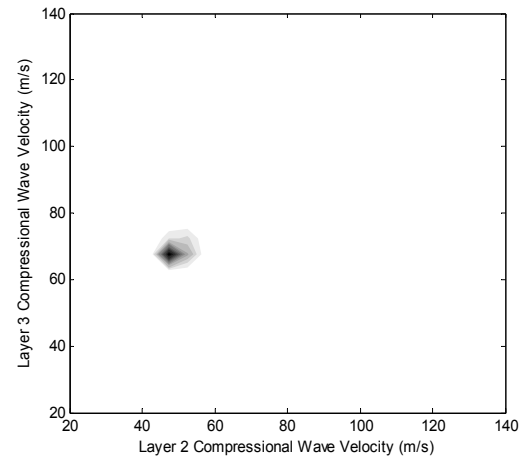


(e)

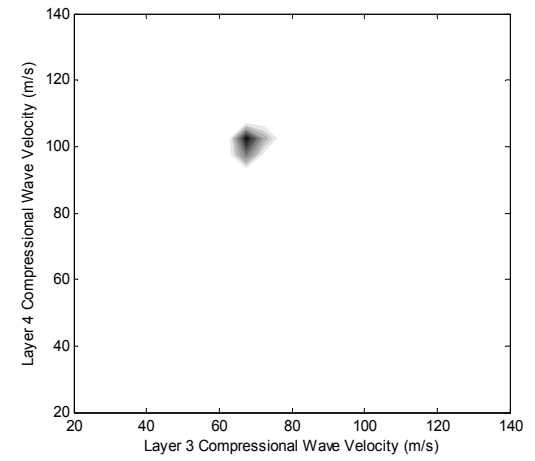
Figure 7-4 - (a, b, c, d and e) Kernel density estimates of marginal a posteriori probabilities for the layer compressional wave velocities.



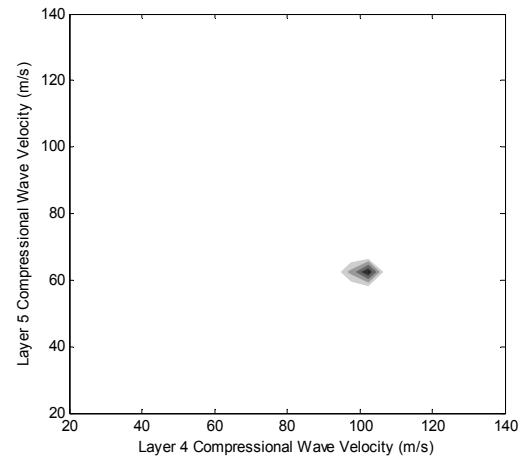
(a)



(b)



(c)



(d)

Figure 7-5 - (a, b, c , and d) Two dimensional kernel density estimates of marginal a posteriori probabilities for the layer compressional wave velocities.

Experimental Waveforms

The test results used in this section were collected as a part of the SPA testing and monitoring performed in the course of a research project on investigation of the pavement material characterization and its seasonal variation conducted jointly by Rutgers University and Stantec Inc. The details of the project and its results have been published in a number of reports and papers [Zaghloul *et al.* 2006].

For the example considered here, acceleration time histories A1, A2 and A3 from a test on a flexible pavement section were considered as the experimental data. While, the device collects much more information than these three time records, only these three accelerometers were considered to illustrate the potential of the waveform inversion technique.

SPA is originally designed to record the changes in acceleration and load in terms of raw analog to digital (A/D) counts and not in terms of actual acceleration and load values. The A/D counts are adequate for implementation of the aforementioned five seismic techniques. Typical acceleration records collected during a test on a flexible pavement, along with the inducing loading wavelet of high frequency hammer measured by the load cell mounted on the hammer, are presented in Figure 7-7 in terms of A/D counts. The translation of these records from the A/D counts to the actual acceleration and load values requires multiplication of the recorded histories by calibration factors, which were not available for this study. However, as will be illustrated below, this step is not necessary for the waveform inversion application presented here.

By inspection of the data in Figure 7-7, it can be observed that the recorded waveforms contain an initial wave packet followed by other oscillations. Intuitively, the

initial packet of the waves at each receiver location, which generally occurs between 0 and 0.001 seconds, contains the major portion of the information carried by the waves. Therefore, for the example presented here, this portion of the wave is windowed using a Hamming window [Oppenheim and Schaffer 1989] and resulting waveforms are considered as input data in the inversion procedure. The windowing functions along with the windowed waveforms are depicted in Figure 7-8.

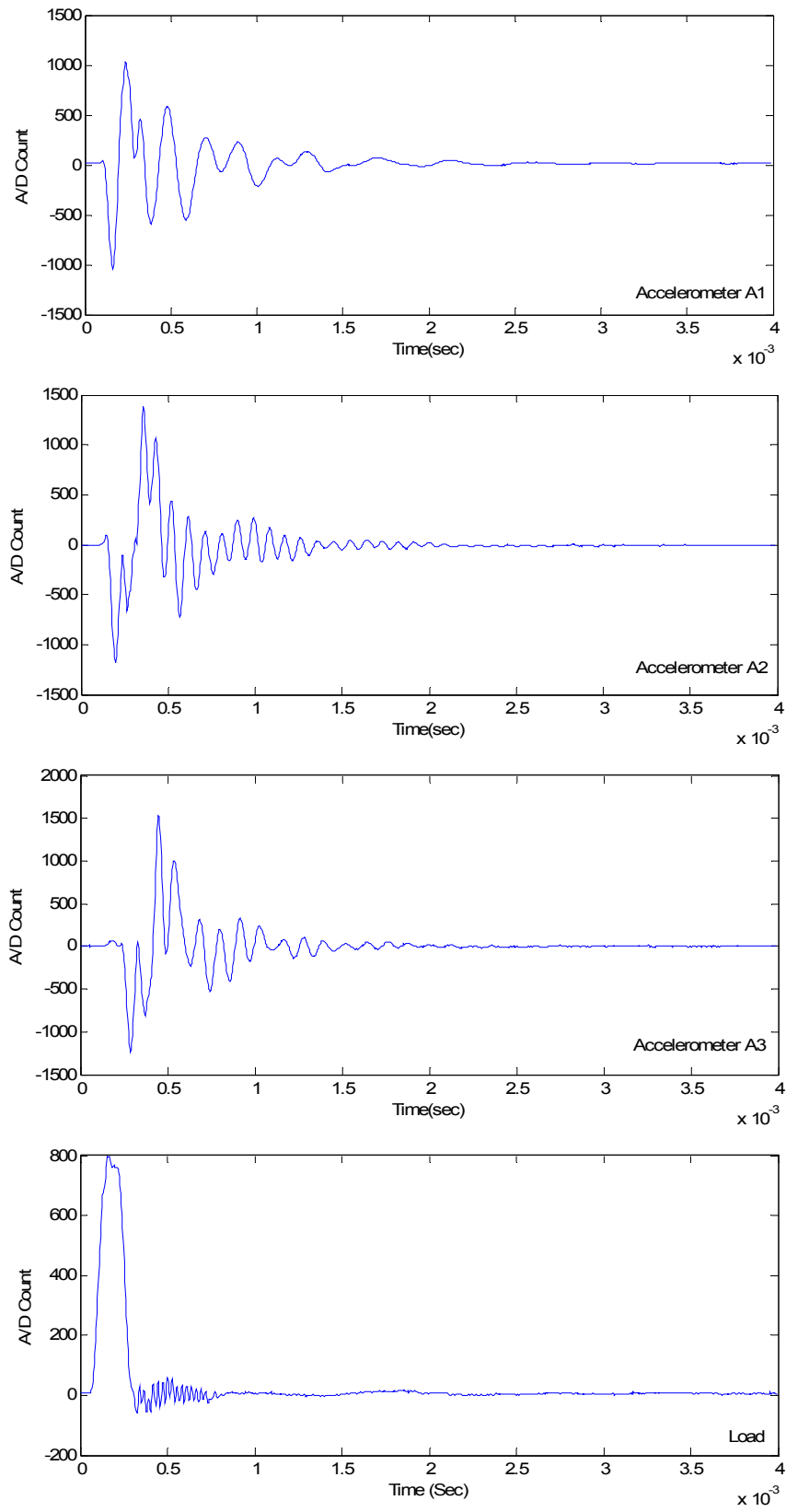


Figure 7-7 –A/D counts from accelerometers A1, A2, A3, and the high frequency hammer from a test on a flexible section.

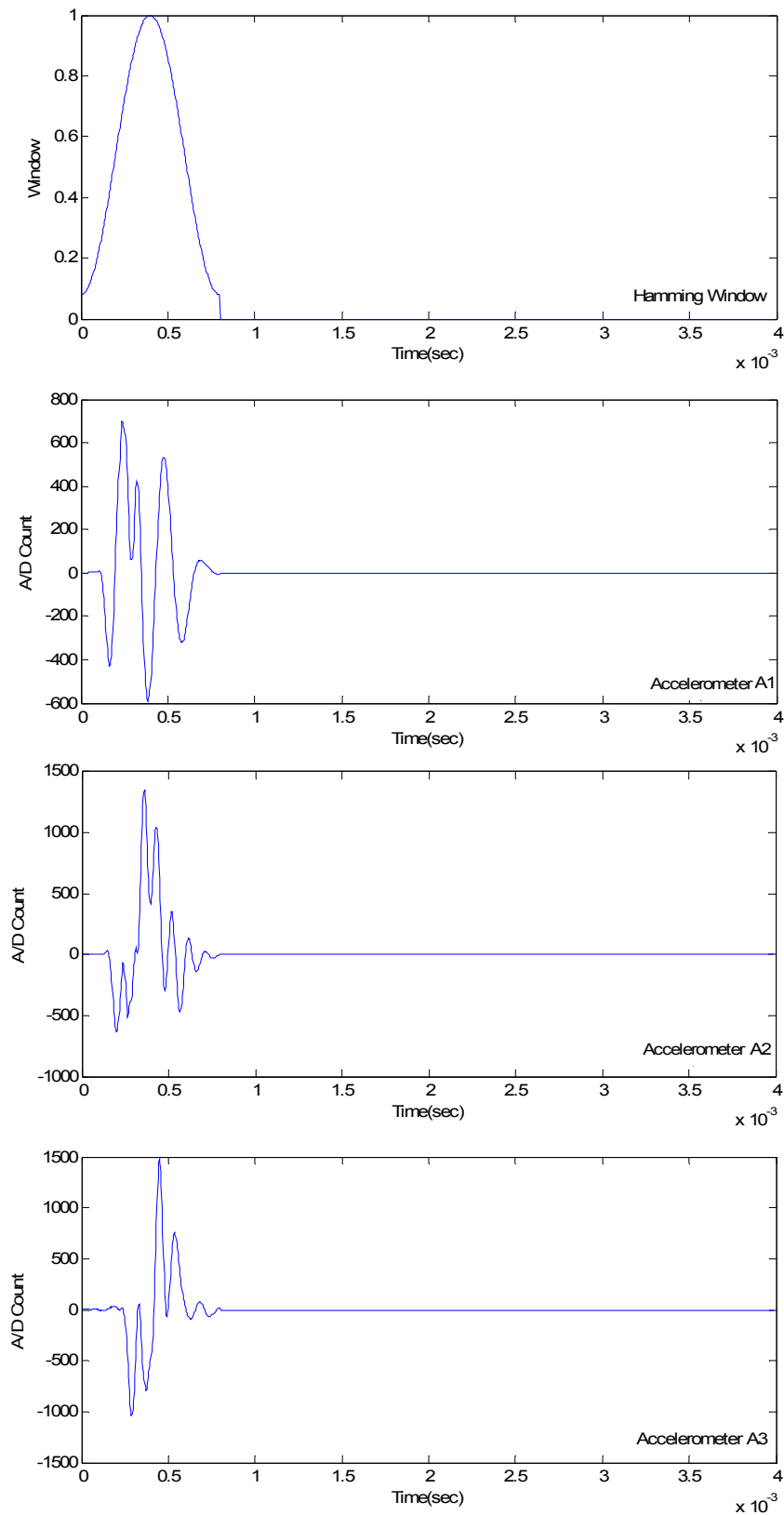


Figure 7-8 – Hamming window function and A/D counts from accelerometers A1, A2, A3 after the windowing operation.

Forward Model

To evaluate the response of a pavement section to various loads, pavements are generally modeled as horizontally layered systems. Due to a low intensity of the excitation in the SPA test, the response of the pavement is essentially a linearly elastic one. Therefore, a spectral element model, as presented in Appendix A, can be used as a representative model and is considered here as the forward model.

To predict the theoretical response of a typical pavement section during a SPA test, the recorded A/D counts of the loading time history, as presented in Figure 7-7, is used as an input to the model. The resulting waveforms are then windowed using the same windowing operations as described earlier. It should be noted that, since the input loading history is given and used in terms of A/D counts, the magnitude of the predicted accelerations from the model can not be realistic. However, since the pavement system is essentially linearly elastic, the relative variation of the acceleration is realistic and can be compared to the relative variation of acceleration in actual recorded data. To perform such a comparison during the inversion, the predicted acceleration time history at each receiver location is scaled so that the value of its maximum matches the value of the maximum acceleration in the actual data. Once this scaling has been performed, the theoretical and experimental data are compared to each other.

Results of Inversion of SPA Data

Using the presented forward model, the SPA data was analyzed to obtain the layer elastic modulus and layer thickness for each layer. For this analysis, the pavement was

modeled as a three layer system; an asphalt layer over a base layer, underlain by an infinite subgrade layer. The combined data and modeling uncertainty covariance was selected to be one unit of A/D count. Obviously, a more comprehensive analysis is required to identify an appropriate value for modeling and data uncertainties. However, in this analysis, a nominal uncertainty value was selected to illustrate the waveform inversion for experimental test data. Kernel density estimates of marginal a posteriori probability densities for the layer moduli obtained from the probabilistic backcalculation are presented in Figure 7-9. A comparison of the acceleration time histories for the pavement section with the most probable layer moduli and the observed data are presented in Figure 7-10. It can be observed that the waveform inversion has identified the layer moduli and thicknesses. However, the uncertainty of the moduli is much lower than the uncertainty of the thicknesses calculated from the inversion analysis. It should be mentioned that the objective of the presented analysis was to validate the applicability of the waveform inversion for experimental data. Although the presented results validate the applicability of the approach, further research is required to completely understand different aspects of the waveform inversion for shallow subsurface investigation. The research should try to address a number of issues, such as evaluation of uncertainties in the modeling by comparing actual and theoretical data and verifying the inversion analysis by comparison of the results to other reference data such as laboratory test results. Such reference data were not available for this preliminary study.

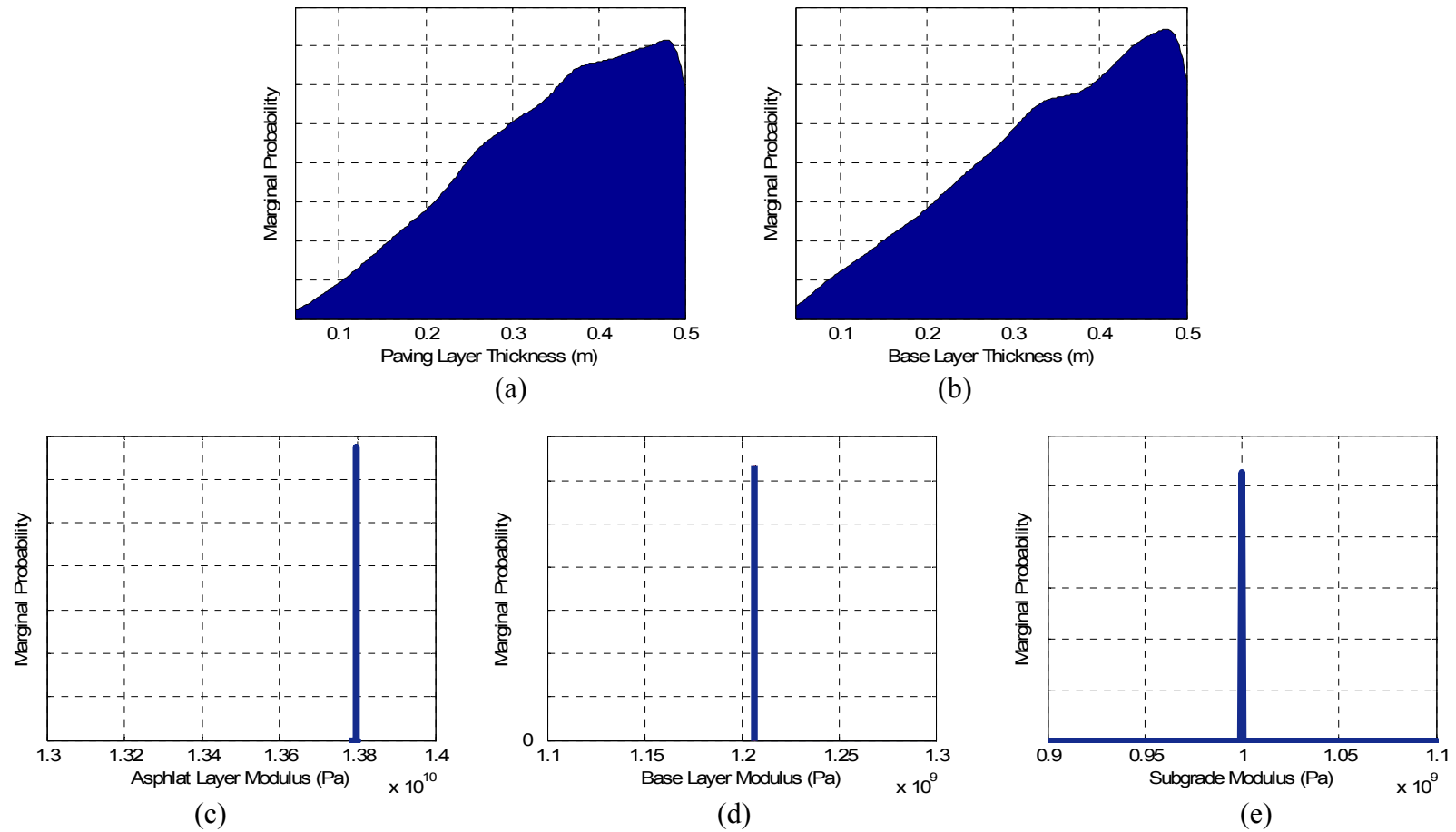


Figure 7-9 – - Kernel density estimates of marginal a posteriori probabilities for the layer thickness (a and b) and layer moduli (c, d, and e) obtained from the probabilistic inversion of the acceleration time histories.

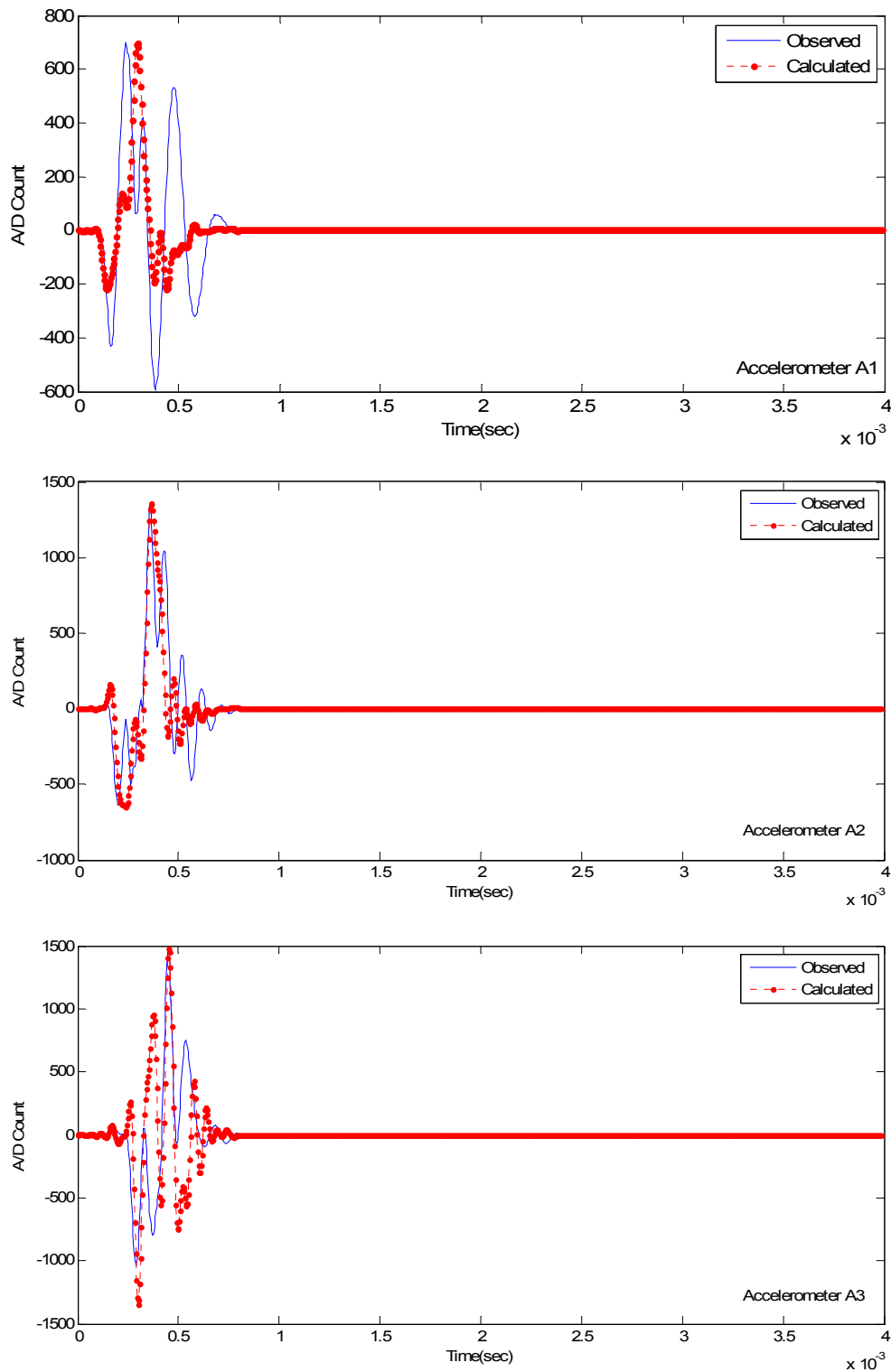


Figure 7-10 – Comparison of the acceleration time histories for the pavement section with the most probable layer moduli and the observed data.

Summary

The probabilistic formulation of the seismic waveform inversion problem for evaluation of subsurface properties in civil engineering was presented in this chapter. Using a set of synthetic data, the potential of the waveform inversion for evaluation of the subsurface profiles was illustrated. It was shown that the waveform inversion is a powerful technique, which is not limited by many of the assumption of other seismic techniques such as Spectral Analysis of Surface Waves (SASW). Finally, by inversion of a set of experimental seismic data collected for a pavement section by Seismic Pavement Analyzer (SPA), the feasibility of the application of the probabilistic waveform inversion approach to real data was illustrated.

References

- ABAQUS (2005), Hibbitt, Karlsson, and Sorensen, Providence, RI.
- Gucunski, N., and Woods, R. D. (1991), "Instrumentation for SASW Testing." Geotechnical Special Publication No. 29, Recent Advances in Instrumentation, Data Acquisition, and Testing in Soil Dynamics, New York: American Society of Civil Engineers, pp. 1-16.
- Nazarian, S., Stokoe, K.H., II and Hudson, W.R. (1983), "Use of Spectral Analysis of Surface Waves Method for Determination of Moduli and Thicknesses of Pavement Systems," Transportation Research Record, No. 930, National Research Council, Washington, D.C., 38-45.
- Nazarian, S. (1984), "In situ determination of elastic moduli of soil deposits and pavement systems by spectral analysis of surface waves method" PhD thesis, Univ. of Texas at Austin, Texas.
- Nazarian S., Baker M.R. and Crain K. (1993), "Development and Testing of a Seismic Pavement Analyzer - Software and Hardware" Report SHRP-H-375, Strategic Highway Research Program, National Research Council, Washington, D.C.
- Oppenheim, A.V., and Schafer R.W., (1989), "Discrete-Time Signal Processing", Prentice-Hall.
- Park, C.B., Miller, R. D., and Xia, J. (1999), "Multichannel Analysis of Surface Waves" Geophysics, Vol. 64, No. 3, pp. 800-808.
- Priestly (1981) "Spectral Analysis of Time Series", Academic Press, New York.
- Reddy, S. (1992), "Improved Impulse Response Testing - Theoretical and Practical Validations" M.S. Thesis, The University of Texas at El Paso.

- Sansalone, M, (1997), “Impact-Echo: The Complete Story” ACI Structural Journal, Vo. 94, No. 6, pp. 777-786.
- Zaghoul, S.M., Gucunski, N., Jackson, H., and Hadidi, R. (2006), “Material Characterization and Seasonal Variation in Material Properties”, Report No. FHWA-NJ-2005-024, New Jersey Department of Transportation, Trenton, NJ.

8 Closure

Summary and Conclusions

In this dissertation, a general probabilistic approach to the solution of the inverse problems was introduced as a better approach to the solution of inverse problems. The mathematical framework required for implementation of this approach was presented in detail. This approach is a new approach to inverse problems in civil engineering and is different from the currently used deterministic approach, where the objective is to find the model of a system, for which the theoretical response best fits the observed data. Following the mathematical formulation of the approach, techniques for direct analytical evaluation and numerical approximation of the probabilistic solution using Monte Carlo Markov Chains (MCMC), with and without Neighborhood Algorithm (NA) approximation, were introduced and explained. The application of the presented concepts and techniques was then illustrated in practical terms using a simple modulus determination experiment.

The probabilistic approach was applied to three important classes of inverse problems in geotechnical/transportation engineering as application examples. These applications were:

- Pavement modulus backcalculation for Falling Weight Deflectometer (FWD),
- Model calibration based on geotechnical instrument measurements, and
- Seismic waveform inversion for shallow subsurface characterization.

A brief summary of the major findings in each application is presented below.

FWD Backcalculation

As the first application, probabilistic FWD backcalculation was introduced formulated, and the results of the backcalculation of synthetic test data were presented. The probabilistic backcalculation was then used as a tool to compare different backcalculation procedures, such as static and dynamic backcalculation procedures. Based on the presented results, it was shown that the static backcalculation procedures fail to capture the essential dynamic nature of the test and consequently can not be relied upon for accurate backcalculation. It was also demonstrated that there is little redundancy in dynamic deflection bowl backcalculation procedures, which can produce large uncertainties in obtained backcalculation results. Among the compared backcalculation procedures, the dynamic deflection time history backcalculation offers the best and most reliable approach in the FWD backcalculation. The application of this approach was then illustrated both on synthetic and actual experimental data. It was also shown that, at least in the case of synthetic data, the deflection time histories carry enough information to simultaneously backcalculate for layer moduli and bedrock depth. Finally, the effect of frequency dependent layer material properties on predicted deflection time histories was

investigated. It was shown that such effects can be significant and produce discrepancies in the backcalculation results.

Model Calibration

As the second application, calibration of a finite element settlement prediction model for a landfill redevelopment project was presented. This example demonstrated how the probabilistic inversion approach can be used to complement the application of the observational method in geotechnical engineering. The basic formulation of the probabilistic solution was described for this problem and the calibration of a settlement prediction model using the probabilistic approach was then outlined and the results of the analysis were presented. It was illustrated that the ability of the probabilistic approach to evaluate the uncertainties of the obtained results provides an engineer with very valuable information regarding the limitations of the data and results. Consequently, it enables him/her to devise an appropriate course of action.

Seismic Inversion

As the last application, the probabilistic formulation of a seismic waveform inversion problem for evaluation of shallow subsurface properties was presented. Using a set of synthetic data, the potential of the waveform inversion for evaluation of the subsurface profiles were illustrated. It was shown that the waveform inversion is a powerful technique, which is not limited by many of the assumption of other seismic techniques, such as Spectral Analysis of Surface Waves (SASW). Finally, the feasibility

of the application of the probabilistic waveform inversion approach to real data was illustrated by inversion of a set of experimental seismic data collected for a pavement section by Seismic Pavement Analyzer (SPA).

Recommendations for Future Research

The following are recommendations for further development of the probabilistic approach and its adoption in engineering practice:

- The probabilistic approach to the solution of inverse problems is a mathematical tool that can be applied to virtually any inverse problem in civil engineering. Advantages of using the probabilistic approach in other civil engineering applications should be further explored.
- To introduce the approach in this research, Matlab® was used as a development environment and generic computer codes were generated for application of the approach. However, to optimize the computational efficiency of the approach and facilitate its implementation, development of efficient stand alone and application oriented codes should be considered.
- One essential component of any inverse problem is the forward model used in generation of the theoretical solution. Development of efficient forward models for each application and evaluation of their uncertainties in comparison to actual measurements will be an essential and necessary next step in further development of the presented approach.

- As outlined in this research, in probabilistic approach, the input parameters of an inverse problem should be accompanied by uncertainty measures represented by a priori information. There limited guidelines in literature addressing the uncertainties in different contexts. A comprehensive review of these guidelines for application in probabilistic approach is required. This review should be followed by development of application oriented guidelines to facilitate the application of this approach as a practical tool.

Appendix A: Spectral Element Method for Analysis of Wave Propagation in Layered Media

Introduction

Finite element method is a general and accepted numerical tool in analysis of wave propagation. However, in spite of the recent advances in computational capabilities, significant resources are still required to perform a reasonably accurate wave propagation analysis using finite element method. In the finite element analysis, the number and type of elements control the computational time required to solve the model. The number of elements required to converge a dynamic finite element model is generally more than a static model and tend to increase with increased excitation frequency. For a structure analyzed at a high excitation frequency, the number of elements may easily exceed the practical number to solve the problem in a timely manner.

For horizontally layered media, over the years, a series of more efficient techniques have been developed, which involves a combination of analytical and numerical solutions. The general similarity of these techniques, referred to here as frequency domain techniques, is that the solution is obtained by a synthesis of waveforms

from superposition of many frequency components, which are in part are obtained analytically. The most notable work in this area has been done by Thomson [1950] and Haskell [1953], who developed the layer transfer matrix method. In this method, for a given layer, the amplitude of displacement and force vector at one interface are related to the amplitude of displacement and force at the other interface for each frequency component through the transfer matrix. Kausel and Roesset [1981] further developed this technique by introducing a layer stiffness matrix similar to those in the finite element method. The transfer and stiffness matrices involve transcendental functions which exhibit numerical complications in implementations.

To overcome this problem, a semi discrete solution was introduced by Lysmer [1970] and was further generalized by Kausel and Roesset [1981]. The basic idea of this solution is to divide layers into sublayers with thicknesses shorter than the wavelength of interest and to approximate the wave in the vertical direction by a linear interpolation between layer interfaces, assuming that the mass of each layer is lumped at the interfaces. By doing so, the transcendental equation will be replaced by a simple eigenvalue problem, which can be solved by standard techniques.

The requirement of subdivision of layers to sublayers of small thickness results in a large system of equations that should to be solved for each frequency component. This makes these techniques rather computationally expensive. The spectral element method [Rizzi and Doyle, 1992, Doyle, 1997] overcomes this issue by modeling the exact mass distribution and using double summation over significant wave numbers and frequencies instead of numerical integration. Consequently, each layer is modeled exactly without the need to subdivide the layer. Hence the method becomes more efficient.

The spectral element method can be described as a variation of p-type convergence analysis in finite element. In dynamic finite element analysis the convergence can be obtained by either increasing the number of elements or increasing the polynomial order of the interpolation functions. If the convergence is obtained by increasing the order of the interpolating function, the convergence is generally referred to as p-type convergence. Typically, the order of the polynomial interpolation function is increased, while the spatial mesh is held constant, until more accurate results are obtained. In spectral elements, the element interpolation functions are based on the eigenfunctions of the differential equation used to represent the dominant mechanics in the problem. This results in the “exact” form of the displacement field for the interpolation function. The interpolation functions of spectral elements are based on trigonometric functions, opposed to polynomial functions of conventional elements. The trigonometric functions incorporate the frequency of the response into the interpolation function. Having the interpolation function based on the eigenfunctions means that a single spectral element will give the “exact” dynamic solution across the element for simple loading and boundary conditions. This results in a reduced number of elements, and thus a reduced model size for a spectral element model as compared to the conventional finite element model.

This appendix provides the basic formulation of the spectral elements and describes its implementation in this research. This appendix is not intended to be a tutorial about this technique. Further details of derivation and implementation of this approach can be found in cited references.

Spectral Wave Analysis

The general form of spectral element analysis approach to wave propagation is presented by Doyle [1997]. This approach is illustrated here for the wave propagation analysis in an axi-symmetric horizontally layered media [Alkhoury et. al 2001].

The general equation of motion for an isotropic elastic material can be represented by the following coupled differential equation:

$$(\lambda + \mu)\nabla\nabla\cdot U + \mu\nabla^2 U = \rho U \quad (\text{A-1})$$

where U is the displacement vector, ρ is the material density, μ and λ are the Lamé constants, ∇ is the vector differential operator, $\nabla\cdot$ is the divergence operation and, ∇^2 is the vector Laplacian operation.

Using Helmholtz decomposition [Achenbach, 1973], the displacement field can be expressed in terms of gradient of a scalar potential function φ and the curl of a vector potential function ψ as:

$$u = \nabla\varphi + \nabla \times \psi \quad (\text{A-2})$$

For an axi-symmetric motion, the vector potential ψ has only one component ψ_θ .

Denoting the displacements in r and z direction by u and w the displacements and potentials are related by:

$$u = \frac{\partial\varphi}{\partial r} - \frac{\partial\psi_\theta}{\partial z} \quad w = \frac{\partial\varphi}{\partial z} + \frac{1}{r} \frac{\partial(r\psi_\theta)}{\partial r} \quad (\text{A-3})$$

and stress-displacement relationships are given by:

$$\begin{aligned} \sigma_{zz} &= (\lambda + 2\mu) \frac{\partial w}{\partial z} + \frac{\lambda}{r} \frac{\partial(ru)}{\partial r} \\ \tau_{zr} &= \mu \left(\frac{\partial u}{\partial z} + \frac{\partial w}{\partial r} \right) \end{aligned} \quad (\text{A-4})$$

These potentials can be obtained by solution of the following differential equations, which are a set of decoupled equations obtained by substitution of Equation (A-3) into Equation (A-1).

$$\begin{aligned} \frac{\partial^2 \varphi}{\partial r^2} + \frac{1}{r} \frac{\partial \varphi}{\partial r} + \frac{\partial^2 \varphi}{\partial z^2} &= \frac{1}{c_p^2} \frac{\partial^2 \varphi}{\partial t^2} \\ \frac{\partial^2 \psi_\theta}{\partial r^2} + \frac{1}{r} \frac{\partial \psi_\theta}{\partial r} + \frac{\partial^2 \psi_\theta}{\partial z^2} - \frac{\psi_\theta}{r^2} &= \frac{1}{c_s^2} \frac{\partial^2 \psi_\theta}{\partial t^2} \end{aligned} \quad (\text{A-4})$$

where c_p and c_s are compressional and shear wave velocities of the medium defined

respectively as $c_p = \left(\frac{\lambda + 2\mu}{\rho}\right)^{1/2}$ and $c_s = \left(\frac{\mu}{\rho}\right)^{1/2}$.

These equations can be transformed to the frequency domain using the Fourier transform:

$$\begin{aligned} \frac{\partial^2 \hat{\varphi}}{\partial r^2} + \frac{1}{r} \frac{\partial \hat{\varphi}}{\partial r} + \frac{\partial^2 \hat{\varphi}}{\partial z^2} &= \frac{1}{c_p^2} \omega^2 \hat{\varphi} \\ \frac{\partial^2 \hat{\psi}_\theta}{\partial r^2} + \frac{1}{r} \frac{\partial \hat{\psi}_\theta}{\partial r} + \frac{\partial^2 \hat{\psi}_\theta}{\partial z^2} - \frac{\hat{\psi}_\theta}{r^2} &= \frac{1}{c_s^2} \omega^2 \hat{\psi}_\theta \end{aligned} \quad (\text{A-5})$$

where hat sign indicates that the expression is in the frequency domain and ω is the frequency. These equations can be solved by separation of variables.

To discretize the solution, a boundary condition is imposed on the problem. Assuming that at the radial boundary $r = R$ (far from load) the amplitude of oscillations vanishes, the generic solution of wave equation can be discretized and is given by double summation over discrete angular frequency ω_n with $n = 1, \dots, N$ and discrete wave number $k_m = \frac{\alpha_m}{R}$ with $m = 1, \dots, M$, where α_m is the m th positive root of Bessel

function of first kind, J_0 . The solution is presented below:

$$\begin{aligned} \varphi &= \sum_n \sum_m A_{mn} e^{-ik_{pmn}z} J_0(k_m r) e^{-i\omega_n t} \\ \psi_\theta &= \sum_n \sum_m B_{mn} e^{-ik_{smn}z} J_1(k_m r) e^{-i\omega_n t} \end{aligned} \quad (\text{A-6})$$

where J_1 is the Bessel function of first kind and order one, A_{mn} and B_{mn} are coefficients to be determined from the boundary conditions and k_{szmn} and k_{pzmn} satisfy the following relations referred to as spectrum relations:

$$\begin{aligned} k_{pzmn} &= \left(\frac{\omega_n^2}{c_p^2} - k_m^2 \right)^{1/2} \\ k_{szmn} &= \left(\frac{\omega_n^2}{c_s^2} - k_m^2 \right)^{1/2} \end{aligned} \quad (\text{A-7})$$

Spectral Element Formulation

The obtained discretized solution can be used to derive the spectral elements formulation. Such a derivation is presented below for a two node layer element and a one node half space element.

Two-Node Layer Element

The two node layer element with a height of h , which is depicted in Figure A-1, can be visualized as a layer confined by two circular surfaces within which the wave is constrained to move. The response at any point in the element is determined by a superposition of incident and reflected waves from each surface. To include both incident and reflected waves, the following general solution that is obtained by adding two potentials is considered. These potentials include waves propagating in both directions:

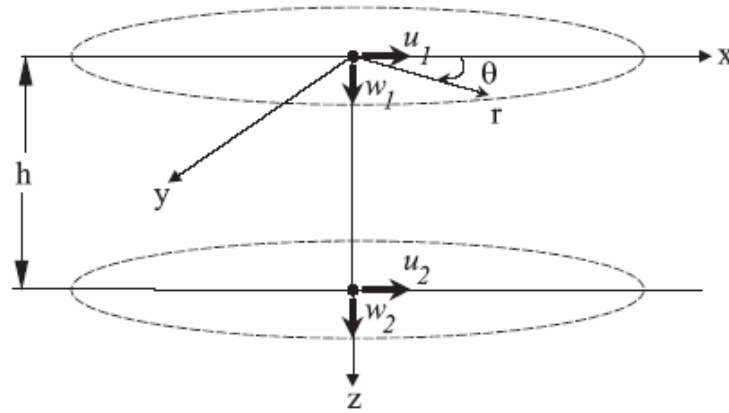


Figure A-1 - Two-node axis-symmetrical layer element [Alkhoury, 2001].

$$\begin{aligned}\varphi_{mn}(r, z, \omega_n, k_m) &= (A_{mn} e^{-ik_{pzm}z} + C_{mn} e^{-ik_{pzm}(h-z)}) J_0(k_m r) \\ \psi_{mn}(r, z, \omega_n, k_m) &= (B_{mn} e^{-ik_{szm}z} + D_{mn} e^{-ik_{szm}(h-z)}) J_1(k_m r)\end{aligned}\quad (\text{A-8})$$

where z is the distance measured from the top surface of the element and A_{mn} , B_{mn} , C_{mn} , and D_{mn} are constants. Substituting the potentials in Equation (A-8) into Equation (A-3) the radial and vertical displacements in the frequency domain are obtained as:

$$\begin{aligned}u_{mn}(r, z, \omega_n, k_m) &= \left(-A_{mn} k_m e^{-ik_{pzm}z} - C_{mn} k_m e^{-ik_{pzm}(h-z)} \right. \\ &\quad \left. + iB_{mn} k_{szm} e^{-ik_{szm}z} - iD_{mn} k_{szm} e^{-ik_{szm}(h-z)} \right) J_1(k_m r) \\ w_{mn}(r, z, \omega_n, k_m) &= \left(-iA_{mn} k_{pzm} e^{-ik_{pzm}z} + iC_{mn} k_{pzm} e^{-ik_{pzm}(h-z)} \right. \\ &\quad \left. + B_{mn} k_m e^{-ik_{szm}z} + D_{mn} k_m e^{-ik_{szm}(h-z)} \right) J_0(k_m r)\end{aligned}\quad (\text{A-9})$$

So the displacements at the top of the layer, u_{1mn} and w_{1mn} , and the bottom of the layer u_{2mn} and w_{2mn} can be related to potential coefficients by:

$$[u_{1mn}, w_{1mn}, u_{2mn}, w_{2mn}]^T = [I_{mn}] [A_{mn}, B_{mn}, C_{mn}, D_{mn}]^T \quad (\text{A-10})$$

where I_{mn} is the matrix of coefficients. The algebra required to obtain I_{mn} in Equation (A-10) is straightforward but it should be performed with significant care. The exact expression of I_{mn} is given by Alkhoury et al. [2001] and will not be repeated here.

Similar to the derivation of Equation (A-10), the surface traction T_k at each interface can be related to the potential coefficients using equations (A-4) and (A-9). To obtain the surface tractions the Cauchy stress principle, $T_k = \tau_{km} n_m$, is used. In this equation, n_m represents the normal to the surface of the layer and τ_{km} is the component of the stress tensor. So the traction at the top of the layer, T_{r1mn} and T_{z1mn} , and the bottom of the layer T_{r2mn} and T_{z2mn} , can be related to potential coefficients by:

$$[T_{r1mn}, T_{z1mn}, T_{r2mn}, T_{z2mn}]^T = [H_{mn}] [A_{mn}, B_{mn}, C_{mn}, D_{mn}]^T \quad (\text{A-11})$$

The exact expression of H_{mn} is also given by Alkhoury et. al. [2001] and will not be repeated here. Upon performing the required algebra to eliminate the coefficient from equations (A-10) and (A-11), the tractions and displacements can be related to each other by a complex and symmetric 4x4 dynamic stiffness matrix.

$$[T_{r1mn}, T_{z1mn}, T_{r2mn}, T_{z2mn}]^T = [k_{mn}] [u_{1mn}, w_{1mn}, u_{2mn}, w_{2mn}]^T \quad (\text{A-12})$$

where:

$$[k_{mn}] = \begin{bmatrix} k_{11mn} & k_{12mn} & k_{13mn} & k_{14mn} \\ & k_{22mn} & -k_{14mn} & k_{24mn} \\ & & k_{11mn} & -k_{11mn} \\ \text{sym} & & & k_{22mn} \end{bmatrix} \quad (\text{A-13})$$

and

$$k_{11mn} = \frac{\mu}{\Delta_{mn}} \{ ik_{pzmn} (k_{szmn}^2 + k_m^2) (k_m^2 Q_{12} Q_{21} + k_{szmn} k_{pzmn} Q_{11} Q_{22}) \}$$

$$k_{12mn} = \frac{\mu}{\Delta_{mn}} \left\{ k_m k_{szmn} k_{pzmn} (-k_{szmn}^2 + 3k_m^2) (Q_{12} Q_{22} - 4 \exp(-ik_{pzmn} h - ik_{szmn} h)) \right. \\ \left. - k_m Q_{11} Q_{21} (k_m^2 k_{szmn}^2 - k_m^4 - 2k_{pzmn}^2 k_{szmn}^2) \right\}$$

$$k_{13mn} = \frac{\mu}{\Delta_{mn}} \{ -2ik_{pzmn} (k_{szmn}^2 + k_m^2) (k_m^2 \exp(-ik_{pzmn} h) Q_{21} + k_{szmn} k_{pzmn} \exp(-ik_{szmn} h) Q_{11}) \}$$

$$k_{14mn} = \frac{\mu}{\Delta_{mn}} \{2k_{pzmn} k_{szmn} (k_{szmn}^2 + k_m^2) (\exp(-ik_{pzmn} h) Q_{22} - \exp(-ik_{szmn} h) Q_{12})\}$$

$$k_{22mn} = \frac{\mu}{\Delta_{mn}} \{ik_{szmn} (k_{szmn}^2 + k_m^2) (k_m^2 Q_{11} Q_{22} + k_{szmn} k_{pzmn} Q_{12} Q_{21})\}$$

$$k_{24mn} = \frac{\mu}{\Delta_{mn}} \{-2ik_{szmn} (k_{szmn}^2 + k_m^2) (k_m^2 \exp(-ik_{szmn} h) Q_{11} + k_{szmn} k_{pzmn} \exp(-ik_{pzmn} h) Q_{21})\}$$

In which:

$$\Delta_{mn} = 2k_m^2 k_{pzmn} k_{szmn} (4 \exp(-ik_{pzmn} h - ik_{szmn} h) - Q_{12} Q_{22}) - (k_{pzmn}^2 k_{szmn}^2 + k_m^4) Q_{11} Q_{21}$$

$$Q_{11} = 1 - \exp(-2ik_{pzmn} h)$$

$$Q_{21} = 1 - \exp(-2ik_{szmn} h)$$

$$Q_{12} = 1 + \exp(-2ik_{pzmn} h)$$

$$Q_{22} = 1 + \exp(-2ik_{szmn} h)$$

One-Node Half Space Element

In a one node half space element waves travel only in one direction. So only the incident wave potential is considered in the derivation of the element matrix. An illustration of the one node half space element is presented in Figure A-2. The steps in the derivation of the stiffness matrix in this case are similar to the steps in the derivation of the two node element presented earlier. Similar to the derivation for the two node element, the stiffness matrix can be obtained as:

$$[T_{r1mn}, T_{z1mn}]^T = [k_{mn}] [u_{1mn}, w_{1mn}]^T \quad (\text{A-14})$$

where:

$$[k_{mn}] = \frac{\mu}{\Delta_{mn}} \begin{bmatrix} ik_{pzm n} (k_{sz}^2 + k_m^2) & (2k_{pzm n} k_{szm n} - k_{szm n}^2 + k_m^2) k_m \\ \text{sym} & ik_{szm n} (k_{sz}^2 + k_m^2) \end{bmatrix} \quad (\text{A-15})$$

and $\Delta_{mn} = k_m^2 + k_{pzm n} k_{szm n}$.

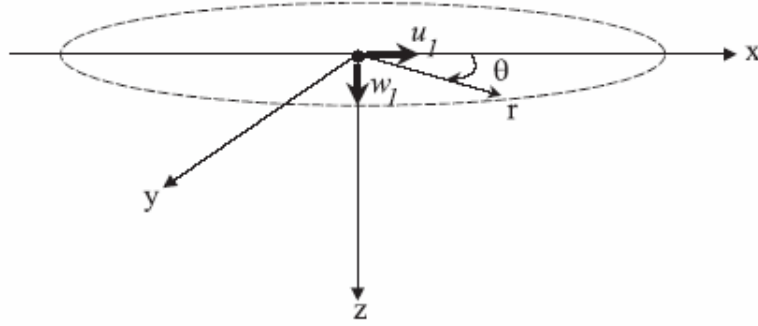


Figure A-2 - One-node axis-symmetrical half space element.
[Alkhoury, 2001].

Assemblage

Assemblage of stiffness matrices follows the usual procedures of the conventional finite element method [Cook, 1974] except that dynamic, rather than static, equilibrium is imposed at each node. The stiffness matrix should be assembled at each frequency and wave number. The same procedure should be followed in assemblage of the global force vector.

Boundary Conditions and Solution of the System for an Impact Load

For an applied load at the surface of a horizontally layered medium the actual displacements are obtained by scaling the response at each frequency and wave number according to the coefficients of the decomposition of the load at that wave number and frequency. To illustrate the procedure, these coefficients are obtained below for a load

with a spatial distribution of q for $0 \leq r \leq a$, as shown in Figure A-3, and a half sine time variation, as presented in Figure A-4,

The scaling factors in the frequency domain, \hat{F}_n , are obtained by Fourier transform. The Fourier transform coefficients can be numerically calculated by applying fast Fourier transform (FFT) to the time variation of the force function. For the half sine force function depicted in Figure A-4, the variation of the magnitude of FFT coefficient with frequency is presented in Figure A-5.

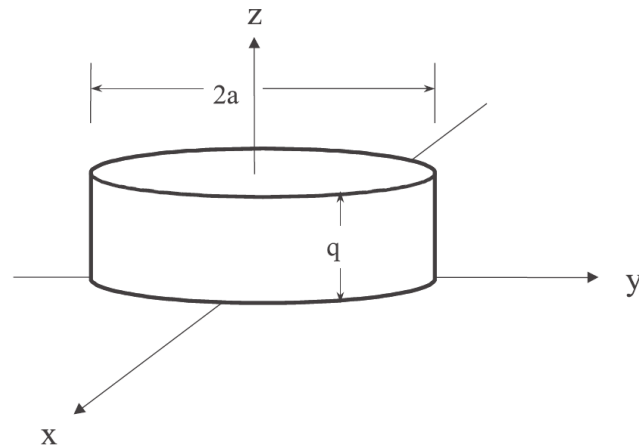


Figure A-3 – Spatial distribution of the load [Alkhoury, 2001].

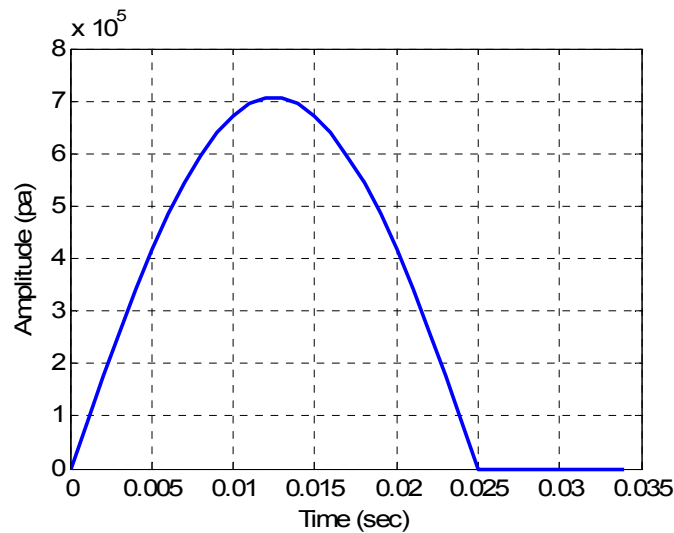


Figure A-4 - Time history of the idealized time wavelet.

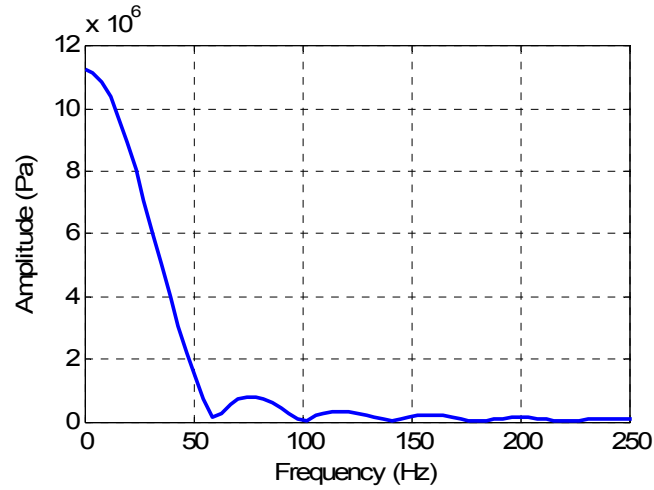


Figure A-5 - Frequency spectrum of the idealized wavelet.

The scaling factors in the wave number domain can be obtained based on Fourier-Bessel theory. For a cylindrical shaped load of a radius a , the Fourier-Bessel coefficients are given by [Kreyszig, 1999]:

$$\hat{F}_m = \frac{2a}{\alpha_m R J_1^2(\alpha_m)} J_1\left(\frac{\alpha_m}{R} a\right) \quad m = 1, \dots, M \quad (\text{A-16})$$

where \hat{F}_m is the coefficient of Fourier Bessel series for a wave number $k_m = \frac{\alpha_m}{R}$ with

$m = 1, \dots, M$, and α_m is the m th positive root of the Bessel function of first kind, J_0 .

The variation of Fourier-Bessel series coefficients for a circular load of a radius a , as depicted in Figure A-3, is presented in Figure A-6.

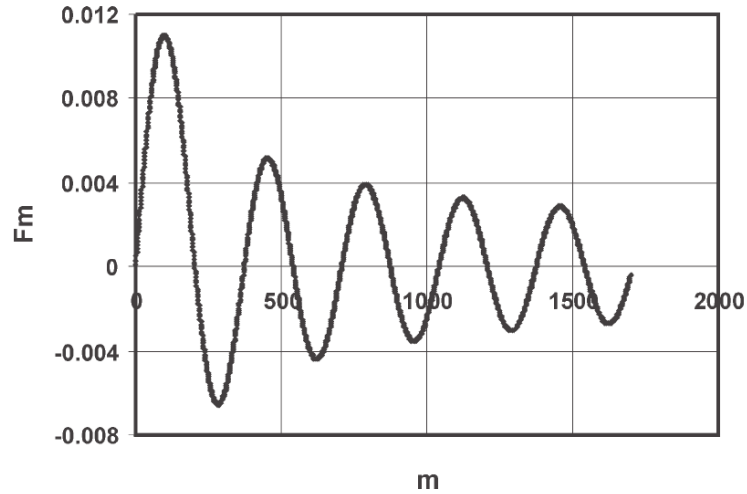


Figure A-6 – Coefficients of Fourier-Bessel series for a circular load of a radius $a = 0.15m$.

Numerical Implementation

The flowchart of the algorithm for implementation of the spectral element method is presented in Figure A-7 [Alkhory et. al. 2001]. A Mathlab® code was developed based on this algorithm to implement the presented spectral element approach. The algorithm can be generally described by the following steps:

- Obtain time and wave number domain scaling factors by FFT and Fourier-Bessel transform of the load function, respectively.
- Form the stiffness matrix of the system for each frequency and wave number.
- Solve for the displacements for a unit load in the frequency-wave number domain for each frequency and wave number combination.
- Scale the calculated response using the obtained scaling factors.
- Sum all the wave number domain responses for each frequency to obtain the response in the frequency domain.

- Use inverse FFT to obtain the response in the time domain.

Illustrative Example

To verify the accuracy of the developed spectral element code, a numerical example is considered and the results of the example are presented. The example considered here is the simulation of the pavement response during the Falling Weight Deflectometer (FWD) test. The pavement layer properties used for the numerical simulation are presented in Table A-1. The spatial and time variation of the load function considered for this example is similar to those presented in previous section.

The predicted surface deflection time histories by the spectral element method are presented in Figure A-7. The response of the same pavement, as calculated by Alkhoury [2001a], is presented in Figure A-8. These results are in very good agreement, which confirms the accuracy of the developed code. Furthermore, as presented in Chapter 5, these results are also in good agreement with finite element results.

Table A- 1 – Geometrical and material properties used in the numerical evaluation and verification of the spectral element method [Alkhoury, 2001].

Material Type	Thickness (m)	Elastic Modulus (MPa)	Poisson's Ratio	Mass Density (kg/m ³)
Asphalt Concrete	0.15	1000	0.35	2300
Aggregate Base Course	0.25	200	0.35	2000
Subgrade	infinity	100	0.35	1500

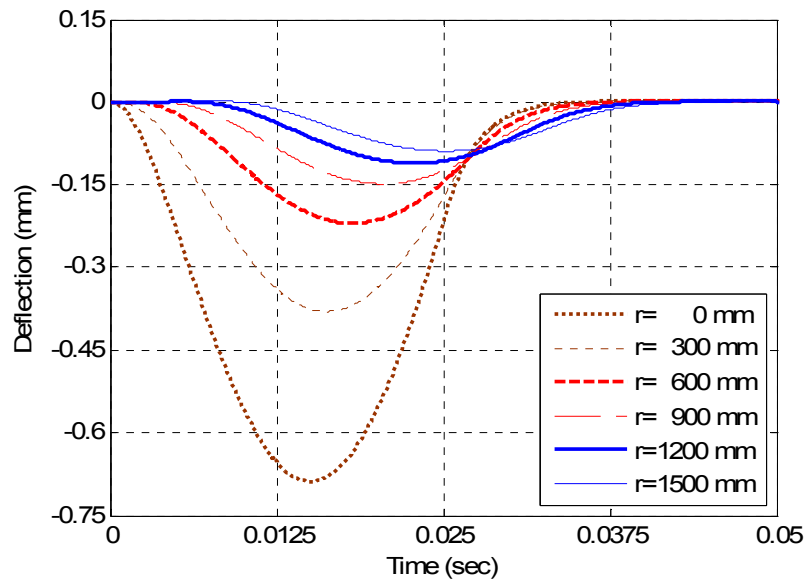


Figure A-7 - Predicted pavement surface deflection time histories from the spectral element analysis.

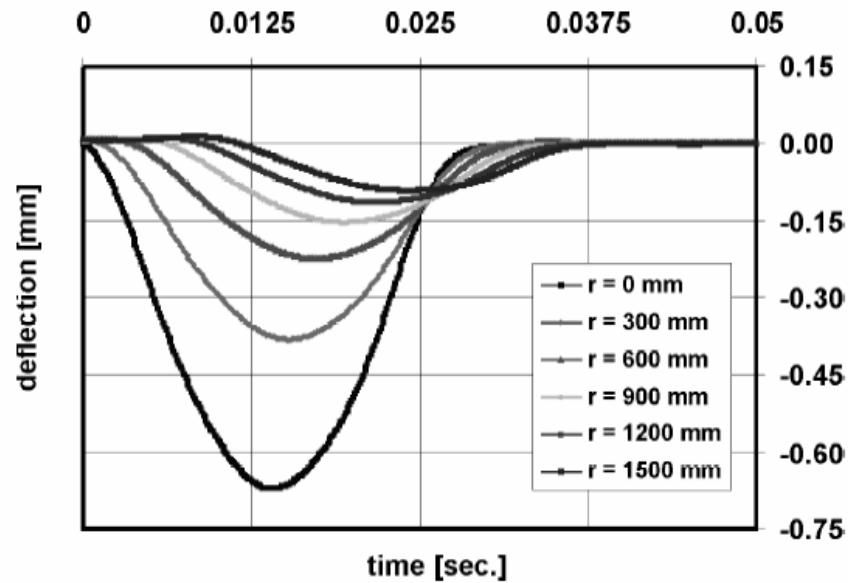


Figure A-8 - Predicted pavement surface deflection time histories from the spectral element analysis [Alkhoury et al., 2001].

Summary

In this appendix, derivation and implementation of the spectral elements technique is presented. Spectral element method, is a frequency domain analysis

technique for horizontally layered media, such as pavements. The method is much more efficient than the traditional finite element technique. The background and basic formulation of the spectral element method was presented in this appendix and its implementation was illustrated by the simulation of the FWD test. It is shown that the results of the developed Matlab® code are in agreement with results published by others.

References

- Achenbach, J. D. (1973), “Wave Propagation in Elastic Solids”, Elsevier, Amsterdam, Netherlands.
- Al-khoury, R., Scarpas, A., Kasbergen, C., Blaauwendraad, J. (2001a), “Spectral Element Technique for Efficient Parameter Identification of Layered Media: Part I: Forward Model”, International Journal of Solids and Structures, Vol. 38.
- Al-khoury, R., Scarpas, A., Kasbergen, C., Blaauwendraad, J. (2001b), “Spectral Element Technique for Efficient Parameter Identification of Layered Media: Part II: Inverse Calculations”, International Journal of Solids and Structures, Vol. 38.
- Cook, R. D., (1974), “Concepts and Application of Finite Element Analysis”, Jon Wiley and Sons, New York, NY.
- Doyle, J.M. (1997), “Wave Propagation in Structures”, Springer-Verlag, NY.
- Haskell, N.A. (1953), “The Dispersion of Surface Waves on Multilayered Media”, Bulletin of Seismological Society of America, Vol. 43, 17-34.
- Kausel, E. and Rosset, J. M. (1981), “Stiffness Matrices for Layered Soils”, Bulletin of Seismological Society of America, Vol. 71, 1743-1761.
- Kreyszig, E. (1999), “Advanced Engineering Mathematics”, 8th. Edition, John Wiley and Sons, New York, NY.
- Lysmer, J., (1970), “Lumped Mass Method for Rayleigh Waves”, Bulletin of Seismological Society of America, V.60, No. 1, pp. 89-104.
- Rizzi, S.A. and Doyle, J.F. (1992), “Spectral Analysis of Wave Motion in Plane Solids with Boundaries”, Trans. of ASME, Journal of Vibration and Acoustics, Vol 114, No. 2, pp. 133-140.
- Thomson, W.T., (1950), “Transmission of Elastic Waves through a Stratified Solid Media”, Journal of Applied Physics, Vol. 21, p. 89-93.

Curriculum Vitae

Rambod Hadidi**Education:**

Ph.D. Civil Engineering, Rutgers University, New Brunswick, NJ, May 2007
 M.Sc. Civil Engineering, Rutgers University, New Brunswick, NJ, May 2003
 B.Sc. Civil Engineering, Sharif University of Technology, Tehran, Iran, June 1999

Academic Experience:

University of Texas at El Paso, El Paso, TX

Lecturer - August, 2006 to December 2006

Rutgers University, Piscataway, NJ - January, 2002 to July 2006

Graduate Research Assistant – Spring, 2002; Summer, 2002; Fall, 2002; Spring, 2003; and Summer 2004

Substitute Lecturer- Spring, 2006

Lecturer- Fall, 2003; Spring, 2004; Fall, 2004; and summer 2005

Graduate Teaching Assistant – Fall 2004

New Jersey Institute of Technology, Newark, NJ – September 1999 to December 2001

Graduate Research Assistant - Fall, 1999; Spring, 2000; and Fall, 2000

Professional Experience:

Paulus, Sokolowski and Sartor, LLC, Warren, NJ

Consultant/Project Geotechnical Engineer - April, 2004 to January, 2007

Transportation Infrastructure Systems Inc., Skillman, NJ

Project Engineer - January, 2003 to January 2004

Qods Niroo Consulting Engineers, Tehran, IRAN

Project Engineer - June 1999 to September 1999

Publications:

Journal and Peer Reviewed Publications:

Hadidi, R. and Gucunski, N. “A Probabilistic Approach to Solution of Inverse Problems in Civil Engineering”, *ASCE Journal of Computing in Civil Engineering*, (Accepted for publication).

Hadidi, R., and Gucunski, N. “A Probabilistic Approach to Falling Weight Deflectometer Backcalculation”, *The 86th Transportation Research Board Annual Meeting*, Washington, DC, 2007.

- Gucunski, N., Hadidi, R., Zaghlouol, S., Maher, A., and Shokouhi, P., “Seasonal and Temperature Adjustment Models of Pavement Properties from Seismic Nondestructive Evaluation”, *Geotechnical Special publication - Proceedings of GeoShanghai International Conference*, Shanghai, China June 6-8, 2006 (accepted for publication).
- Gucunski, N., Zaghlouol, S., Maher, A., Hadidi, R., and Shokouhi, P., “Development of Seasonal Variation Models of Pavement Properties Using Seismic Nondestructive Testing (NDT) Techniques”, *Geotechnical Special Publication, Proceedings of Geo-Institute Congress – Geotechnical Engineering in Information Technology Age*, Atlanta, Georgia, February 26 to March 1, 2006.
- Hadidi, R. and Saadeghvaziri, M.A., “Transverse Cracking of Concrete Bridge Decks: the State-of-the-Art”, *ASCE Journal of Bridge Engineering*, Volume 10, Number 5, September/October 2005, pp 503-510.
- Saadeghvaziri, M.A. and Hadidi, R., “Transverse Cracking of Concrete Bridge Decks: Effects of Design Factor”, *ASCE Journal of Bridge Engineering*, Volume 10, Number 5, September/October 2005, pp 511-519.
- Hadidi, R., Saadeghvaziri, M.A., and Hsu, T.H. “A Practical Tool to Accurately Estimate Tensile Stresses in Concrete Bridge Decks to Control Transverse Cracking”, *ASCE Practice Periodical on Structural Design and Construction*, Volume 8, Number 2, 2003, pp74-82.
- Hadidi, R., and Saadeghvaziri, M.A., “State of the Art of Early Age Transverse Cracking of Concrete Bridge Decks”, *The 82nd Transportation Research Board Annual Meeting*, Washington, DC, January 15, 2003.